Faculdade de Engenharia da Universidade do Porto
Instituto de Ciências Biomédicas Abel Salazar da Universidade do Porto

Polymeric-based nanoparticles targeting the CCR5 co-receptor as an innovative approach for the delivery of antiretroviral compounds

Catarina Castanheira Coutinho

Dissertation for the Master Degree in Bioengineering – Molecular Biotechnology

Supervisor: José das Neves, Ph.D.
Co-supervisor: Bruno Sarmento, Ph.D.

September, 2017

“A confiança consegue realizar
as coisas mais impossíveis.”

(J. Kentenich)

Resumo

A infeção pelo vírus da imunodeficiência humana (VIH), o agente causador da síndrome da imunodeficiência adquirida (SIDA), continua a ser uma causa significativa de morbidade e mortalidade em todo o mundo. Enquanto uma cura eficaz ainda é elusiva, a prevenção tornou-se crucial na luta contra o VIH/SIDA. Em particular, o desenvolvimento de microbicidas anti-VIH tópicos tem sido foco de investigação significativa nos últimos anos, especialmente para a prevenção da transmissão do homem para a mulher. Neste contexto, os sistemas baseados em nanotecnologia têm atraído um interesse considerável devido ao potencial melhoramento dos perfis de eficácia e segurança das formulações microbicidas. Para isso, o conceito de entrega direcionada de compostos ativos, embora pouco explorado na área, pode ser particularmente vantajoso, visto que permitiria a sua entrega específica aos primeiros intervenientes na transmissão do VIH. Este trabalho tem como objetivo o desenvolvimento de nanopartículas (NPs) de base polimérica direcionadas para o receptor de quimiocinas C-C do tipo 5 (CCR5). Estes nanossistemas poderiam ser utilizados como transportadores de fármacos anti-retrovirais inovadores, direccionados para as células suscetíveis ao VIH que estão normalmente envolvidas na transmissão inicial do vírus na mucosas cervicovaginal e colorretal.

As NPs foram desenvolvidas utilizando copolímeros de poli(ácido lático-*co*-ácido glicólico) (PLGA)-polietilenoglicol (PEG) e funcionalizadas com D-Ala-Péptido T-Amida (DAPTA), um péptido com afinidade para o receptor CCR5. Um copolímero de PLGA-PEG com grupos carboxílicos terminais (PLGA-PEG-COOH) foi sintetizado por acoplamento mediado por carbodiimida, com um rendimento em massa de 24.4%. O polímero obtido foi caracterizado por Espectrometria de Massa de Ionização e Dessorção a Laser Assistida por Matriz-Tempo de Voo (MALDI-TOF MS), Espectroscopia de Infravermelho por Transformada de Fourier (FTIR) e Ressonância Magnética Nuclear de Protão (RMN de ^{1}H). Enquanto a análise de MALDI-TOF permitiu apenas confirmar a presença de PEG, tanto FTIR como RMN de ^{1}H indicaram a presença de ambos os polímeros nas amostras de PLGA-PEG-COOH obtidas. NPs de PLGA-PEG contendo 90% de PLGA-PEG e 10% de PLGA-PEG-COOH, sintetizado ou comercialmente disponível, foram produzidas por nanoprecipitação. As NPs obtidas foram depois

funcionalizadas com o péptido DAPTA por acoplamento mediado por carbodiimida. A presença de DAPTA associado às NPs foi confirmada por análise de RMN de ^{1}H. A morfologia das NPs foi caracterizada por Microscopia Eletrónica de Transmissão (TEM), enquanto o tamanho (diâmetro hidrodinâmico médio) e a carga superficial (potencial zeta) foram determinados usando Dispersão de Luz Dinâmica (DLS) e Dispersão de Luz Eletroforética (ELS), respectivamente. Todas as formulações de NPs, incluindo nanossistemas não funcionalizados e nanossistemas modificados com DAPTA, apresentaram valores médios de diâmetro hidrodinâmico entre 160 e 180 nm, sendo relativamente monodispersas (valores de índice de polidispersão abaixo de 0.1). Os valores de potencial zeta, compreendidos entre -9 e -3 mV, indicaram que as NPs apresentaram carga superficial praticamente neutra.

O potencial de toxicidade das NPs na linha celular GHOST (3) $CCR5^{+}$ (Ghost Hi-5) foi ainda estudado através da avaliação da atividade metabólica utilizando o ensaio de redução de brometo de 3-(4,5-dimetiltiazol-2-il)-2,5-difeniltetrazólio (MTT). Tanto NPs funcionalizadas como não funcionalizadas apresentaram um potencial de citotoxicidade baixo. Finalmente, NPs contendo cumarina-6 foram utilizadas para avaliar a capacidade do péptido DAPTA para aumentar a interação das NPs com as células Ghost Hi-5. Os estudos quantitativos de captação de NPs foram feitos utilizando Separação de Células Ativada por Fluorescência (FACS). Dados preliminares sugeriram que as NPs modificadas com DAPTA não melhoraram significativamente a associação com células em comparação com NPs não funcionalizadas.

Em conclusão, NPs de PLGA-PEG modificadas com DAPTA foram produzidas com sucesso e as suas propriedades físico-químicas e biológicas relevantes foram caracterizadas. Em particular, os dados obtidos sugeriram que as NPs funcionalizadas apresentam características gerais adequadas para o seu potencial uso no desenvolvimento de microbicidas. No entanto, uma maior associação a células que expressam CCR5 não foi demonstrada e são necessários estudos adicionais para perceber melhor as interações entre NPs e células.

Palavras-chave: VIH/SIDA; profilaxia pré-exposição; microbicidas; nanotecnologia; nanopartículas de PLGA-PEG; entrega direcionada

Abstract

Infection by the human immunodeficiency virus (HIV), the causative agent of acquired immune deficiency syndrome (AIDS), continues to be a significant cause of morbidity and mortality worldwide. While an effective cure is still elusive, prevention has become crucial in the battle against HIV/AIDS. In particular, the development of topical anti-HIV microbicides has been the focus of significant research in recent years, especially for preventing male-to-female transmission. In this context, nanotechnology-based systems have attracted considerable interest due to the potential improvement of efficacy and safety profiles of microbicide formulations. For that, the concept of targeted delivery of active compounds, although little explored in the field, may be particularly advantageous, as it would allow specific delivery to early key players in HIV transmission. This work aims at developing polymeric-based nanoparticles (NPs) targeting the C-C chemokine receptor type 5 (CCR5). Such nanosystems may pose as innovative antiretroviral drug carriers targeting HIV-susceptible cells that are typically involved in early viral transmission at the cervicovaginal and colorectal mucosae.

NPs were developed by using poly(lactic-*co*-glycolic acid) (PLGA)-polyethylene glycol (PEG) copolymers and further functionalized with D-Ala-Peptide T-Amide (DAPTA), a peptide with reported affinity towards the CCR5 receptor. A PLGA-PEG copolymer with terminal carboxylic groups (PLGA-PEG-COOH) was synthesized through carbodiimide-mediated coupling, with a mass yield of 24.4%. The obtained polymer was characterized by Matrix Assisted Laser Desorption Ionization-Time of Flight Mass Spectrometry (MALDI-TOF MS), Fourier Transform Infrared Spectroscopy (FTIR) and Proton Nuclear Magnetic Resonance (^{1}H NMR). While MALDI-TOF analysis allowed only to confirm the presence of PEG, both FTIR and ^{1}H NMR indicated the presence of both polymers in the obtained PLGA-PEG-COOH samples. PLGA-PEG NPs containing 90% of PLGA-PEG and 10% of either synthesized or commercially available PLGA-PEG-COOH were produced by nanoprecipitation. Obtained NPs were then functionalized with the DAPTA peptide through carbodiimide-mediated coupling. The presence of DAPTA associated to NPs was confirmed by ^{1}H NMR analysis. NP morphology was characterized by using Transmission Electron Microscopy (TEM), while size (mean hydrodynamic diameter) and

surface charge (zeta potential) were determined using Dynamic Light Scattering (DLS) and Electrophoretic Light Scattering (ELS), respectively. All NP formulations, including non-functionalized and DAPTA-modified nanosystems, had average hydrodynamic diameter values between 160 and 180 nm and were relatively monodisperse (polydispersity index values below 0.1). Zeta potential values ranging from -9 to –3 mV indicated that NPs presented nearly neutral surface charge.

The toxicity potential of NPs in the GHOST (3) $CCR5^+$ cell line (Ghost Hi-5) was further assessed by estimating the metabolic activity using the 3-(4,5-dimethylthiazol-2-yl)-2,5-diphenyltetrazolium bromide (MTT) reduction assay. Both functionalized and non-functionalized NPs presented low cytotoxic potential. Finally, coumarin-6-loaded NPs were used to evaluate the ability of DAPTA to enhance the interactions of NPs with Ghost Hi-5 cells. Quantitative NP uptake studies were performed using Fluorescence-Activated Cell Sorting (FACS). Preliminary data suggested that the proposed DAPTA-modified NPs did not significantly improve the association with cells as compared to non-functionalized NPs.

In conclusion, DAPTA-modified PLGA-PEG NPs were successfully produced and characterized for relevant physicochemical and biological properties. In particular, obtained data suggested that functionalized NPs present suitable general features for potential use in microbicide development. However, enhanced association to CCR5-expressing cells was not demonstrated and additional studies are required in order to better understand NP-cell interactions.

Key words: HIV/AIDS; pre-exposure prophylaxis; microbicides; nanotechnology; PLGA-PEG nanoparticles; targeted delivery

Acknowledgements

First of all, I would like to thank my supervisor, Dr. José das Neves, for having accepted me as a master student, for all the support and patience throughout this journey. I'm thankful for all the great advice he gave me, for passing me a bit of his deep knowledge and experience, for the valuable suggestions and for all the time he spent helping me and teaching me how the world of research works. I'm also thankful for always saying the right words at the right time, either for encouragement or stimulus.

I would also like to thank my co-supervisor, Prof. Bruno Sarmento, for having accepted me in his team, for all the advice, kindness, support and for being an example of excellence and professionalism.

To all my team colleagues in the *Nanomedicines & Translational Drug Delivery* group, particularly those who helped me the most – Mafalda and Elisabete, for all the help they gave me in the beginning; Rute, for always being willing to help me and teach me all she could, even when her time was so short; Patrick, Cláudia and Francisca for all the valuable advice they gave me; Flávia and Andreia, for all the support, help and good mood; Karla for the joy and laughter she brought to the lab; Inês, for being the best college and lab mate I could ever find. Thank you for your help, company and, above all, for all the friendship!

A heartfelt thanks to Mariana Andrade, to Sílvia Maia and, especially, to Carlos Fernandes, for their valuable contributions to the development of my work.

My sincere acknowledgements to *i3S - Instituto de Investigação e Inovação em Saúde* for having accepted me in its laboratories and for all the facilities I used in my dissertation. This is an institution "where ideas grow", but also "where people grow" and, mainly, "where our passion for science grows"! I'm also thankful for all the wonderful people I could meet in this institute, not only in our group, but also our lab and other labs as well.

My acknowledgements also to FEUP and ICBAS for receiving me and for all the learning and skills provided.

To all my friends in MIB, for all the company, the laughter, the complicity, the good moments, the challenges we faced together and for making these five year journey one of the

best of my short life. To Ana Martins, Inês, Débora, Rita Ribeiro, Nélson, Hélia, Ana Rodrigues, Isabel, Daniela, Vítor, Mariana and Sara, a heartfelt thank you! For everything!

To all the friends I met at the Cluny Residence, for all the company, the plans and good moments that could always help relieve the weight of a difficult day. A special thanks to Ana Martins, Ana Rocha, Mariana Domingues and Clara Alves.

To my eternal flatmate, Rita Rebouta, for all the adventures in the years we lived together, for the ones that came after, for the special and unique friendship we built and never changed no matter what were the circumstances!

And last but not least, I would like to thank my amazing family! Thanks to my parents, for their love, support and guidance during my academic journey. Thanks for always believing in me and never let me give up; for encouraging me and for being an example of perseverance, hard work and dedication to others. Thanks to my brother Pedro and my little sister Mariana, for being my joy and always putting a smile on my face, no matter how difficult the week had been. And thanks to all my other family members, for all their love and support, even from a distance. Without you, this would never be possible!

Table of contents

List of figures

List of tables

Abbreviations and symbols

List of abbreviations

^{1}H NMR	Proton nuclear magnetic resonance
a	adsorbed
AIDS	Acquired immunodeficiency syndrome
ANOVA	One-way analysis of variance
APC	Allophycocyanin
ATR	Attenuated Total Reflection
BCA	Bicinchoninic acid
CCR5	C-C chemokine receptor type 5
CD1a	Cluster of differentiation 1a
CD4	Cluster of differentiation 4
CD45	Cluster of differentiation 45
CD195	Cluster of differentiation 195
cDNA	Complementary deoxyribonucleic acid
CXCR4	C-X-C chemokine receptor type 4
Cy-3	Cyanine dye 3
Cy-5	Cyanine dye 5
DAPI	4',6-diamidino-2-phenylindole
DAPTA	D-ala-peptide T-amide
DC	Dendritic cell
DCC	*N*,*N*'-Dicyclohexylcarbodiimide
DCM	Dichloromethane
DC-SIGN	Dendritic Cell-Specific Intercellular adhesion molecule-3-Grabbing Non-integrin
DCTB	*trans*-2-[3-(4-*tert*-Butylphenyl)-2-methyl-2-propenylidene]malononitrile
DIC	*N*,*N*'-Diisopropylcarbodiimide
DIPEA	*N*,*N*-Diisopropylethylamine
DLS	Dynamic Light Scattering
DMEM	Dulbecco's Modified Eagle medium

DMSO	Dimethyl sulfoxide
EDC	1-ethyl-3-(3-dimethylaminopropyl)carbodiimide
EDTA	Ethylenediamine tetraacetic acid
ELS	Electrophoretic Light Scattering
EMA	European Medicine Agency
f	functionalized
Fab	fragment, antigen-binding
FACS	Fluorescence-activated cell sorting
FBS	Fetal bovine serum
FDA	United States Food and Drug Administration
FITC	Fluorescein isothiocyanate
FSC-A	Forward scatter area
FSC-H	Forward scatter height
FTIR	Fourier Transform Infrared
Gly	Glycine
gp120	Glycoprotein 120
gp41	Glycoprotein 41
GPC	Gel Permeation Chromatography
HIV	Human immunodeficiency virus
HLA-DR	Human Leukocyte Antigen – antigen D Related Intercellular Adhesion Molecule
ICAM	Intercellular Adhesion Molecule
IR	Infrared
ISO	International Organization for Standardization
LC	Langerhans cell
LFA-1	Lymphocyte function-associated antigen 1
MALDI-TOF MS	Matrix-assisted laser desorption/ionization – time-of-flight mass spectrometry
MES	2-(*N*-morpholino)ethanesulfonic acid
MFI	Mean fluorescence intensity
MTT	3-(4,5-dimethylthiazol-2-yl)-2,5-diphenyltetrazolium bromide
Mw	Molecular weight
MWCO	Molecular weight cut-off
NHS	*N*-hydroxysuccinimide
NIH	National Institutes of Health
NP	Nanoparticle
OPA	*ortho*-phthalaldehyde
PBMC	Peripheral blood mononuclear cell
PBS	Phosphate buffered saline
PCL	Poly(ε-caprolactone)
PdI	Polydispersity index
PEG	Polyethylene glycol

PFA	Paraformaldehyde
PLGA	Poly(lactic-co-glycolic acid)
PrEP	Pre-Exposure Prophylaxis
PVP	polyvinylpyrrolidone
RANTES	Regulated on Activation, Normal T Cell Expressed and Secreted
RMSD	Root mean square deviation
SD	Standard deviation
SEC	Size Exclusion Chromatography
siRNA	small interfering ribonucleic acid
SLS	Static Light Scattering
SNAP-23	Synaptosome-associated 23-kDa protein
SSC-A	Side Scatter Area
Sulfo-NHS	*N*-hydroxysulfosuccinimide
TEM	Transmission Electron Microscopy
THF	Tetrahydrofuran
TMS	Tetramethylsilane
TNPO3	Transportin 3
UNAIDS	Joint United Nations Programme on HIV/AIDS

List of symbols

δ	Chemical shift (in NMR)
δ	Bending vibration (in FTIR)
ε	Dielectric constant
υ	Stretching vibration (in FTIR)
τ	Twisting vibration (in FTIR)
ζ	Zeta (in ζ-potential)

CHAPTER 1

Motivations, Objective and Document Structure

1.1. Context and motivations [1]

Infection by the human immunodeficiency virus (HIV), the causative agent of acquired immune deficiency syndrome (AIDS), continues to be one of the most relevant healthcare problems at the global level and is still a significant cause of morbidity and mortality worldwide (1). HIV infects and destroys the $CD4^+$ cells of the immune system, leading to immune deficiency and increased susceptibility to lethal opportunistic infections that may subsequently arise (2). According to official estimates of the Joint United Nations Programme on HIV and AIDS (UNAIDS), an additional 2.1 million new HIV infections occurred during 2015, rising the number of infected individuals to a total of 36.7 million people (3). HIV sexual transmission is held accountable for around 80% of all infections, with roughly half of the affected individuals being women (4). The advent of combined antiretroviral therapy has been crucial for controlling the infection and reducing morbidity and mortality (5). However, a cure for HIV/AIDS is still elusive and prevention remains crucial. In the case of sexual transmission, condom use, promotion of changes in sexual behavior, sexual counselling and testing, male medical circumcision, antiretroviral therapy in serodiscordant couples and oral pre-exposure prophylaxis (PrEP) are currently well established as effective measures (6). Still, all these options have not been fully successful in averting new infections and additional strategies are therefore deemed necessary.

Similarly to antiretroviral drugs used for oral PrEP, topical microbicides have been proposed for blocking early transmission events at the vaginal or rectal mucosae. These last comprise products intended to be self-administered in the vagina or rectum, prior or around

[1] This section has been partially published as "Coutinho C, Sarmento B, das Neves J. Targeted microbicides for preventing sexual HIV transmission. J Control Release. 2017; 266:119-128."

the time of sexual intercourse, with potentially fast onset of high local concentrations of antiviral compounds but reduced systemic exposure (7-9). Microbicides for vaginal use are currently in advanced stages of development, with various products based on antiretroviral drugs already under clinical testing. In particular, a vaginal ring allowing to sustain the vaginal levels of dapivirine, a non-nucleoside reverse transcriptase inhibitor, for several weeks, has been shown effective in reducing transmission by 27-31% (10, 11). Despite mild effectiveness, the product is seen as particularly advantageous since it may be used irrespective of the time of sexual intercourse (coitus-independent use), contrary to other microbicides based on gel, tablet or film formulations (12). The dapivirine ring is currently undergoing additional clinical testing and is expected to get regulatory approval for use by women at high risk of infection over the next few years.

The microbicides field has come a long way since the first disappointing trials of products containing non-specific active compounds (13). Despite current trends supporting the use of potent antiretroviral drugs and increasing efforts being made to develop products that can sustain mucosal drug levels (14, 15), targeted delivery of promising microbicide compounds has been little explored. The ability to preferentially deliver active molecules to cells, tissues or structures particularly relevant to HIV transmission presents the potential to enhance protection, while reducing undesirable effects. Such strategy has been widely used in other fields, namely in cancer therapy and diagnostics research, and nanotechnology in particular has been playing a pivotal role in developing targeted drug carriers and probes (16, 17). Targeted delivery of drugs and other biologically active agents of interest might also be useful in managing infectious diseases by exploiting host/pathogen differences and blocking their interactions (18). Microbicides, in particular, may potentially take advantage of such approaches, as they would allow specific delivery to early key players in HIV transmission and spread, and subsequent inhibition of viral replication, thus likely increasing the efficacy and safety profiles of microbicide formulations.

1.2. Objective and rationale of the work

The objective of this work was to develop polymeric-based nanoparticles (NPs) targeting the C-C chemokine receptor type 5 (CCR5), a receptor involved in HIV entry into susceptible cells (19). Promising nanosystems emerging from this work are intended to be considered in the future as potential antiretroviral drug carriers in the context of microbicide development.

For the purpose of this work, poly(lactic-*co*-glycolic acid) (PLGA)-polyethylene glycol (PEG) copolymers have been selected for the development of polymeric NPs, which were further functionalized with D-Ala-Peptide T-Amide (DAPTA), a peptide with reported high affinity towards the CCR5 receptor. PLGA is a biocompatible and biodegradable polymer

composed by glycolic and lactic acid monomers linked by ester bonds (20). It is approved by the United States Food and Drug Administration (FDA) and the European Medicines Agency (EMA) for use in drug delivery systems for parenteral administration, having been widely explored in the design of NPs for drug delivery purposes in a wide range of biomedical applications (21). PLGA has also been proposed for the development of nanotechnology-based microbicides (22). PEG is a widely used polymer in the biomedical field for conferring improved solubility, stealth-like behavior (*i.e.*, decreased uptake by the reticuloendothelial system) and non-immunogenic properties to nanosystems (23). This polymer has further been proposed for densely coating microbicide nanosystems, allowing to reduce their interactions with mucins and favor their distribution and transport across mucus (24). For these reasons, PLGA-PEG copolymers (**Figure 1.1A**) have been chosen as building blocks for the polymeric NPs developed herein.

Regarding the targeting ability towards CCR5, several compounds have been developed as therapeutic drugs and/or microbicide candidates that can bind the CCC5 receptor. These can block the membrane receptor used by the virus and inhibit its entry (25, 26). Compounds binding to CCR5 with high affinity could also hold promise for the development of targeted systems towards HIV-susceptible cells. One example is the herein proposed DAPTA peptide (**Figure 1.1B**), the protease resistant analog of peptide T. DAPTA comprises an eight amino acid peptide derived from the V2 region of the HIV gp120 protein that inhibits HIV cell entry upon direct binding to CCR5 (27). DAPTA had been evaluated in early phase clinical trials for improving HIV neuropsychological symptoms (neuro-AIDS) with good efficacy and safety outcomes (28). DAPTA was therefore selected as a targeting ligand for PLGA-PEG NPs in this work.

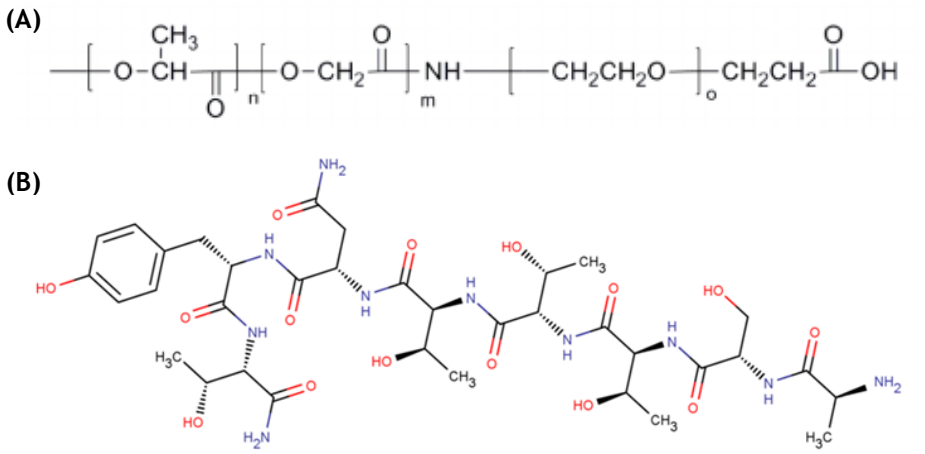

Figure 1.1. Structure of the copolymer and peptide used in this work. **(A)** General structure of PLGA-PEG copolymers. **(B)** Structure of the DAPTA peptide. Image in **(A)** is reprinted with permission from (29), Copyright 2013 American Chemical Society.

Specific aims of the work included the synthesis and characterization of PLGA-PEG copolymers that would further allow the production and functionalization with DAPTA of NPs, alongside relevant physicochemical characterization. Additionally, obtained NPs were intended to be tested *in vitro* for their cytotoxicity, as well as targeting ability to CCR5-expressing cells.

1.3. Structure of the dissertation

This dissertation is organized in five chapters. Chapter 1 explores the motivations behind the present work and delineates its main objective. In Chapter 2, the most relevant literature is revised, describing the state of the art of research involving targeted nanosystems for application as anti-HIV microbicides. The next two chapters pertain to the performed experimental work: Chapter 3 is dedicated to the description of materials, experiments and methodologies used, while Chapter 4 presents the results and their critical and concise analysis. In the last chapter, Chapter 5, the main findings of this work are summarized and prospects for future studies are presented.

CHAPTER 2

Literature Review [2]

2.1. Targeted microbicides: targeting what?

Defining actual and potential viral and host targets that can be useful for specific delivery of antiretroviral compounds is a crucial initial step in guiding the engineering of delivery systems. Most targets can be inferred from the general viral life cycle (**Figure 2.1**).

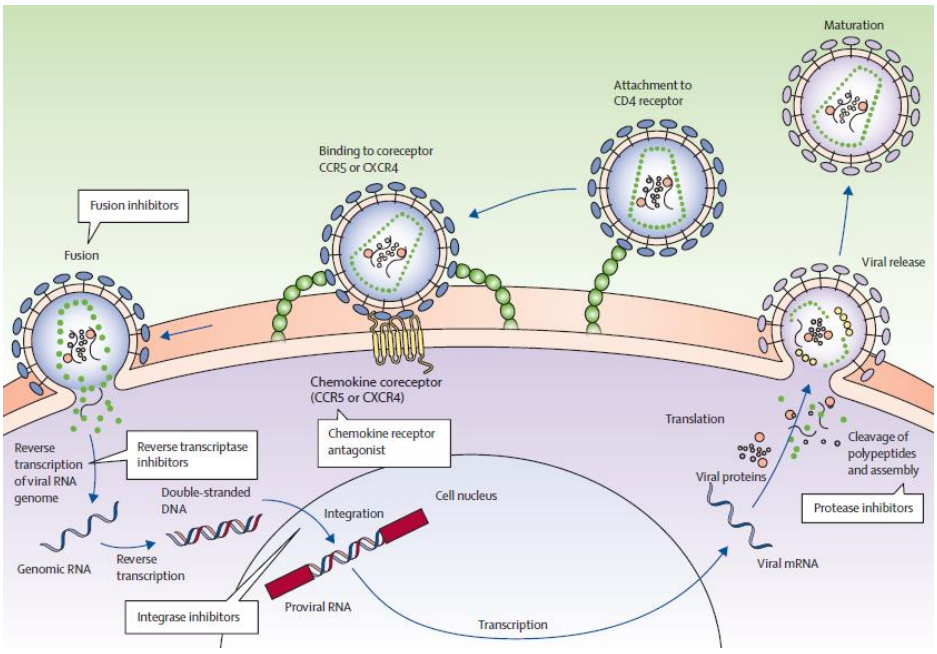

Figure 2.1. HIV life cycle and the sites of action of different classes of antiretroviral drugs. Reprinted from (30), Copyright (2014), with permission from Elsevier.

[2] This section has been partially published as "Coutinho C, Sarmento B, das Neves J. Targeted microbicides for preventing sexual HIV transmission. J Control Release. 2017; 266:119-128."

HIV typically infects susceptible cells in a highly specific manner that depends on the interaction of distinct viral and host proteins. Entry of HIV into susceptible cells requires the initial interaction of the viral envelope glycoprotein gp120 with the host CD4 cell membrane receptor and then with one chemokine co-receptor, usually CCR5 or CXCR4 (19). Cells expressing these surface molecules, namely at the cervicovaginal mucosa, include mainly macrophages, T cells and dendritic cells (DCs) (31). After sequential binding to receptor and co-receptor, the fusion of HIV and the host cell membrane is mediated by the viral envelope protein gp41 (32). Targeting either viral gp120 or gp41, or host CD4, CCR5 or CXCR4 has been quickly recognized as beneficial, not only for direct blocking of infection (as in the case of entry inhibitors used in therapeutics (33)) but also as a straight forward strategy for delivering antiretroviral compounds. Various studies focusing on this last possibility have been described over the years for therapeutic purposes. For example, Clayton and co-workers (34) developed PEG-modified liposomes coated with ligands derived from the Fab fragment of F105, a gp120-directed monoclonal antibody. Liposomes were evaluated as targeted carriers for a new protease inhibitor (PI1), showing great specificity to HIV-infected cells bearing gp120 at the membrane (**Figure 2.2**) and allowing greater and longer drug activity than the free drug or non-targeted liposomes. The same Fab fragment fused to protamine had been previously used to deliver different siRNA molecules, being the obtained systems shown able to silence the expression of specific genes and to inhibit viral replication in HIV-infected T cells (35). In another study, Zhou *et al*. (36) proposed aptamer-siRNA chimeras, composed by siRNA silencing a *tat*/*rev* common exon sequence and an anti-gp120 aptamer conferring targeting ability to the conjugate. Chimeras were specifically internalized into cells expressing gp120, either ectopically or resulting from HIV infection. Also, conjugates efficiently inhibited HIV replication both *in vitro* in T cells and, in a later study (37), in HIV-infected humanized mice. Endsley and Ho (38) reported on the development of PEGylated liposomes incorporating the protease inhibitor indinavir and functionalized with two peptides with reported affinity to CD4. The liposomes were shown to selectively bind and efficiently deliver the drug to $CD4^+$ cells, presenting higher anti-HIV activity as compared to non-targeted liposomes or the free drug.

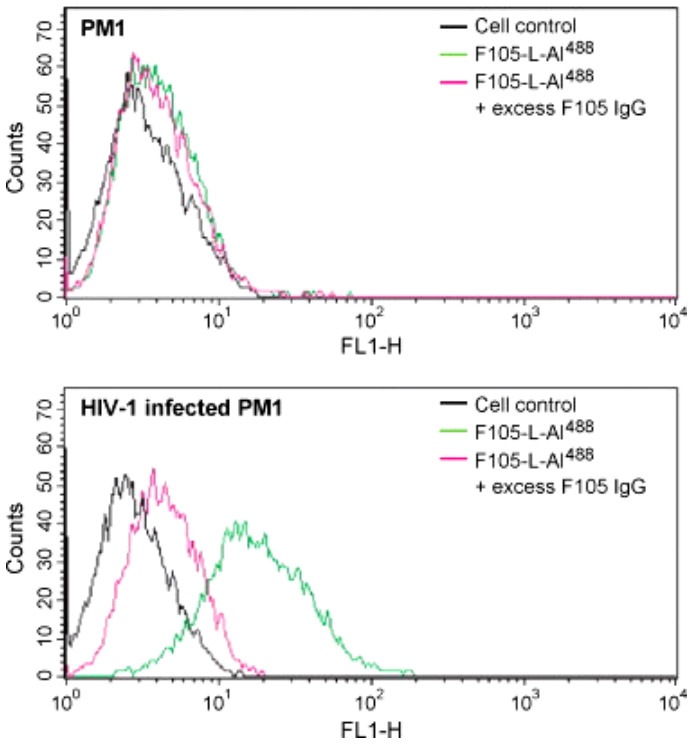

Figure 2.2. Fluorescence-activated cell sorting (FACS) histograms showing binding and uptake of F105-functionalized liposomes labeled with Dextran Alexa Fluor 488 (F105-L-Al^{488}) by uninfected and HIV-1-BaL-infected PM1 CD4$^+$ T cells, either alone or in competition with an excess of F105 IgG. Reprinted from (34), Copyright (2009), with permission from Elsevier.

After cell entry, the HIV core disassembles and its RNA genome is converted into complementary DNA (cDNA) by the viral reverse transcriptase. Newly formed cDNA migrates to the nucleus, where it is integrated into the host genome by the viral integrase. From that point on, the cell becomes permanently infected and is able to produce new virions (39). Viral molecules involved in the intracellular part of the life cycle, namely reverse transcriptase, integrase and protease, have been extensively studied as targets for developing new drugs, but these seem unfeasible from a drug delivery perspective. Intracellular targeting would likely require being associated with pre-cellular targeting and, thus, be redundant in terms of delivering relevantly higher levels of antiretroviral compounds to the site of action.

Beyond more general considerations regarding the viral life cycle, events occurring specifically during sexual transmission of HIV, as schematically represented in **Figure 2.3**, provide important hints towards the identification of potential targets. HIV can be deposited in the vaginal or colorectal lumen either in the free form or associated to cells, mostly upon ejaculation. These viral particles and infected leukocytes can immediately be targeted by microbicide nanosystems and prematurely inactivated (40). Specific molecules at the surface of HIV (namely those described above) and immune cells, such as the leukocyte common antigen CD45, can be tentatively selected for such purpose. Still at the mucosal lumen, mucus has long been regarded as a preferential target for drug carriers, namely by

engineering the previous to bear mucoadhesive properties (41). This allows, in principle, to prolong residence after administration with consequent increased drug levels at one of the first hurdles that the virus encounters. However, it is currently known that interacting with mucus might actually be detrimental since the barrier properties of mucosal fluids can be compromised, thus facilitating HIV crossing towards the underlying epithelium (42). For example, current trends in nanotechnology-based microbicides seem to favor approaches that use systems bearing non-mucoadhesive surfaces, namely by densely coating these last with relatively low molecular weight PEG that reduces interactions with mucins (24). Alternative strategies to PEGylation are also being developed for increasing diffusivity of nanosystems (43).

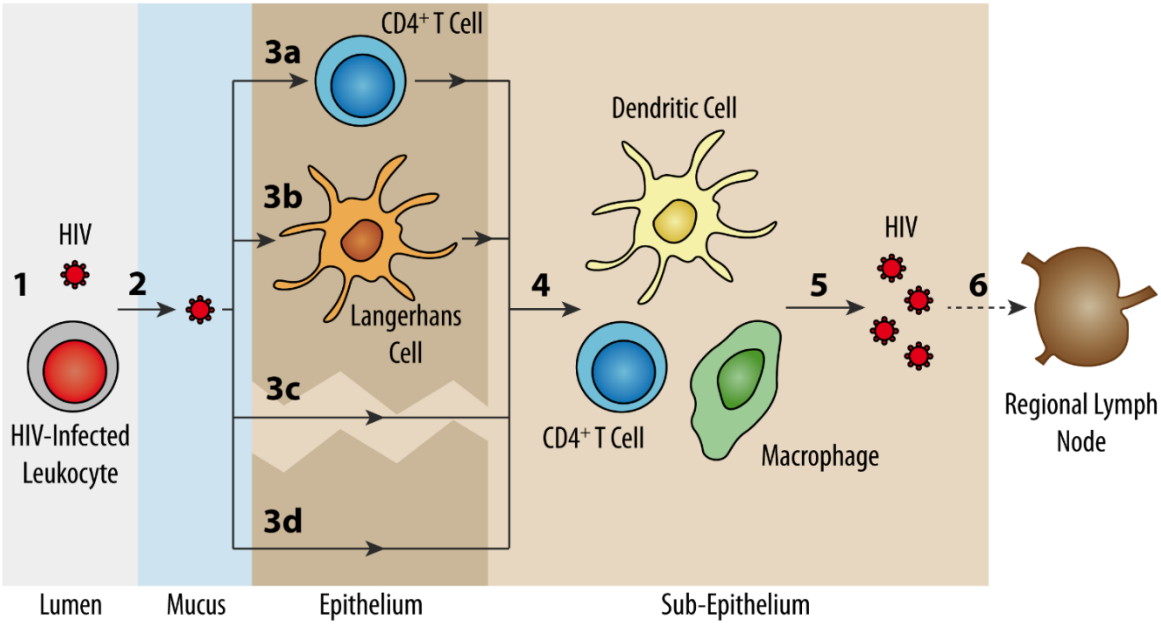

Figure 2.3. Schematic representation of the main events involved in the sexual transmission of HIV occurring at the mucosal level. **(1)** HIV is deposited alongside semen in the cervicovaginal or colorectal lumen, either in the free form or associated to leukocytes. **(2)** The virus is then required to tackle mucus and reach the epithelial barrier. HIV may cross the epithelium through different mechanisms, namely by: **(3a)** accessing and infecting intraepithelial $CD4^+$ T cells or other leukocytes; **(3b)** accessing intraepithelial Langerhans cells that capture viral particles and help mediate crossing to the sub-epithelium without cell infection; **(3c)** crossing through epithelial breaches that can occur naturally in healthy individuals (for instance, related with microtrauma due to sexual intercourse) or result from pathological conditions (*e.g.*, inflammation, other infections); or **(3d)** direct crossing of the epithelium, which is limited in intact stratified squamous epithelia at the ectocervix and vagina but common in simple columnar epithelia present at the endocervix and colorectum. **(4)** HIV reaching the sub-epithelium can then infect target cells, including dendritic cells, $CD4^+$ T cells and macrophages. **(5)** These last, mainly $CD4^+$ T cells, promote initial amplification of the virus. **(6)** Finally, free or cell-associated HIV migrates to regional lymph nodes, where cell infection is further propagated before

systemic spreading (not necessary in the case of the colorectum due to the presence of lymphoid cells and follicles at the sub-epithelium).

Once past mucosal fluids, viral particles are required to cross the epithelium in order to access susceptible cells that are abundant at the lamina propria. It should be noted that epithelial cells do not support viral replication and provide a noticeable physical barrier to HIV, particularly at the vagina (44). Thus, targeting the epithelium, including its underlying basement membrane, as a depot site for drug nanocarriers may be explored as an approach to enhance protection. There are several major mechanisms through which HIV can migrate across the epithelium, namely (i) by penetrating regions of thinned or damaged epithelium; (ii) by accessing intraepithelial $CD4^+$ T cells and Langerhans cells (LCs), which can mediate transepithelial transport; and (iii) by bypassing the simple columnar epithelium of the endocervix and colorectum through transcytosis (free virions) or via intercellular gaps (both in the free form or in infected cells) (45, 46). Intraepithelial immune cells can be relevant when considering these potential routes. In the particular case of LCs, the lumen-lamina propria HIV translocation mechanism and transmission to $CD4^+$ T cells without productive infection (possibly mediated by C-type lectin receptors such as langerin) can be of particular interest for targeting purposes (47). Therefore, typical but not exclusive markers of LCs, such as langerin and CD1a, may be helpful in establishing targeting strategies.

Susceptible cells present at the lamina propria, particularly $CD4^+$ T cells, are able to provide crucial local amplification of infection before the virus is transferred to regional lymph nodes (48). Such cells are therefore preferential targets for specific delivery of antiretroviral compounds. Again, cell surface proteins described above for the general life cycle of the virus, namely CD4, are prone to be selected for targeting. Moreover, and in addition to being susceptible to HIV infection, DCs can promote infection of other immune cells without being productively infected, either by membrane fusion and establishment of infectious synapses, or by endocytosis of HIV followed by incorporation into endosomal multivesicular bodies and release as exosomes (49). This type of interactions may also provide means for viral transport to lymph nodes. C-type lectin cell membrane receptors, mainly dendritic cell-specific ICAM-grabbing non-integrin (DC-SIGN), have been implicated in such processes (50, 51), making it an important target for mediating specific antiretroviral drug delivery at the mucosal level. Targeting past the mucosa, namely at regional lymph nodes, may already be considered off-limits to microbicides. Still, seminal work on the topic has been described (52, 53) and such possibility should not be immediately discarded.

2.2. 'Smart' microbicides: examples of targeted systems

The number of studies concerning targeted delivery of antiretroviral compounds in the context of topical prevention of sexual HIV transmission is still reduced but has been increasing over recent years. Drug delivery trends already being applied to other medical fields are being adopted and creating novel ways of thinking about microbicides engineering. The following sections will discuss the most relevant approaches in the design of targeted systems, mostly macromolecular constructs or nanocarriers. Both passive and active targeting strategies are overviewed, being defined in a similar way as previously for anticancer therapy (54). In the case of the former, targeted delivery can be achieved by taking advantage of natural biological phenomena (*e.g.*, preferential uptake of nanoparticulate systems by HIV-susceptible cells), while in the latter, surface modification of nanocarriers with particular moieties that can recognize/be recognized by biological structures is sought.

2.2.1. Passive targeting

Passive targeting seeks to take advantage of natural biological processes in order to modulate the bioavailability, biodistribution and/or targeting of active moieties. Inherent properties of nanosystems, such as size, shape and surface charge, can be engineered with such purpose. Passive targeting may be particularly relevant in achieving enhanced cell-associated drug levels. Such objective is considered interesting for both HIV therapy and prevention and rely simply on the typical phagocytic ability of HIV-susceptible cells (55-57). Improving the uptake by epithelia lining anogenital mucosae may also be of interest, namely in establishing local depot sites for prolonging tissue residence of microbicide compounds. Mucosal retention can also be achieved by modifying the ability of microbicide systems to interact with non-cellular structures such as mucus, namely by enhancing the mucoadhesive properties of nanomaterials (24, 58). This has been a popular approach when developing nanotechnology-based carriers for preventing sexual HIV transmission (59, 60). However, growing evidence that mucoadhesive nanosystems may disrupt the natural mucus barrier and potentially enhance viral infection has led to the progressive abandonment of such strategy as a possibility for developing microbicides. Alternatively, mucus-penetrating nanosystems have been shown useful in enhancing mucosal distribution and retention (61-63), serving as preferential platforms for further functionalization and specific targeting.

Our research group has been engaged over recent years in studying the ability of multiple nanocarriers to passively target different cell types (64). In particular, polymeric NPs (mean diameter of 170-200 nm) based on poly(ε-caprolactone) (PCL) or poly(lactic-*co*-glycolic acid) (PLGA) have been designed to deliver dapivirine, one of the most promising microbicide drug candidates. Such systems were shown to be readily taken up by different immune and epithelial cell types as assessed by fluorescence microscopy (65-67). More important,

cell-associated levels of dapivirine provided by nanocarriers were significantly higher (up to nearly 30-fold) in different immune cells as compared to the free drug (**Figure 2.4**) (65). These observations were also correlated with moderately enhanced *in vitro* activity against HIV infection in human peripheral blood mononuclear cells (PBMCs) and a co-culture model of DCs and $CD4^+$ T cells. Conversely, dapivirine-loaded NPs did not generally modify intracellular dapivirine levels when anogenital epithelial cell lines were tested, thus indicating that passive targeting of immune cells (potentially susceptible to HIV infection) could be achieved. Such behavior was, however, highly dependent on the surface properties of NPs: for example, positively-charged nanosystems presented increased cell-associated drug levels even in epithelial cells, likely due to enhanced electrostatic interactions with negatively-charged cell membranes (65, 66).

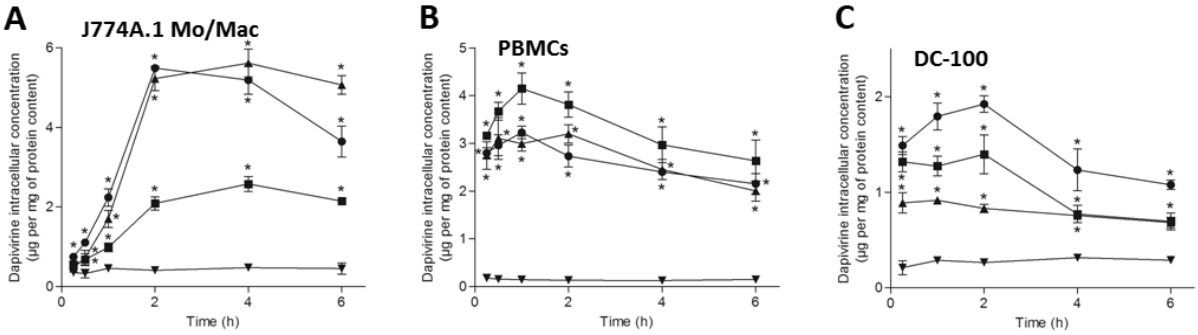

Figure 2.4. Cell-associated levels of dapivirine in (**A**) murine macrophages (J774A.1 Mo/Mac), (**B**) human PBMCs and (**C**) human DC-100 DCs after incubation with the drug at 5 µM concentration. Levels are expressed as drug content per cell protein content. Results presented as mean and standard deviation (n=3). (*) denotes p<0.05 as compared to free dapivirine. Legend: dapivirine-loaded polyethylene oxide-modified PCL NPs (●), dapivirine-loaded sodium lauryl sulfate-modified polycaprolactone NPs (■), dapivirine-loaded cetyltrimethylammonium bromide-modified polycaprolactone NPs (▲), and free dapivirine (▼). Modified from (65), Copyright Springer Science + Business Media, LLC 2011, with permission of Springer.

As mentioned above, nanosystems may also allow non-specific accumulation of active compounds at genital epithelia and contribute to extended protection windows from viral infection. For example, Ham *et al*. (68) demonstrated the ability of PLGA NPs (mean diameter around 260 nm) to enhance the penetration and accumulation of PSC-RANTES, an analog of the Regulated on Activation Normal T cell Expressed and Secreted (RANTES) chemokine and promising microbicide candidate, in human vaginal mucosa. Data from *ex vivo* experiments showed that PSC-RANTES was found present deep into the epithelium as mediated by NPs, while negligible penetration was achieved when the analog was added in the free form (**Figure 2.5**). Work from our group also demonstrated that drug-loaded polymeric NPs can enhance dapivirine accumulation in pig vaginal and rectal mucosa (66), likely due to the ability of NPs to penetrate and retain in epithelia (67).

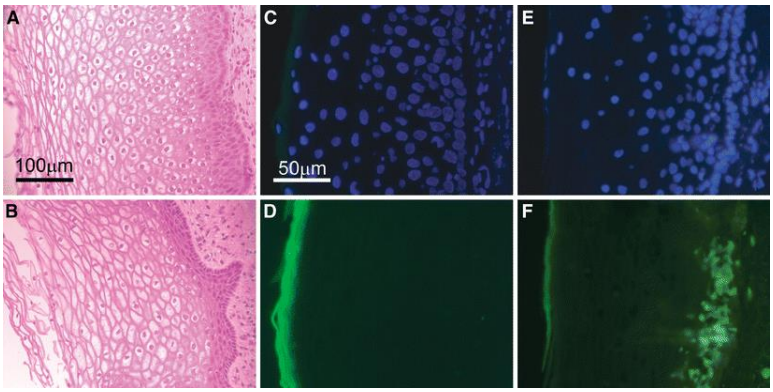

Figure 2.5. Representative hematoxylin & eosin stained microscopy images of ectocervical tissue **(A)** pre-NP exposure and **(B)** post NP exposure *ex vivo*, indicating no apparent morphologic changes. **(C-F)** Representative fluorescent microscopy images of ectocervical tissue with FITC (green) or DAPI (blue) filters at 40× magnification. Ectocervical tissue treated *ex vivo* with unformulated PSC-RANTES-biotin for four hours and stained with **(C)** DAPI (indicating cell nuclei in blue) or **(D)** streptavidin-FITC (indicating PSC-RANTES-biotin in green). Ectocervical tissue treated *ex vivo* with PSC-RANTES-biotin encapsulated nanoparticles for four hours and stained with **(E)** DAPI or **(F)** streptavidin-FITC. Reproduced from (68), Copyright Springer Science + Business Media, LLC 2008, with permission of Springer.

2.2.2. Active targeting

Targeting specific viral or host factors involved in HIV transmission allows increasing the specificity of microbicide constructs or systems towards structures/sites of interest. Such goal can be achieved by directly modifying microbicide molecules or their carriers with targeting moieties (54). Targeting viral envelope glycoproteins can be seen as an obvious approach, allowing direct binding of microbicide systems to HIV, thus hampering interactions of HIV with immune cells. Additionally, targeting infected cells displaying envelope glycoproteins (*e.g.*, gp120) at their membranes can be sought, although this strategy may only applicable to the early inactivation of pre-infected leukocytes transported in semen or late inhibition of viral amplification at mucosae. This last approach has indeed been mostly explored for therapeutic purposes as described for examples provided in section 2.1. Alternatively, targeting host factors may be considered as more effective due to the substantial variability of HIV structure, namely at the envelope level (69). From a preventive viewpoint, it also seems more suitable to affect the mucosal lining of defense before potential exposure to HIV, namely by providing protective antiretroviral drug levels, rather than trying to block infection after the virus is deposited in the vagina or rectum. Another potential advantage of targeting host factors is to directly compete with the virus for cell membrane receptors used for infection. In the following, different examples of targeted microbicides using either approach are discussed.

2.2.2.1. Targeting viral factors

Targeting viral surface proteins, mostly gp120, has been extensively explored in the microbicides field as a strategy to directly bind and inactivate HIV. One approach involves the development of different nanosystems presenting surface groups capable of establishing low specificity binding with viral particles (22). Even if such systems present intrinsic activity, it is reasonable to consider that similar strategies may be useful for targeting the delivery of other associated microbicide molecules. For example, an early report by Hayakawa *et al*. (70) suggested that concanavalin-A-tethered NPs (mean diameter around 400 nm) could target gp120 with high affinity and efficiently block HIV infectivity, thus presenting the potential to be used as microbicides. Other types of NPs have since been proposed. For instance, Di Gianvincenzo *et al*. (71) proposed gold NPs (mean diameter around 2-3 nm) coated with multiple amphiphilic sulfated ligands to target HIV, particularly at gp120. High affinity towards gp120 was demonstrated by using surface plasmon resonance. Also, NPs were shown to possess substantial anti-HIV activity in neutralization assays in MT-2 cells against a CXCR4-tropic virus. In another study, Lara *et al*. (72) developed silver NPs (mean diameter around 30-50 nm) with polyvinylpyrrolidone (PVP) immobilized at the surface. These researchers showed that the system could inhibit the infection of human cervical explants. Although PVP-modified NPs were able to target gp120 present at the envelope, other mechanisms of action may also be implicated in the overall antiviral activity (73).

The most studied systems in this category, however, have been dendrimers (74). The SPL7013 dendrimer has been in the forefront of the microbicides field, being developed as a gel (VivaGel®, Starpharma, Australia). The fourth generation dendrimer is composed of a benzhydrylamine amide core linked to poly-L-lysine branches capped with anionic naphthalene disulfonate groups, these last being responsible for interacting with gp120 (**Figure 2.6**) (75-77). Despite promising *in vitro* and *in vivo* animal data (78, 79), the development of VivaGel® as a microbicide seems to have been halted due to, among other reasons, safety issues identified in early clinical testing (80, 81). Alternative microbicide dendrimers sharing similar gp120 targeting ability have been proposed, including G2-S16, a second generation carbosilane dendrimer capped with sulfonate groups (82). Promising results were obtained *in vivo* with a vaginal gel containing 3% of G2-S16: 84% protection was observed in humanized mice treated before intravaginal exposure to HIV, contrasting with no protection in the placebo gel group (83).

Viral gp41 may be regarded as another possibility for allowing direct targeting to HIV, although nearly any data is available. Steric hindrance caused by associated gp120, leading to reduced accessibility to gp41 at the viral surface, may be an important hurdle to circumvent in order to allow proper targeting. Still, various potential targeting moiety candidates can be identified and selected for such purpose (84-86). For instance, Wickline *et al*. (87) acknowledged the possibility of modifying perfluorocarbon-based nanoemulsions with either antibodies or aptamers targeting gp41 in a 2011 patent, although no details on the proposed

systems or biological outcomes were provided. These researchers have been engaged on the development of such nanoemulsions as carriers of melittin, a peptide component of bee venom capable of reducing the infectivity of HIV by direct envelope shedding (88).

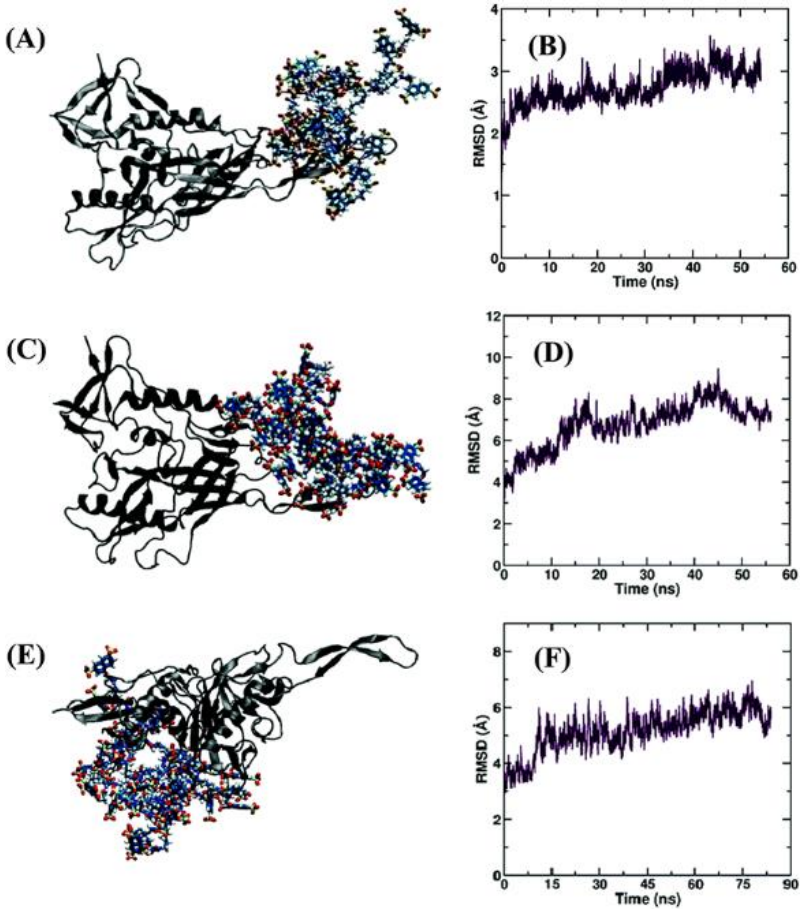

Figure 2.6. Binding of SPL7013 dendrimer to gp120 alone. Snapshots of the gp120-SPL7013 complexes predicted by ZDOCK (an automated protein docking server) as **(A)** rank 8 and **(C)** rank 1, after equilibration using molecular dynamics simulations (gp120 is in grey). **(B, D)** The corresponding root mean square deviations (RMSD) of the complex with respect to their initial configurations. **(E)** A snapshot of the Patchdock (another automated protein docking server) structure with the dendrimer blocking the CD4 binding site. **(F)** RMSD of the complex shown in (E) with respect to its initial configuration. Reproduced from (75), with permission of The Royal Society of Chemistry (Copyright 2015).

2.2.2.2. Targeting host factors

Mimicking HIV in its ability to infect particular host cells is the most popular approach for achieving targeted delivery of microbicide compounds. Expression of both CD4 and at least one of two chemokine co-receptors, CCR5 and CXCR4, is a generic hallmark of most HIV-susceptible cells. These have been the main membrane receptors explored for targeted microbicides, despite the fact that possible interference with their normal immune functions

may raise some concerns, particularly in the case of CD4 (89). One example of the use of the CD4 receptor has been detailed by Wheeler and co-workers (90). These researchers used a previously developed anti-CD4 aptamer (91) and conjugated it to different siRNAs. Resultant chimeras were designed to target CD4 via aptamer recognition and deliver siRNAs for silencing host (*CCR5*) or viral (*gag* and *vif*) genes. The macromolecular constructs were efficiently and selectively taken up by primary $CD4^+$ T cells and monocyte-derived macrophages, as well as specifically by $CD4^+$ T cells when added to a mixed PBMC population. Internalization results correlated well with the specific knockdown of CCR5 in both T cells and macrophages when using chimeras containing anti-CCR5 siRNA, with expression levels being reduced to around 10% of those for chimeras featuring scrambled siRNA sequences or the anti-CD4 aptamer alone. Furthermore, inhibition of post-infection HIV replication *in vitro* was observed for conjugates comprising either a mixture of siRNAs against *gag* and *vif* or siRNA against *CCR5*. The aptamer alone also showed inhibitory activity against the virus, albeit with less efficiency than the conjugate, thus suggesting that CD4 targeting leads to competitive blockage of the receptor (90). Moreover, pre-treatment with chimeras against *CCR5*, both *gag* and *vif*, or all three genes allowed inhibition of HIV infection in polarized human cervicovaginal explants and a humanized mouse model (90, 92). Even when incorporated in a gel vehicle, anti-*CCR5* chimeras fully prevented transmission in these mice following viral challenge up to around four days post intravaginal administration (92). In another work, Yang *et al*. (93) attempted to selectively deliver saquinavir, a protease inhibitor, to $CD4^+$ cells by conjugating an anti-CD4 antibody to the surface of PLGA NP carriers (mean diameter around 200-300 nm). Although targeting ability was not clearly demonstrated, intracellular drug levels in $CD4^+$ Sup-T1 T cells incubated with saquinavir-loaded targeted NPs were mildly increased (up to two fold) as compared to non-targeted NPs. Moreover, no differences were observed for targeted and non-targeted NPs in $CD4^-$ VK2/E6E7 vaginal epithelial cells.

The crucial role of CCR5 or CXCR4 in the ensuing viral fusion makes these chemokine receptors potential targets for prevention. CCR5, in particular, appears to be an optimal candidate for targeting due to its involvement in most new HIV infections (94). Moreover, interference with its function does not seem to be associated with immunological disturbances (95), while impairment of normal CCR5 function, such as in the case of naturally occurring homozygous *CCR5Δ32* variants, leads to increased resistance to HIV infection (96). These advantageous features have indeed stimulated the development of numerous therapeutic drugs and microbicide candidates that directly compete with the virus for its co-receptor (25, 26). Such array of compounds provides scientists interested in developing targeted microbicides with multiple options for targeting CCR5. An interesting approach is the one recently reported by Zhou *et al*. (97), in which various anti-CCR5 aptamers were developed and conjugated to siRNA against *TNPO3* coding for transportin-3, a cellular factor that facilitates the transport of HIV pre-integration complex into the nucleus. Although the possibility of using these constructs in the development of topical microbicides was not the

main goal of this work, application to prevention was proposed. Specific cell targeting was successfully demonstrated for selected aptamer-siRNA conjugates in $CCR5^+$ cells (CEM-NKr-CCR5 cells and PBMCs) when compared to siRNA alone, as shown in **Figure 2.7**, while no differences were observed in cells negative for CCR5 (parental CEM-NKr cells). Specific gene silencing was further shown for chimeras, contrasting with the results for non-targeted conjugates in the absence of transfection reagents, as well as prevention of infection of PBMCs *in vitro* (97). Contrasting with CCR5, CXCR4 seems to be of less importance for sexual transmission of HIV and this reason alone may justify that no microbicide system targeting such receptor is under development. However, the possibility has been explored for developing CXCR4-targeted drug nanocarriers with other applications, namely for cancer therapy (98, 99).

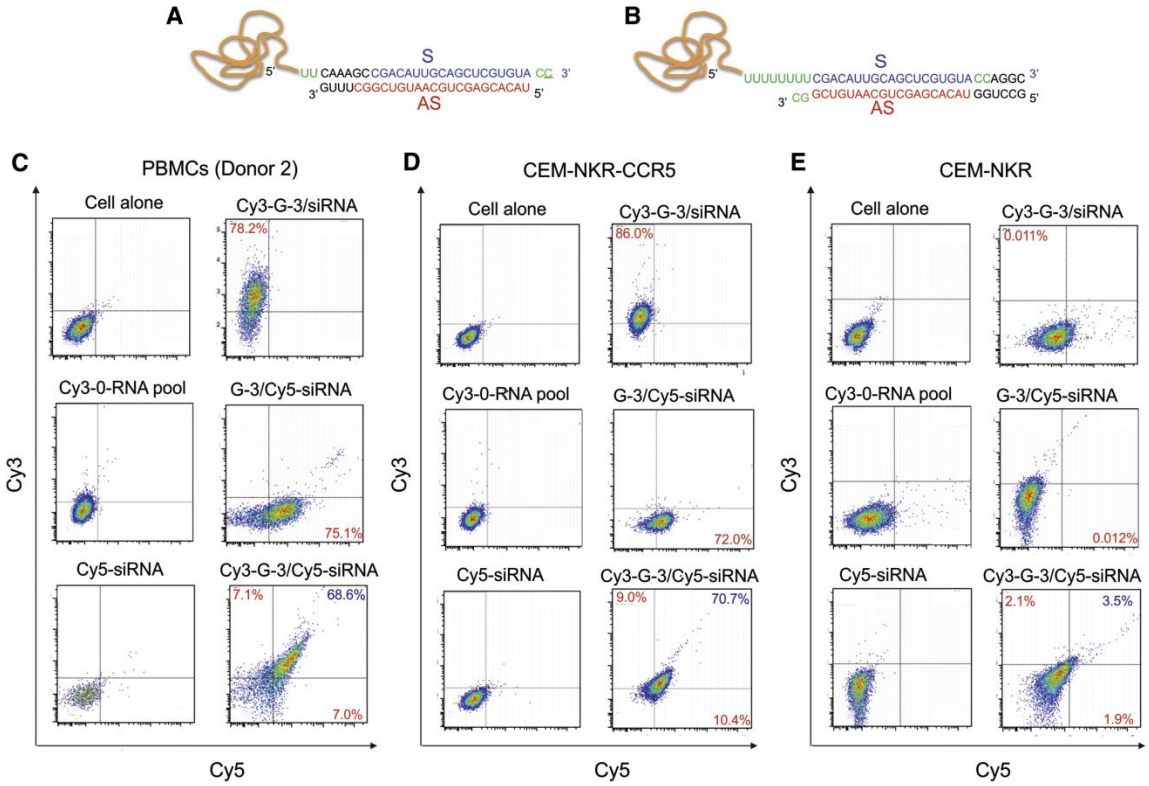

Figure 2.7. The design and binding affinity of aptamer-siRNA chimeras. **(A, B)** Schematic of CCR5 aptamer-siRNA chimeras. The region of the aptamer is responsible for binding to CCR5, and the siRNA is targeting the *TNPO3* gene. A linker (2 or 8 U) between the aptamer and siRNA is indicated in green. Two versions, **(A)** G-3-TNPO3 OVH chimera and **(B)** G-3-TNPO3 Blunt chimera, were designed. **(C-E)** Cell surface binding of fluorescent dye-labeled RNAs was assessed by flow cytometry. The Cy3-labeled 0-RNA pool and Cy5-labeled siRNA were used as a negative control. The G-3-TNPO3 OVH chimera was chosen for a binding affinity test with **(C)** PBMC-$CD4^+$ cells, **(D)** CEM-NKr-CCR5 positive cells, and **(E)** CEM negative cells. The aptamer-sense strand and antisense strand of the chimera were labeled by the Cy3 and Cy5 dyes, respectively. They were then annealed to form the aptamer-siRNA chimera. Modified from (97), Copyright (2015), with permission from Elsevier.

Apart from the major targets discussed above, other immune cell-specific receptors have further been explored in the development of anti-HIV microbicide systems, including DC-SIGN, lymphocyte function-associated antigen 1 (LFA-1) and human leukocyte antigen-antigen D related (HLA-DR). Targeting DCs through DC-SIGN seems to be a promising approach for preventing mucosal HIV transmission due to the early role of such cells in the infection cascade, namely in mediating cell-cell transmission and transport of the virus to lymph nodes (49). Again, most of the work exploring DC-SIGN as a target has been conducted with systems bearing intrinsic antiviral activity rather than serving as carriers. Interesting examples are the ones from Martínez-Ávila *et al*. (100, 101) on gold NPs coated with different oligomannosides mimicking carbohydrate structures of gp120; Garcia-Vallejo *et al*. (102) on poly(amidoamine) (PAMAM) glycodendrimers carrying various Lewis-type antigens; and Berzi *et al*. (103) and Varga *et al*. (104) on a polyvalent glycodendrimer carrying six units of a glycosidic DC-SIGN ligand (polyman 19). All systems exhibited high affinity for DC-SIGN and were able to reduce viral infection to different extents in cell-based assays and/or human cervical tissue explants. Another interesting immune cell surface molecule for targeting purposes is LFA-1. This integrin has been shown to participate in the transmission of HIV between T cells through the establishment of virological synapses (105). Thus, targeting LFA-1 may have the dual benefit of specific delivery of active compounds and direct inhibition of cell-mediated viral infection. For instance, Kim and co-workers (106) developed hyaluronan-coated liposomes functionalized with a conformation-insensitive antibody to LFA-1, which can target both activated and naïve T cells. The nanosystem (approximately 100 nm mean diameter) was used for the intracellular delivery of associated siRNA targeting either *CD4* or *CCR5*. *In vitro* data indicated that functionalized liposomes were able to deliver their payload to LFA-1^{+} human leukocytes, allowing silencing of CD4 with high efficiency, contrasting with the poor results for non-targeted liposomes. Although not tested *in vivo* for preventing sexual transmission of HIV, systemic administration of targeted liposomes containing anti-*CCR5* siRNA to a humanized mouse model allowed prolonged gene silencing and provided protection from subsequent HIV intraperitoneal challenge (106). These interesting results seem to indicate that such systems could be useful for topical PrEP, although safety issues related with immunogenicity and possible interference with LFA-1 function may arise. Another possible target for microbicide development is HLA-DR, which has been reported as one of the most predominant host-derived cell membrane receptor being incorporated into the viral envelope upon release from the cell (107). Its presence facilitates further infection through the interaction with CD4 of other susceptible cells. In this particular case, targeting both host cells and HIV may be possible, as previously described for immunoliposomes (108, 109). Within the specific scope of microbicides, an interesting approach has been recently proposed by Gu *et al*. (110) using PEG-modified PLGA/polyethylenimine NPs (mean diameter around 200 nm) functionalized with an anti-HLA-DR antibody for siRNA delivery. The synaptosome-associated 23-kDa protein (SNAP-23) was selected for silencing due to its involvement in the exocytosis of secretory

vesicles and correct virus particle production. NPs were further incorporated into a thin biodegradable polymeric film intended for suitable vaginal administration. *In vitro* data reported by these researchers demonstrated enhanced uptake of targeted NPs in HLA-DR$^+$ mKG-1 DCs as compared to non-targeted counterparts, while no differences were observed in vaginal epithelial VK2/E6E7 cells (negative for HLA-DR). Moreover, targeted NPs appeared to be quickly released from the film, penetrate an epithelial cell monolayer and maintain the ability to selectively target DCs (around 3-times higher uptake than for non-targeted NPs) as assessed in a cell-based co-culture model (**Figure 2.8**). *SNAP-23* gene knockdown was also efficiently achieved, being significantly higher for targeted NPs (110). The proposed nanosystem revealed to be a promising platform for preventing vaginal HIV transmission, although further testing is required, namely regarding *in vivo* performance.

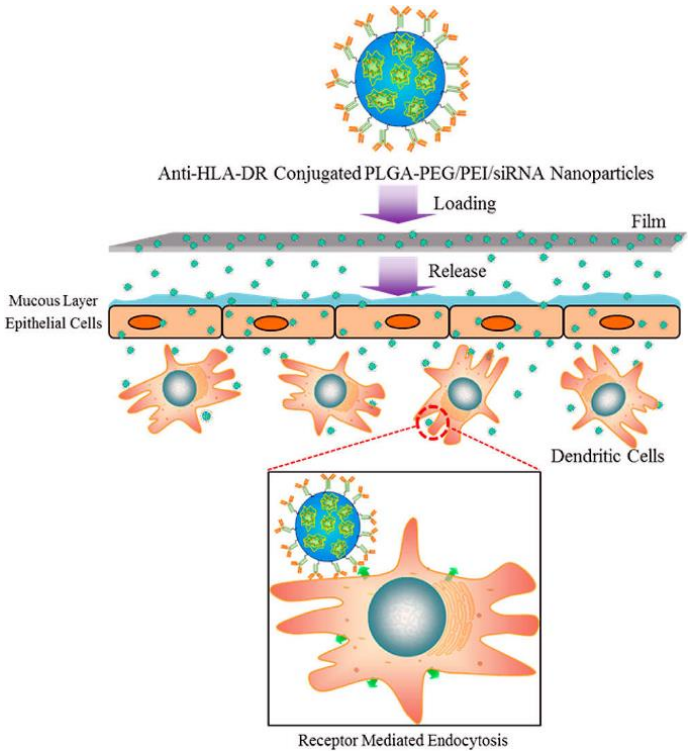

Figure 2.8. Schematic representation of targeted NPs formulated into a biodegradable film for targeting siRNA delivery into HLA-DR$^+$ DCs using a co-culture cell model. Targeted NPs are homogeneously dispersed in a biodegradable film and, upon administration, the film is expected to disintegrate within the vaginal lumen allowing NPs to penetrate across the vaginal mucosa and deliver siRNA in a targeted manner to HLA-DR$^+$ mKG-1 dendritic cells. Reprinted from (110), Copyright (2015) American Chemical Society.

2.3. Future perspectives for targeted microbicides

Recent years have seen an increasing interest in the development of topical PrEP strategies using microbicides. Building on the relative success of large-scale clinical trials

testing products such as the dapivirine ring, different advanced solutions have further been proposed and are currently under active development. In particular, systems that are able to target important assets for HIV transmission may allow enhancing the amount of active compounds at specific cells, tissues or structures relevant to HIV transmission through the vaginal and/or rectal routes, thus potentially increasing efficacy while reducing adverse effects. This literature review discussed potential targets for such purposes and explored several examples of targeted systems engineered as potential microbicide candidates. Despite significant efforts and advances so far, the field of targeted microbicides is still in its infancy and many uncertainties and questions need to be addressed. Several targets presented herein have been little explored, while some promising targeted systems require further assessment in order to confirm and/or optimize their usefulness. In particular, specific engineering of microbicide molecular constructs and drug carriers intended for vaginal or rectal delivery may be more complex than simply transposing strategies that have been shown useful for other purposes or even different routes of administration. The singular features of such mucosal environments must be considered in order to successfully develop effective systems. Also, safety issues may arise when host cell membrane molecules playing relevant immune roles are selected for targeting. Other more general but highly pertinent issues to microbicide development that also need to be considered include: (i) the selection of suitable delivery platforms for targeted microbicide candidates – films (111) appear to be interesting choices for vaginal administration of nanosystems, while no clear option seems optimal for rectal use (112) –; (ii) selection and scaling-up of manufacturing processes for both intermediates and final formulations; and (iii) affordability of the final products that are mostly needed in settings characterized by poor economic resources, namely in sub-Saharan Africa.

CHAPTER 3

Materials and Methods

3.1. Materials, reagents and cell lines

PLGA-COOH (Purasorb PDLG 5004A; 50:50 lactide:glycolide molar ratio; inherent viscosity midpoint of 0.4 dl/g. corresponding to approximately 44 kDa in molecular weight (Mw)) was kindly provided by Corbion (Amsterdam, The Netherlands). Monodisperse amine PEG Carboxyl (H_2N-PEG-COOH, HCl salt, Mw 7.5 kDa) was purchased from JenKem Technology USA (Plano, TX, USA). Poly(ethylene glycol) methyl ether-block-poly(lactide-*co*-glycolide) (PLGA-PEG; 50:50 lactide:glycolide molar ratio; PLGA number average molecular weight (Mn) 55 kDa; PEG Mn 5 kDa) was purchased from Sigma Aldrich (St. Louis, MO, USA) and carboxylic acid endcap PLGA-PEG (PLGA-PEG-COOH, 50:50 lactide:glycolide molar ratio; PLGA Mw ~40 kDa; PEG Mw ~5 kDa) from PolySciTech (West Lafayette, IN, USA). D-Ala-Peptide T-Amide (DAPTA; D-Ala-Ser-Thr-Thr-Thr-Asn-Tyr-Thr-NH_2) was acquired from Tocris Bioscience (Bristol, UK).

Ethyl ether, methanol, acetone and dimethyl sulfoxide (DMSO) were purchased from Merck Millipore (Billerica, MA, USA). Dichoromethane (DCM) was acquired from Riedel-de Haën (Seelze, Germany) and chloroform from Panreac AppliChem (Darmstadt, Germany). 1-ethyl-3-(3-dimethylaminopropyl)-carbodiimide (EDC), *N*-hydroxysuccinimide (NHS), *N*-hydroxysulfosuccinimide (Sulfo-NHS), *N*,*N*-diisopropylethylamine (DIPEA), 2-(*N*-morpholino) ethanesulfonic acid (MES), deuterated DMSO (Dimethyl Sulfoxide-*d6*), glycine and coumarin 6 (C6) were purchased from Sigma Aldrich. All solvents and reagents were of analytical grade or equivalent.

GHOST (3) $CCR5^+$ cells (Hi-5 cells; CCR5-expressing cells originated from human osteosarcoma) available from the NIH Aids Reagent Program (113) were kindly provided by Prof. Nuno Taveira, iMed.ULisboa, University of Lisbon. Human cervical HeLa cells were purchased from the American Type Culture Collection (ATCC, Manassas, VA, USA) (114). Dulbecco's Modified Eagle medium (DMEM) was acquired from Lonza (Basel, Switzerland);

fetal bovine serum (FBS), penicillin-streptomycin and trypsin-EDTA from Invitrogen (Carlsbad, CA, USA). Triton™ X-100 was purchased from SPI-Chem (West Chester, PA, USA) and Versene™ from Thermo Fisher Scientific (Waltham, MA, USA). 3-(4,5-dimethylthiazol-2-yl)-2,5-diphenyltetrazolium bromide (MTT) and paraformaldehyde (PFA) were purchased from Sigma Aldrich. Sodium azide was acquired from Panreac AppliChem. The allophycocyanin (APC)-labelled anti-CCR5 antibody (CD195 (CCR5) Monoclonal Antibody (NP-6G4), APC, eBioscience™) was obtained from Labclinics (Barcelona, Spain).

3.2. Synthesis of PLGA-PEG-COOH copolymer

3.2.1. Synthesis reaction

The PLGA-PEG-COOH copolymer was synthesized through carbodiimide/NHS-mediated conjugation of PLGA-COOH to H_2N-PEG-COOH (115), by adapting methods previously reported by Langer, Farokhzad and collaborators (116, 117). Briefly, PLGA-COOH (880 mg, 0.02 mmol) was activated to PLGA-NHS in DCM, in the presence of excess EDC (19.2 mg, 0.1 mmol) and NHS (11.5 mg, 0.1 mmol) under stirring for 2h. PLGA-NHS was then precipitated with ice-cold ethyl ether:methanol (1:1) and collected by centrifugation at 2,700×*g* (Eppendorf 5810R Refrigerated Centrifuge). The polymer was re-dissolved in DCM and the precipitation process repeated twice as described, in order to remove residual EDC and NHS. After drying under vacuum, PLGA-NHS (440 mg, 0.01 mmol) and H_2N-PEG-COOH (112.5 mg, 0.015 mmol) were dissolved in 10 mL of chloroform. *N*,*N*-diisopropylethylamine (DIPEA) (15.5 mg, 0.15 mmol) was added to the mixture, which was left under stirring for 24h. The resulting polymer was precipitated with ethyl ether:methanol (1:1) at -80 ˚C and was either left at -80 ºC for 1-2h or at -20 ºC for a 2-3 days, to enhance the recovery of the polymer. PLGA-PEG-COOH was then collected by centrifugation at 2,700×*g*, re-dissolved in chloroform and the precipitation process repeated twice in order to remove non-conjugated H_2N-PEG-COOH. Finally, the co-polymer was dried under vacuum, characterized and used for the production of NPs without further treatment. A schematic representation of the reaction described herein is presented in **Figure 3.1**.

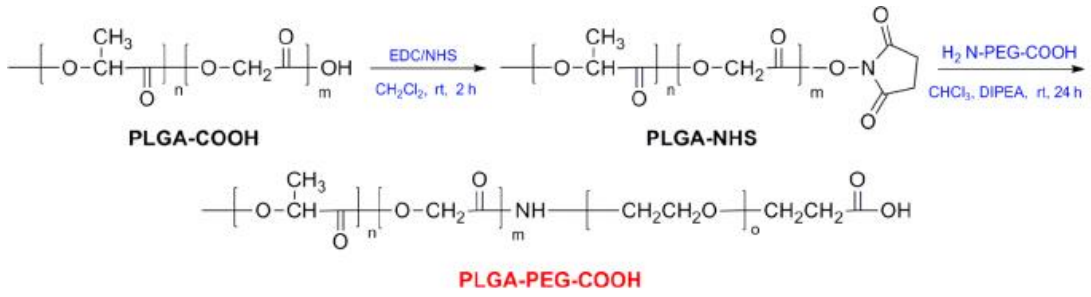

Figure 3.1. Synthesis of the PLGA-PEG-COOH copolymer, using standard carbodiimide/NHS-mediated chemistry. Adapted with permission from (29), Copyright 2013 American Chemical Society.

In order to improve the precipitation method for the recovery of the PLGA-PEG-COOH copolymer, several preliminary experiments were performed using commercially available PLGA-PEG from Sigma Aldrich. Tested solvents included ethyl ether and methanol, either alone or mixed in different proportions. A small amount of polymer was dissolved in chloroform and then recovered by addition to different solvent systems dropwise at -80 ºC. Mixtures were left at -80 ºC for 1-2h and afterwards centrifuged at 13,000 rpm (Labnet Spectrafuge 16M – Labnet, Edison, NJ, USA). Then, the supernatants were removed, the polymer was dried under vacuum and weighted for mass yield calculation.

3.2.2. Polymer characterization

3.2.2.1. Matrix Assisted Laser Desorption Ionization – Time of Flight Mass Spectrometry

Matrix Assisted Laser Desorption Ionization - Time of Flight Mass Spectrometry (MALDI-TOF MS) analysis of polymers was performed in an ultrafleXtreme mass spectrometer (Bruker, Bremen, Germany), controlled by the *Compass for flexSeries 1.4* software. Both reflector and linear modes were used, with laser powers set to 70% and 95%, respectively. The mass ranges were 0.2-3.5 kDa for the reflector mode and 2-210 kDa for the linear mode. For sample preparation, three milligrams of each polymer were dissolved in acetonitrile. Equal volumes of sample and *trans*-2-[3-(4-*tert*-Butylphenyl)-2-methyl-2-propenylidene] malononitrile (DCTB) (Bruker) matrix solution were pre-mixed. One microliter of each mixture was applied to a ground steel target (Bruker). One thousand shots were accumulated per run.

3.2.2.2. Fourier Transform Infrared Spectroscopy

Attenuated Total Reflection Fourier Transform Infrared Spectroscopy (ATR-FTIR) spectra of polymers were generated by using an ABB MB3000 FTIR spectrometer from ABB (Zurich, Switzerland) equipped with a MIRacle single reflection attenuated total reflectance (ATR) accessory from PIKE Technologies (Madison, WI, USA). All spectra were collected by performing 256 scans in the region of 4000-600 cm^{-1} at a resolution of 4 cm^{-1}. Commercial polymers used in synthesis reactions (used as controls) were dissolved and precipitated in the same manner as synthesized ones prior to the analysis.

3.2.2.3. Proton Nuclear Magnetic Resonance

Proton Nuclear Magnetic Resonance (^1H NMR) analysis of the polymers was performed using an Avance III spectrometer from Bruker operating at 400 MHz (9.4 Tesla). Three

milligrams of each sample were dissolved in 600 µL of deuterated DMSO and placed on appropriate NMR quartz tubes. Analyses were performed at room temperature and chemical shift values were expressed in δ (ppm), relative to tetramethylsilane (TMS), which was used as internal reference. An estimated PEG "bonding" efficiency was determined by comparing the areas of PLGA and PEG peaks, normalized by the 5.2 ppm PLGA peak. Peak areas were determined using *Mnova* software (Mestrelab Research, Santiago de Compostela, Spain) and the PEG "bonding" efficiency was estimated through Equation 1 (118, 119).

$$PEG\ "bonding"\ efficiency\ (\%) = \frac{Peak\ area_{3.6\ ppm}/4}{(Peak\ area_{5.2\ ppm} + Peak\ area_{4.8\ ppm} + Peak\ area_{1.4\ ppm})/6} \times 100 \qquad (1)$$

3.3. Production, functionalization and characterization of nanoparticles

3.3.1. Nanoparticle production

PLGA-PEG NPs were produced by nanoprecipitation as depicted in **Figure 3.2** (120). Batches of 20 mg total polymer were produced, containing 90% (w/w) of PLGA-PEG (55 kDa - 5 kDa, from Sigma Aldrich) and 10% of PLGA-PEG-COOH, either commercially available (40 kDa – 5 kDa, from PolySciTech) or synthesized (44 kDa – 7.5 kDa) as described above. Briefly, the polymers were dissolved in a 1 mL mixture of acetone and DMSO (1:1) and the solution was injected slowly into 10 mL of ultrapure water under magnetic stirring (200 rpm) using a 200 µL pipette. The NP dispersion was left under stirring for 2h in order to allow partial evaporation of organic solvents. NPs were then concentrated and washed thrice with 10 mL of ultrapure water by centrifugation at 2,100 rpm for 12 min (Eppendorf 5810R Refrigerated Centrifuge) using Amicon Ultra-15 Centrifugal Filter Units (Millipore) with a molecular weight cut-off (MWCO) of 100 kDa. The volume of NP suspensions was adjusted to 1-2 mL with ultrapure water. Fluorescent NPs (30 mg batches) were similarly obtained by incorporating C6 (1 mg/mg of polymers) in the organic phase before the addition to the aqueous phase.

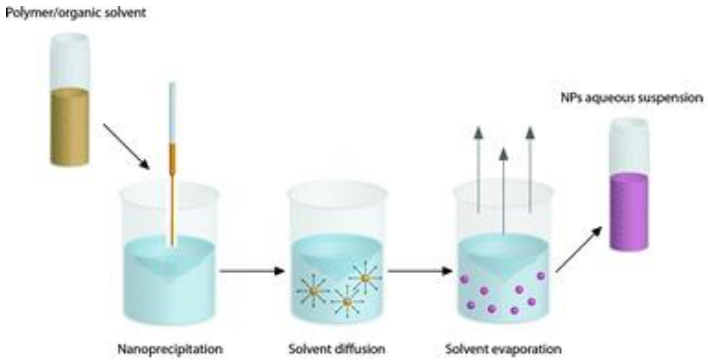

Figure 3.2. Schematic representation of the general nanoprecipitation technique for the production of polymeric NPs. The polymer(s) is/are dissolved in a water-miscible organic solvent and injected into the

aqueous phase. The rapid diffusion of the solvent within the water leads to the precipitation of the polymers in the form of NPs, followed by partial or total evaporation of the solvent. Adapted from (120), with permission of The Royal Society of Chemistry (Copyright 2013).

3.3.2. Nanoparticles functionalization

The functionalization of NPs with the DAPTA peptide was attained through carbodiimide-mediated coupling to terminal carboxylic acid groups from PLGA-PEG-COOH, based on previously reported methods (115, 121-124). Briefly, 10 mg of either plain or fluorescent NPs were incubated with 20 mM EDC/Sulfo-NHS in MES buffer (MES 0.1 M, pH 6.0) for 30 min under gentle stirring. The resulting NHS-activated NPs were concentrated and washed thrice with 10 mL of ultrapure water by centrifugation at 2,100 rpm for 12 min using Amicon Filters (Millipore, MWCO 100 kDa). The NPs were then resuspended in phosphate buffered saline (0.1 M, pH 7.4) and incubated with approximately 0.04 mM of DAPTA for 8h under gentle stirring. Finally, the DAPTA-functionalized NPs were concentrated and washed thrice with ultrapure water using Amicon Filters as described and stored at a final volume of 1 mL. Non-functionalized NPs were treated likewise, without the addition of the peptide or EDC/Sulfo-NHS. Control NPs were produced with withdrawal of either EDC/Sulfo-NHS or DAPTA (NHS-activated and DAPTA-adsorbed NPs, respectively). In another control formulation, DAPTA was replaced with 0.04 mM glycine in order to cap reactive NHS-activated groups. Treatments for different tentative functionalization of NPs are summarized in **Table 3.1**, as well as the abbreviated designations used throughout this work.

Table 3.1. Different conditions used during the functionalization protocol of NPs.

Designation	Description	Added reagents		
		EDC/Sulfo-NHS	Glycine	DAPTA
NPs	Non-functionalized plain NPs	No	No	No
DAPTA-f-NPs	DAPTA-functionalized plain NPs	Yes	No	Yes
C6-NPs	Non-functionalized fluorescent NPs	No	No	No
C6-NHS-NPs	NHS-activated fluorescent NPs	Yes	No	No
C6-gly-NPs	Glycine-capped fluorescent NPs	Yes	Yes	No
C6-DAPTA-a-NPs	DAPTA-adsorbed fluorescent NPs	No	No	Yes
C6-DAPTA-f-NPs	DAPTA-functionalized fluorescent NPs	Yes	No	Yes

3.3.3. Nanoparticles characterization

Size (mean hydrodynamic diameter) and polydispersity index (PdI) of all NP formulations were determined by Dynamic Light Scattering (DLS) using a Zetasizer Nano ZS instrument (Malvern Instruments, Malvern, UK). The same equipment was used for assessing surface

charge (zeta potential) of NPs by Electrophoretic Light Scattering (ELS). All assays were performed after 100× dilution of NP dispersions with 10 mM sodium chloride solution. Three runs were performed per sample.

The morphology of plain NPs was characterized by Transmission Electron Microscopy (TEM) using a JEOL JEM 1400 Transmission Electron Microscope (JEOL, Tokyo, Japan). Images were recorded using a SC 1100 ORIUS CCD camera (Gatan, Warrendale, PA, USA). NPs were diluted ten times in ultrapure water and 10 µL of each NP suspension were dropped onto a 300-mesh nickel grid. Samples were stained with lanthanum acetate after removal of the excess of suspension with filter paper and the same was done before TEM analysis. The processing of TEM images was performed using ImageJ software (125). It comprised a background subtraction, which consisted on subtracting a fixed pixel intensity (below the intensity of all particles images), using "Math Subtract" function and also "Subtract Background" function (with a rolling ball radius of 150 pixels, above particles size). In some cases, a bandpass filter procedure was applied, using a Fast Fourier Transform. When all the background was black (zero intensity), the "Find Connected Regions" plug-in was used to mark the particles and to uniform their intensity. Then, a "Threshold" was applied to the resulting image, so that all particles detected were delimited. The particles were analyzed excluding those on edges and controlling circularity (between 0.3 and 1). The area of each particle allowed an estimation of its size. The resulting histograms were fitted to Gaussian distributions.

In order to assess the effectiveness of the functionalization of NPs, functionalized and non-functionalized NPs were analyzed through MALDI-TOF MS, ATR-FTIR and ^{1}H NMR, as described above. For MALDI-TOF MS and ATR-FTIR analysis, 10 mg of lyophilized NPs were used, while for ^{1}H NMR the water content was evaporated in a fume hood at room temperature. ^{1}H NMR analyses were performed using an Avance III HD spectrometer from Bruker operating at 600 MHz (14.1 Tesla). DAPTA alone (500 µg for ATR-FTIR and 100 µg for ^{1}H NMR) and commercial precursor polymers were also analyzed as controls.

3.4. Cell culture and maintenance

Ghost Hi-5 cells (passages 7-25) and HeLa cells (passages 73-74) were maintained in DMEM supplemented with 10% (v/v) fetal bovine serum and added with 100 U/mL penicillin and 100 µg/mL streptomycin (further referred as complete DMEM). Cells were kept in a cell culture incubator (Binder, Tuttlingen, Germany) at 37 °C and 5% CO_2, under a water saturated atmosphere. Cells were sub-cultured every 3-4 days, using trypsin–EDTA as dissociation reagent.

3.5. *In vitro* cell studies

3.5.1. Cytotoxicity of DAPTA and nanoparticle formulations

The cytotoxic potential of DAPTA and NP formulations in Ghost Hi-5 cells (passages 22-23) was assessed by measuring the metabolic activity using the MTT reduction assay. For that, cells were seeded on 96-well plates at a density of 10^4 cells/well in 200 µL of complete DMEM. After 24h of incubation, the medium was removed and the cells were washed twice with 200 µL of PBS. Cells were then treated with different concentrations of DAPTA and NPs in complete DMEM. Treatments with medium only and 2% (v/v) Triton™ X-100 were used as positive and negative controls, respectively. All conditions were tested in triplicate. After incubation for 24h, cells were washed twice with 200 µL of PBS and treated with 200 µL of MTT solution (0.5 mg/mL in complete DMEM). After 4h incubation, the MTT solution was removed and the formazan crystals, resulting from the reduction of MTT by viable cells, were solubilized using 200 µL of DMSO. The plates were placed in an orbital shaker at 100 rpm for 15 min in the dark at room temperature. Finally, the absorbance at 570 nm and 630 nm (used for subtraction of unspecific absorption) was measured using a Synergy Mx microplate reader (BioTek, Winooski, VT, USA). After subtracting background reading (*i.e.*, absorbance values at 570 nm of wells without any initial cells), viability was determined according to Equation 2.

$$Cell\ Viability\ (\%) = \frac{Final\ absorbance\ value\ of\ sample}{Final\ absorbance\ value\ of\ positive\ control} \times 100 \quad (2)$$

3.5.2. CCR5 expression assay

To confirm the expression of the CCR5 receptor on the surface of Ghost Hi-5 cells, a preliminary fluorescence-activated cell sorting (FACS) study, using an APC-labelled anti-CCR5 antibody, was performed. Ghost Hi-5 cells at passages 9 and 20 were evaluated, while HeLa cells (passage 73) were used as a negative control. The cells were detached from cell culture flasks using trypsin-EDTA and around 10^6 cells in complete DMEM were placed in 1.5 mL Eppendorf tubes. The cells were then centrifuged at 4 °C, 300×*g*, for 7 min (Eppendorf 5417R Refrigerated Centrifuge), the supernatants were removed, and cells were resuspended in 100 µL of FACS buffer (PBS containing 10% (v/v) FBS and 0.1% (w/v) sodium azide). Five microliters (0.25 µg) of the APC-labelled anti-CCR5 antibody were added to selected tubes and all samples were incubated for 1h at 37 °C. Then, cells were washed by centrifugation (300×*g*, 4°C, 7 min), resuspended in 200 µL of PBS and transferred to FACS tubes. The samples were immediately analyzed by FACS using a BD FACSCanto II instrument (BD Biosciences, San Jose, CA, USA), equipped with three lasers: 405 nm, 488 nm and 633 nm. Upon excitation with the 633 nm laser, stained cells were detected through the APC channel. The results were analyzed using the *FlowJo v10.0.7* software (FlowJo LLC, Ashland, OR, USA).

3.5.3. Nanoparticle uptake studies

The association of fluorescent NPs to Ghost Hi-5 cells was evaluated by FACS. Cells were seeded on 24-well plates at a density of 5×10^4 cells/well in 500 µL of complete DMEM. After 24h of incubation, the medium was removed and the cells were washed twice with 500 µL of PBS. Then, cells were treated with the NPs at 0.01% (w/v) in 500 µL of DMEM without supplements and incubated for 15 min, 30 min, 1h or 2h. After incubation, the NP suspensions were removed, the cells were washed twice with 500 µL of PBS and treated with 250 µL of Versene™ for detaching from the plate. After incubation for 20 min, the cells were collected into 1.5 mL Eppendorf tubes. This process was repeated once more, then 1 mL of complete DMEM was added to each tube and cells were immediately placed on ice. Cells were then centrifuged at 4 °C, 300×*g*, for 7 min. The supernatants were removed, the cells were resuspended in 200 µL of FACS buffer and transferred to FACS tubes. The samples were analyzed in the BD FACSCanto II instrument, with excitation by the 488 nm laser and detection at the FITC channel. The results were analyzed using *FlowJo v10.0.7*.

3.6. Statistical analysis

All experiments were performed in triplicate, unless otherwise stated. Results are presented as mean values ± standard deviation (SD). Statistical analyses were performed using one-away analysis of variance (ANOVA) in order to compare multiple groups, unless otherwise stated. Differences between groups were assessed using Tukey's honestly significant different *post hoc* test. Differences were considered significant at $p<0.05$. Statistical significance was denoted if the p value was lower than 0.05 by * ($p<0.05$), ** ($p<0.01$) and *** ($p<0.001$). All analyses were performed with the *GraphPad Prism 5.0* software.

CHAPTER 4

Results and Discussion

4.1. Synthesis and characterization of PLGA-PEG-COOH copolymer

The synthesis of the PLGA-PEG-COOH copolymer from PLGA-COOH and H_2N-PEG-COOH was performed *via* carbodiimide chemistry using 1-ethyl-3-(3-dimethylaminopropyl)-carbodiimide (EDC)/*N*-hydroxysuccinimide (NHS), a process that has been widely applied to obtain this type of polymer conjugates (29, 116-118, 122, 123, 126-129). A schematic of the reaction is presented in **Figure 4.1**. Carbodiimides mediate the coupling between carboxylates and amines through the formation of amide bonds (amidation). They react with carboxylic acids to form reactive *o*-acylisourea intermediates that promptly react with primary amines, thus forming amide bonds (115). Among several carbodiimide molecules that can be used to promote this type of amidation reactions, EDC has been one of the most commonly used crosslinking agent, especially when in conjunction with NHS, or the water-soluble *N*-hydroxysulfosuccinimide (Sulfo-NHS) (115). These last allow the formation of a more stable NHS ester intermediate, as opposed to the hydrolysable *o*-acylisourea intermediate that is formed when EDC is used alone. Therefore, the yield of amide bond formation significantly increases in the presence of NHS or Sulfo-NHS (130). Data on the production and characterization of this PLGA-PEG-COOH copolymer are presented and discussed in the following.

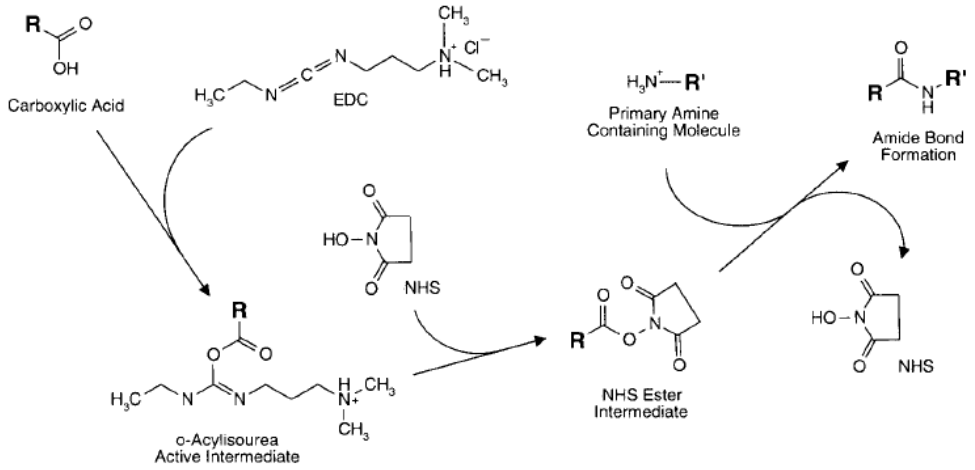

Figure 4.1. General mechanism of the carbodiimide/NHS-mediated coupling reaction. The efficiency of an EDC-mediated reaction may be increased through the formation of a NHS ester intermediate. The NHS ester is more effective at reacting with amine-containing molecules. Thus, higher yields of amide bond formation may be realized using this two-step process as opposed to using a single-step EDC reaction. Adapted from (115), Copyright (2008), with permission from Elsevier.

4.1.1. Copolymer formation and recovery

4.1.1.1. Activation of PLGA-COOH to PLGA-NHS

The activation of PLGA-COOH to PLGA-NHS was performed in DCM, initially using a five-times molar excess of EDC/NHS relative to PLGA-COOH (117). Nevertheless, due to persistent difficulties in obtaining the final PLGA-PEG copolymer, PLGA-NHS polymers synthesized with 10- and 20-times excess of EDC/NHS were also procured for the following procedures. The mass recovery for PLGA-COOH of each reaction is listed in **Table 4.1**.

Table 4.1. Mass recovery for the activation of PLGA-COOH to PLGA-NHS.

Excess EDC/NHS	Recovery
5-times (first batch)	99.7%
5-times (second batch)	86.2%
10-times	88.2%
20-times	86.4%

All reactions presented high mass recovery values as the activated polymer precipitated readily in ethyl ether/methanol, especially when added dropwise and very slowly to the solution. A resting period of around 12 hours at -20 ˚C was necessary for near complete precipitation when addition to the non-solvent system was performed rapidly. The

vacuum-dried polymer had a white vitreous aspect, being then used for the following conjugation with H_2N-PEG-COOH.

4.1.1.2. Production of PLGA-PEG-COOH

The conjugation reaction between PLGA-NHS and H_2N-PEG-COOH was performed using an 1.5-times molar excess of H_2N-PEG-COOH relative to PLGA-NHS (117). The main issue identified during the process was related to the difficulty in selecting an adequate non-solvent system that would allow extensive precipitation of the final product of the conjugation reaction. Several solvents or solvent mixtures have been reported for both the reaction and precipitation steps (29, 116-118, 122, 123, 126, 127) and this information guided the selection approach. In particular, reported reactions were mainly performed in either DCM or chloroform, and precipitation was conducted using ethyl ether, methanol or their mixture (1:1). Therefore, two separate reactions were performed, either in chloroform or DCM, each mixture being then divided in three portions, which were precipitated with either ethyl ether, methanol or ethyl ether:methanol (1:1). The polymer/solvent/non-solvent mixture was further placed at -80 ˚C for 1-2 hours in order to further reduce the solubility of the polymer. The solvent/non-solvent systems used and polymer recovery for each reaction are presented in **Table 4.2.**

Table 4.2. Solvents used and mass recovery for the production of PLGA-PEG-COOH.

Reaction Solvent	Precipitating Agent	Recovery
DCM	Methanol	0%
	Ethyl ether:methanol (1:1)	5.8%
	Ethyl ether	88.1%
Chloroform	Methanol	0%
	Ethyl ether:methanol (1:1)	17.5%
	Ethyl ether	68.4%

When precipitation was attempted with methanol, either from reactions in DCM or chloroform, the solutions looked clear even after centrifugation or rest at -80 ºC or -20 ºC for 2-3 days, with no polymer being recovered. In the case of ethyl ether, the polymer was able to partially precipitate immediately, forming a cloudy dispersion. Storage for one hour at -80 ˚C seemed to increase precipitation and the polymer was then able to sediment well after centrifugation. This behavior was maintained throughout the remaining precipitation and centrifugation steps needed for washing, allowing the recovery of a substantial mass of white vitreous polymer after drying under vacuum, both for reactions occurring in either

chloroform or DCM (68.4% and 88.1% mass yields, respectively). In the case of ethyl ether:methanol (1:1), the polymer did not precipitate immediately but still some turbidity was detected upon addition to the non-solvent mixture. In this case, storage at -80 ºC was crucial for copolymer precipitation and was more evident in the chloroform case. In this last instance, a solid deposit was formed, which was then easily collected upon centrifugation. This behavior was kept throughout the remaining washing steps; however the pellets obtained were less compact and the solvent mixture had to be carefully removed to avoid disturbing the pellet. It was possible to recover around 25 mg of polymer for the chloroform case (17.5% mass recovery). Regarding the DCM case, it was necessary to store the suspension at -20 ˚C for 2-3 days for precipitation to occur since no differences were observed after 2-3 hours at -80 ˚C. After the first centrifugation and decantation, around 2h at -80 ˚C were enough to obtain a loose pellet, which can be explained by the absence of DCM that would otherwise counterpoint precipitation. However, only around 10 mg of polymer were obtained after drying (5.8% mass recovery). As all the removed supernatants had a cloudy aspect, both for ether only and ether:methanol precipitations, they were also stored at -20 ˚C for 2-3 days. It was possible to gradually recover a few milligrams of polymer from these supernatants.

Considering the results described above, ethyl ether alone seemed to be best alternative for the precipitation step of the complete process for polymer preparation, especially when using DCM as the reaction solvent. However, as PEG is not soluble in ethyl ether and was in excess, it is possible that this polymer might still be present in the final recovered product (23). Conversely, the use of methanol allows free PEG removal as it is considered a good solvent for this polymer (131, 132). Ethyl ether, in turn, helps to precipitate the PLGA-PEG-COOH copolymer, since it is a poor solvent for PLGA, often used to precipitate this polymer, as well as for PEG (23, 133). However, precipitation with ethyl ether:methanol had low mass yields, with practical experience indicating that possibly a significant amount of polymer was being lost in the supernatants.

The above mentioned problems, alongside the possibility that copolymer formation may have not occurred in large extension, motivated the performance of additional precipitation experiments using commercially available PLGA-PEG (55 kDa – 5 kDa) obtained from Sigma Aldrich. Furthermore, the possibility of reducing the amount of methanol in the non-solvent mixture was considered, as it could still allow the removal of PEG and presumably promote better precipitation (128, 129). Therefore, precipitation in ethyl ether:methanol (4:1) was also performed. Sequential addition of equal amounts of plain ethyl ether and plain methanol was also evaluated. Each experiment, except for ethyl ether alone, was performed twice. In all cases, 8 mg of copolymer was dissolved in 130 µL of chloroform and added to the different non-solvent systems (600 µL). In an attempt to further reduce the copolymer solubility, the precipitating solutions were pre-cooled to -80 ˚C, while proper care was taken in order to assure that the temperature was kept around such value upon addition of the copolymer.

After resting at -80 ˚C for one hour, a pellet was formed after centrifugation in all cases, though it was apparently more compact for the case of ethyl ether used alone. After removing the supernatants and drying under vacuum, the mass recovered for each precipitation procedure was assessed and these values are presented in **Table 4.3**.

Table 4.3. Solvents used and mass recovered for the precipitation experiments. Different values for recovered PLGA-PEG using the same precipitating agent indicate different replicas.

Reaction Solvent	Precipitating Agent	PLGA-PEG amount	Recovered PLGA-PEG	Mass Yield
Chloroform	Ethyl ether	8 mg	8.1 mg	~100%
	Ethyl ether:methanol (4:1)		5.3 mg	66.0%
			6.1 mg	71.6%
	Ethyl ether:methanol (1:1)		6.0 mg	74.5%
			4.4 mg	55.0%
	Ethyl ether, followed by addition of methanol		5.6 mg	70.5%
			5.5 mg	68.1%
	Methanol		4.3 mg	53.8%
			6.1 mg	76.5%

With the exception of precipitation with ether alone, all other precipitation methods led to a significant loss of PLGA-PEG, which is in agreement with the experiments performed in-house for obtaining PLGA-PEG-COOH. However, the mass yields obtained herein were significantly higher than those of the conjugation protocol, which may indicate that copolymer formation was not indeed complete. Nevertheless, cooling the non-solvent systems down to -80 ˚C prior and during the precipitation step could also have contributed to this increase in recovery. Since some replicas presented dissimilar results, no particular precipitation method could be selected as definitive. However, it was apparent that further testing could help optimizing the recovery process but was not conducted due to time constraints.

Due to the problems identified during recovery of the polymers and attempts to optimize this step, the products obtained in the initial reactions were not in sufficient amount to proceed with subsequent production of NPs. Thus, a new batch was produced, now using 10-times excess of PLGA-NHS. Ethyl ether:methanol (1:1) was kept as precipitating agent, mainly to assure proper washing of unreacted H_2N-PEG-COOH. The ethyl ether:methanol mixture was kept at -80 ˚C prior and during the precipitation procedure. Chloroform was selected as reaction solvent as it seemed to have yielded better results for the ethyl ether:methanol case. These changes did not seem to substantially affect the whole process, with the polymer precipitating only partially and with some polymer still being recoverable

from the washing supernatants. Indeed, a relatively large and compact pellet could be recovered from these last after storage at -20 ˚C for a week. Overall, around 126 mg of copolymer were able to be recovered with a mass recovery of 24.4%. This product was further used in subsequent experiments.

Although the yield of the procedure was still low and substantial margin for improvement seems obvious, some guidance can be inferred from performed experiments that can be useful for future work. Importantly, storage in a cold environment seems to be crucial for improving precipitation, with -80 ˚C appearing to work better than -20 ˚C. One possible alternative for increasing the reaction yield could be the replacement of EDC by dicyclohexyl carbodiimide (DCC) or diisopropyl carbodiimide (DIC), water-insoluble carbodiimide molecules commonly used in organic synthesis applications (115). As this reaction is performed in an organic solvent, such reagents would be suitable and perhaps could yield better results. Regarding the reaction solvents used, it has been described that coupling with EDC should be carried out in solvents with a low dielectric constant, as is the case of DCM (ε=8.93) and chloroform (ε=4.81) (134). However, other solvents with higher dielectric constants that would presumably have lesser impact during precipitation with non-solvents could be useful. An important point to be optimized regards, as already mentioned, the ratio between ethyl ether and methanol. In this case, introducing experimental designs for response surface methodology could be of value.

4.1.2. Polymer characterization

MALDI-TOF MS, FTIR and ^{1}H NMR were used to verify the chemical structure of the PLGA-PEG-COOH products obtained using the above mentioned conditions and confirm the success and extension of the amidation reaction. Precursors used in the reaction, namely PLGA-NHS, PLGA-COOH and H_2N-PEG-COOH, alone or in physical mixture, were also tested for comparison purposes.

4.1.2.1. MALDI-TOF Mass Spectrometry

Mass spectrometry (MS) allows the determination of the Mw of a given compound, upon its ionization into charged molecules and determination of their mass to charge ratio (m/z) (135). MALDI-TOF MS, in particular, requires co-crystallization of the analyte with an organic matrix, being then desorbed and ionized with a laser beam (135). It allows the determination of Mw values in the range of 0.1 kDa to 100 kDa (136), being therefore suitable for determination of the molecular weight of the polymers considered in this work. The expectable average Mw of each sample (as inferred from data provided from suppliers) is

shown in **Table 4.4**, while representative MALDI-TOF spectra for each polymer type are presented in **Figure 4.2.**

Table 4.4. Expectable average Mw values for the polymer samples analyzed using MALDI-TOF MS.

Sample	Average Mw
PLGA-COOH	~44 kDa
H_2N-PEG-COOH	~7.5 kDa
PLGA-NHS	~44.1 kDa
PLGA-PEG-COOH	~51.5 kDa

Given the expectable Mw values, a MALDI-TOF analysis in the range of 20-100 kDa should be suitable for detection of polymers containing PLGA, while PEG could be detected in the 2-20 kDa range. However, it was not possible to detect any peaks in the 20-100 kDa range for any of the samples tested. Only peaks in low Mw regions (0-2 kDa and 2-20 kDa) could be detected for PLGA-COOH and PLGA-NHS samples (**Figure 4.2A** and **Figure 4.2C**). In the case of PEG, only a slight raise of intensity could be detected in the 2-20 kDa range, while in the PLGA-PEG-COOH samples only a broad band centered around 7.8 kDa could be detected, roughly confirming the presence of PEG (**Figure 4.2B** and **Figure 4.2D**). These results indicated that PLGA polymers may have been degraded by the action of the laser beam. PLGA contains degradable ester bonds and it has been demonstrated that its degradability can be accelerated upon laser irradiation, depending on the laser wavelength (137). Thus, this technique was not helpful to assess on the success of the reaction, requiring further experimental optimization in order to minimize PLGA degradation.

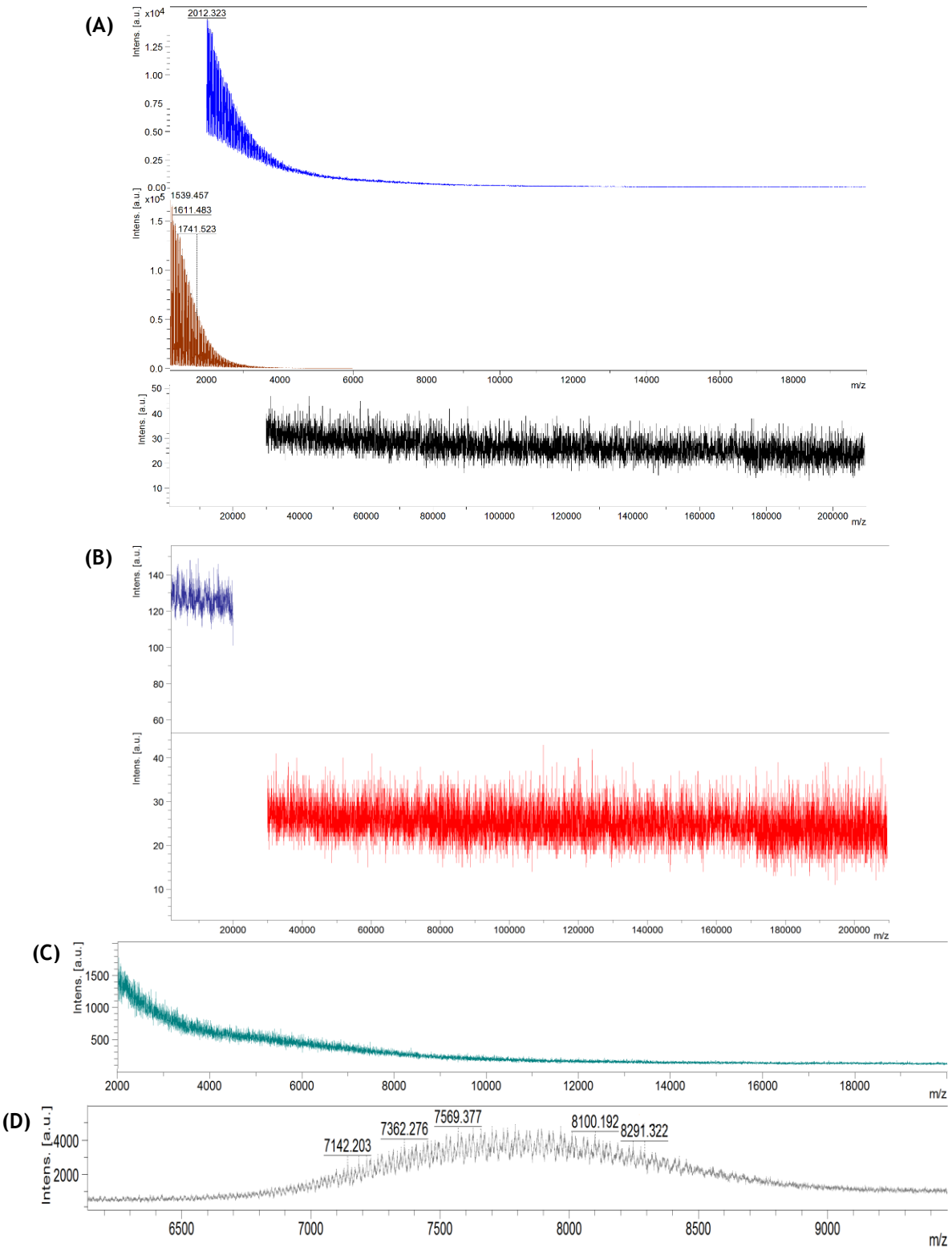

Figure 4.2. MALDI-TOF spectra of **(A)** PLGA-COOH (0-2 kDa, 2-20 kDa and 30-210 kDa), **(B)** H_2N-PEG-COOH (2-20 kDa and 30-210 kDa), **(C)** PLGA-NHS (2-20 kDa) and **(D)** synthesized PLGA-PEG-COOH (6-10 kDa).

4.1.2.2. Fourier Transform Infrared Spectroscopy

The infrared (IR) spectrum of a sample can provide information about what functional groups are present through the detection of absorption bands that are due to vibrations of specific chemical bonds. In FTIR, Fourier transforms are used to enhance the spectral resolution over a wider spectral range (138). In the scope of this work, FTIR could be useful to confirm the presence of typical PLGA and PEG functional groups in the newly formed PLGA-PEG-COOH. Moreover, the formation of an amide bond, due to the carbodiimide-mediated amidation reaction, could presumably be detected by FTIR, as the amide bond presents two characteristic absorption bands: the amide I, at the region of 1,600-1,700 cm^{-1}, due to vibrations of C=O bond; and the amide II, in the region of 1,500-1,600 cm^{-1}, caused by the vibrations of both the C-N and N-H bonds (139).

The FTIR spectra obtained and normalized at the absorption maximum for each sample tested are represented in **Figure 4.3**. The precursor polymers PLGA-COOH and H_2N-PEG-COOH were previously dissolved, precipitated and dried in a similar manner as the synthesized copolymer. The same procedure was used for the physical mixture of PLGA-COOH and H_2N-PEG-COOH (maintaining the molar proportions used in the reaction). This last mixture served as a negative control for the amidation reaction. A representative spectrum of PLGA-NHS samples is also presented, as well as three PLGA-PEG-COOH samples: "PLGA-PEG-COOH (DCM)" and "PLGA-PEG-COOH (chloroform 1)" designate the polymers obtained from the first amidation reactions using ethyl ether:methanol (1:1) as precipitating agent; "PLGA-PEG-COOH (chloroform 2)" designates the polymer obtained in higher amount, from the last reaction performed using the same precipitating agent.

The analysis of the spectrum of PLGA-COOH reveals a band in the region of 2,850-3,000 cm^{-1} attributed to the C-H stretching of CH_2 and CH_3 groups (asymmetric stretch H-C-H at *ca.* 2,926 cm^{-1} and symmetric stretch at around 2853 cm^{-1}), $\upsilon(CH_2 + CH_3)$, and a strong main peak around 1,750 cm^{-1} corresponding to the stretch of the carbonyl group, υ(C=O) (140). A set of peaks in the region 1,350-1,480 cm^{-1} indicate the bending frequency of the C-H single bond, $\delta(CH_2+CH)$ and $\delta(CH_3)$. Another small peak at *ca.* 1,250 cm^{-1} is due to the twisting of CH_2 group out-of-plane, $\tau(CH_2)$. A set of strong peaks in the region 1,000-1,200 cm^{-1} are related with C-O bonds: the stretching of =C-O at 1,170 cm^{-1}, υ(=C-O); the stretching of C-O-C moiety at 1,090 cm^{-1}, υ(C-O-C); and the one of –C-O at around 1,050 cm^{-1}, υ(-C-O) (140). The small peaks around 2,400 cm^{-1} may be due to the signal of environmental carbon dioxide.

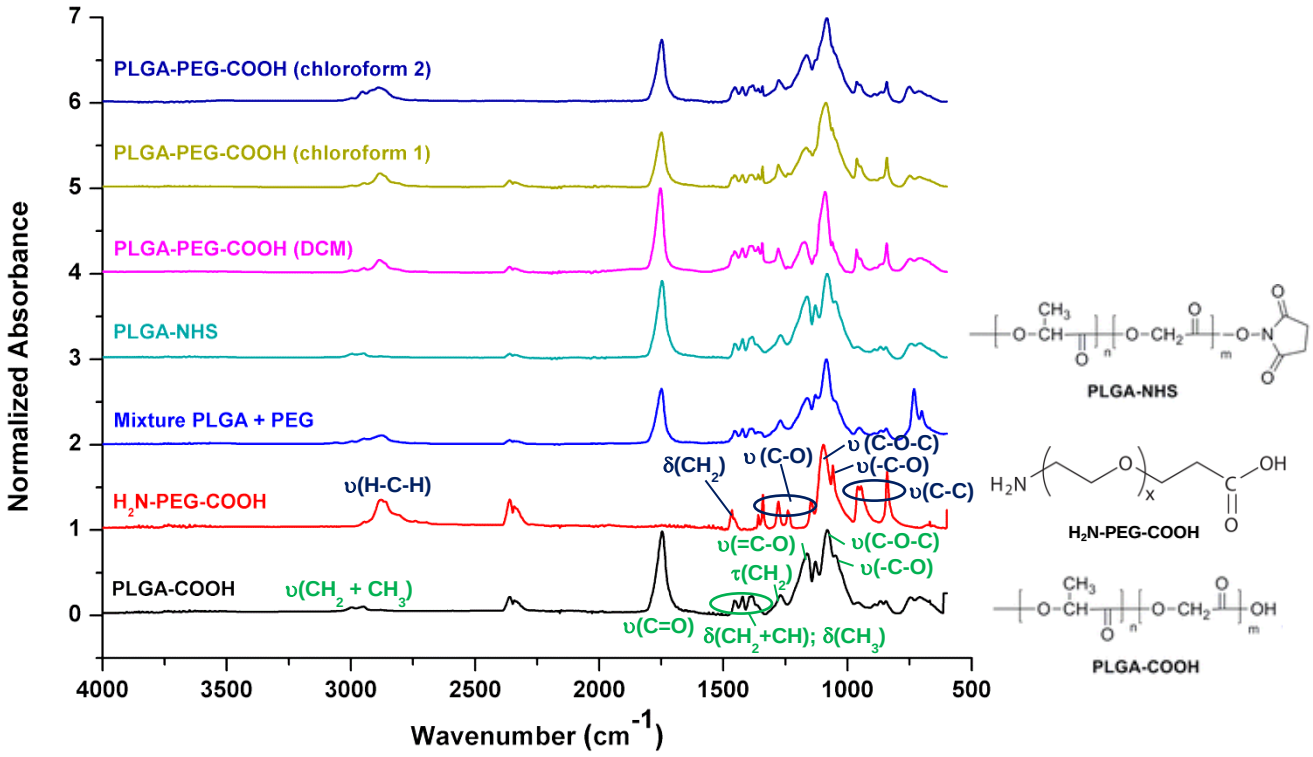

Figure 4.3. Representative FTIR spectra of PLGA-COOH, H_2N-PEG-COOH, PLGA-COOH/H_2N-PEG-COOH physical mixture (mixture PLGA + PEG), PLGA-NHS and PLGA-PEG-COOH samples. PLGA-COOH characteristic vibration modes are shown in green, while H_2N-PEG-COOH vibrations are shown in dark blue. Chemical structures of PLGA-COOH, H_2N-PEG-COOH and PLGA-NHS are also included for convenient analysis of the correspondence between band/peak and chemical bonds.

The same vibration frequencies related to the stretching modes of C-O were observed in the spectrum of PEG, as well as the band around 2,850 cm^{-1} corresponding to the C-H symmetrical stretching vibrations (141). The band at 1,470 cm^{-1} is due to in-plane scissoring of CH_2 group, while those in the region 1,000-1,320 cm^{-1} can be attributed to C-O vibrations (as observed for PLGA). The sharp bands at lower frequencies, 960 and 843 cm^{-1}, are attributed to C-C skeletal stretching vibrations (142).

The IR spectrum of PLGA-NHS is similar to that of PLGA-COOH, as expected, since the amount of NHS groups compared to the extension of the polymer (estimated 0.26% w/w) is too low to allow its detection. The spectra of the mixture PLGA+PEG and of the three PLGA-PEG-COOH samples do not clearly emphasize the presence of PEG, despite some differences, mainly in the region 800-1,300 cm^{-1}, relatively to the IR spectrum of PLGA. The additional band around 750 cm^{-1} in PLGA-PEG-COOH spectra can be attributed to solvent residues (DCM or chloroform), as this frequency is characteristic of the C-Cl stretching vibration (139).

In order to attempt to detect the presence of amide moieties, a magnification of the previous spectra was made in the region of 1,400-1,900 cm^{-1} (**Figure 4.4**), but no IR characteristics of amide moieties (1,600-1,700 cm^{-1} and 1,500-1,600 cm^{-1}) were apparent.

This may be due to the low content of amide moieties compared to the extension of the polymer (estimated 0.08% w/w), as already pointed out in the case of PLGA-NHS.

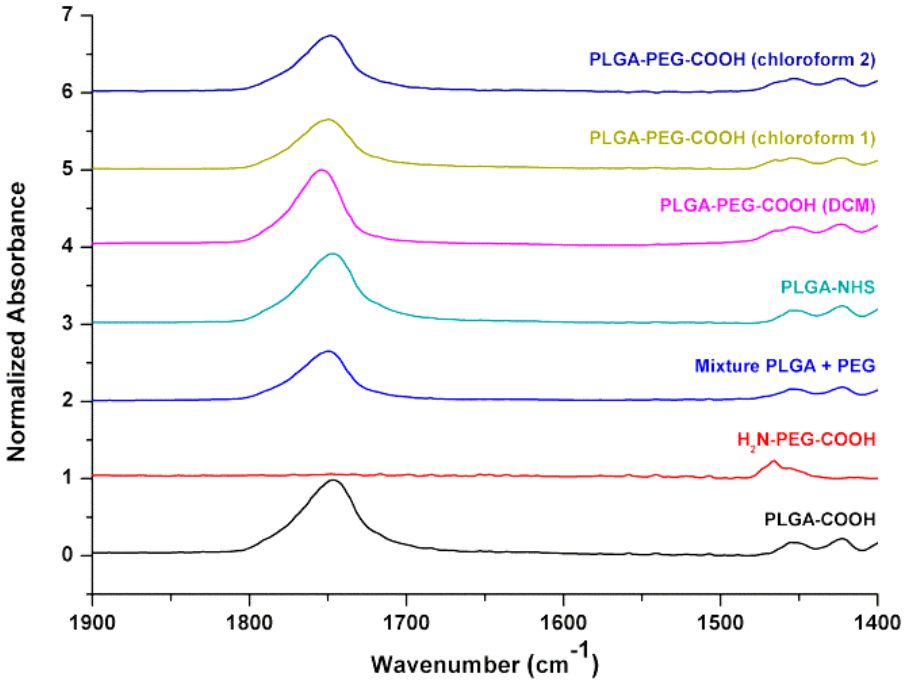

Figure 4.4. Magnification of the FTIR spectra previously presented in Figure 4.3 for polymer samples in the 1,400-1,900 cm^{-1} region.

In order to further confirm the presence of PEG in the samples tested, as well as to attempt to detect the amide bands, the normalized IR spectrum of PLGA-COOH was subtracted from the spectra of all the samples that supposedly contained both PLGA and PEG (also normalized at the peak at 1,750 cm^{-1}). The results are shown in **Figure 4.5**, evidencing several bands typical of PEG in the spectra resulting from the subtraction of PLGA IR identity. In fact, the main features of the several subtracted spectra resemble roughly the PEG IR signature, especially in the PLGA-PEG-COOH samples. However, no amide bands could be detected. Therefore, the presence of an amide bond between PLGA and PEG could not be confirmed by FTIR.

Nevertheless, as the intensity of the IR bands that result from the subtraction is expected to be proportional to the ratio between PLGA and PEG amounts, if no conjugation had occurred, the washing procedure with ethyl ether/methanol would likely have removed, at least partially, the unlinked PEG, leaving the sample mostly with PLGA. In that case, a significant decrease of the intensity of PEG bands would be expected in comparison with the PLGA+PEG mixture, which was precipitated with ethyl ether only. This possibility was not supported by data in **Figure 4.5**, thus possibly indicating that the conjugation was successful. Additionally, different peak shapes are observable for the mixture as compared with PLGA-PEG-COOH samples. However, further studies would be required to confirm such hypothesis.

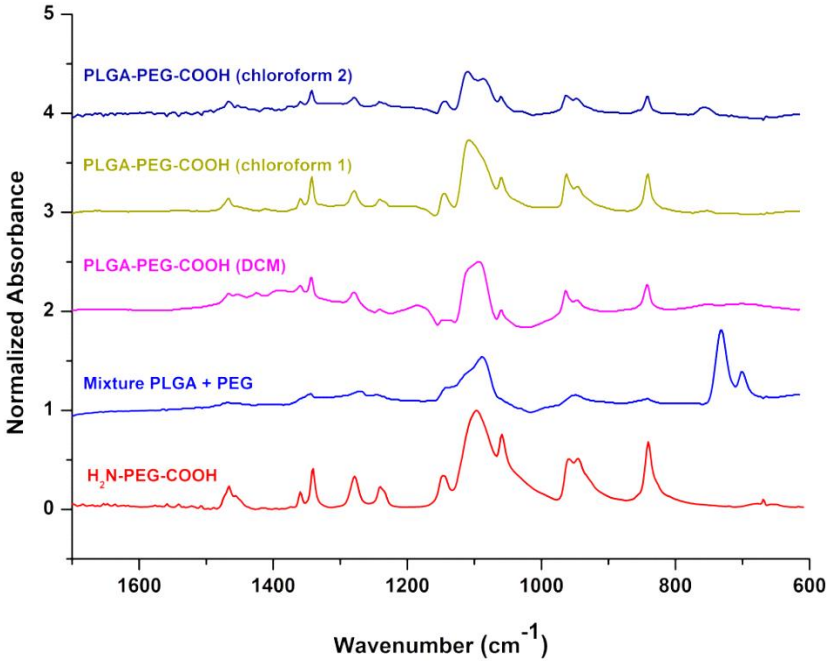

Figure 4.5. Representative FTIR spectra previously presented in Figure 4.3 after subtraction of normalized PLGA-COOH spectrum.

4.1.2.3. Nuclear Magnetic Resonance

Analyzes using ^{1}H NMR were performed to further assess the success and efficiency of the formation of the PLGA-PEG-COOH copolymer. NMR is a technique based on the interaction of active nuclei, such as ^{1}H and ^{13}C, with an applied magnetic field, leading to the absorption of electromagnetic radiation at a characteristic frequency. Resonant absorption by nuclear spins will occur only when electromagnetic radiation of a given frequency is applied and matches the energy difference between the nuclear spin levels in a constant magnetic field (143). The intramolecular magnetic field around an atom in a molecule changes this resonance frequency, providing information of its electronic structure, individual functional groups and neighbouring substituents. NMR spectra represent these resonance frequencies relative to a standard (TMS), the chemical shift, expressed in ppm by frequency (143).

For the case of the present work, several possibilities and limitations of ^{1}H NMR analysis may be expected. For example, specific values of PLGA and PEG protons can potentially be detected and, based on the comparison of areas of normalized PLGA and PEG peaks, an estimation of the efficiency of PLGA-PEG bonding may possibly be determined (118, 119). However, the relatively low amount of protons associated with amide groups in PLGA-PEG-COOH could hamper its detection. Such issue could also be true for detecting the presence of NHS-related groups (4 protons comparing with the number of protons related with the PLGA polymer). Moreover, since amide protons are acidic, they may exchange with

the deuterium from protic solvents, like those present in DMSO-*d6*. Since deuterium (^2H) does not show up in ^1H NMR spectra, amide peaks may shrink or disappear during analysis (144).

The ^1H NMR spectra obtained for polymer samples are presented in **Figure 4.6**, highlighting both comparisons to establish bonding of NHS to PLGA-COOH (**Figure 4.6A**) and the formation of amide groups between PLGA-NHS and H_2N-PEG-COOH (**Figure 4.6B**). All spectral data were normalized relatively to the highest peak and calibrated through the DMSO-*d6* peak at 2.5 ppm. All spectra showed a characteristic H_2O peak at 3.3 ppm. Other unlabeled peaks may represent solvent residue, namely ethyl ether (1.1 ppm) and DCM (5.8 ppm) (145).

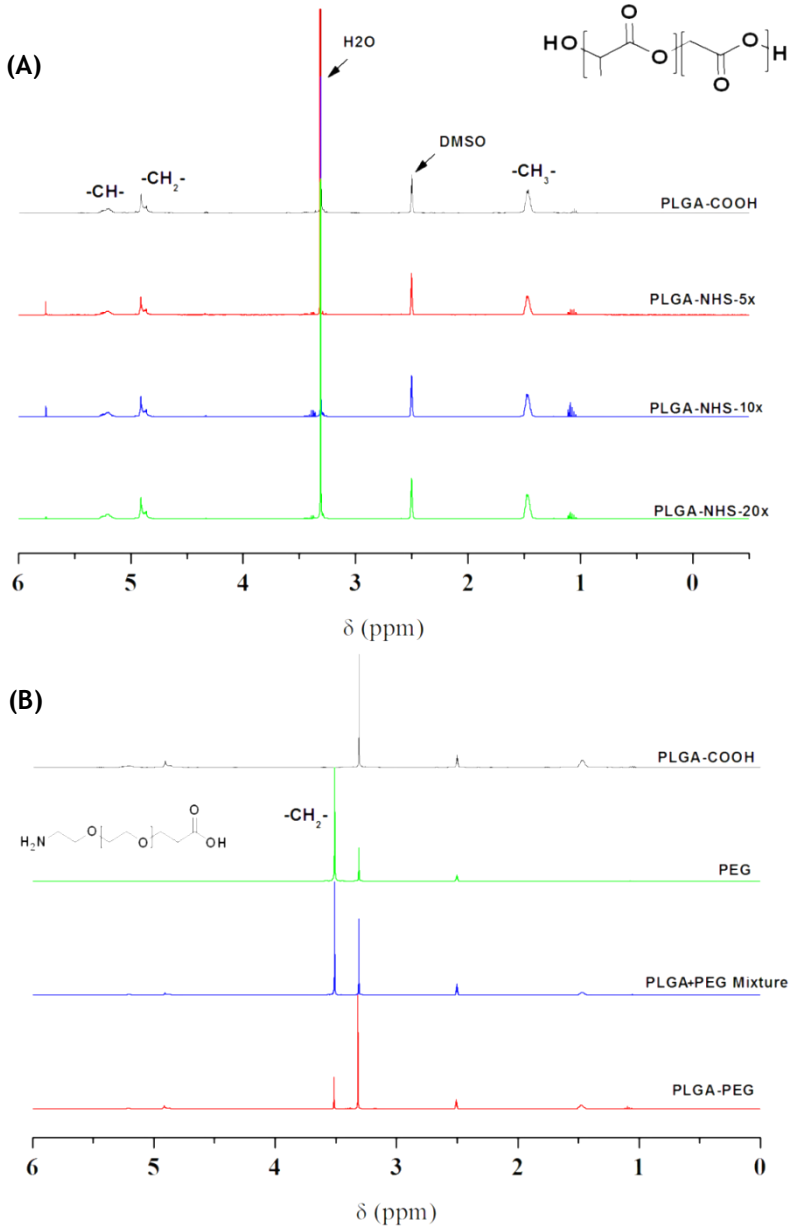

Figure 4.6. Representative ^1H NMR spectra of **(A)** PLGA-COOH and PLGA-NHS (5x, 10x and 20x represent the excess of EDC/NHS used in the activation reaction); **(B)** PLGA-COOH, H_2N-PEG-COOH (denoted "PEG"), their physical mixture and a representative spectrum of PLGA-PEG-COOH samples, in DMSO-*d6* at 400 MHz.

It was possible to observe that all polymers containing PLGA presented typical peaks at 1.4 (3H), 4.8 (2H) and 5.2 ppm (1H), related to the $-CH_3$, $-CH_2$ and -CH protons of the polymer chain, respectively (29). The samples functionalized with NHS did not show any significant difference when compared with the data obtained for the PLGA-COOH sample (**Figure 4.6A**). This may simply have occurred due to the inability of NMR to detect the expectably reduced number of NHS protons. H_2N-PEG-COOH, in turn, presented only one peak at 3.6 ppm (2H), corresponding to $-CH_2-$ protons, which is in accordance with the literature (146). When both PLGA-COOH and H_2N-PEG-COOH were in solution, either mixed or chemically linked, characteristics peaks from both polymers were presented in NMR spectra, thus providing evidence of the presence of both polymers in the final product of the reaction (**Figure 4.6B**). By comparing the normalized areas of PLGA-COOH and H_2N-PEG-COOH peaks, an estimated PEG bonding efficiency was calculated according to Equation 1 presented in Chapter 3 (118, 119). The results for different PLGA-PEG-COOH samples are presented in **Table 4.5.** Bonding efficiency was 66.1% for the first amidation reaction performed ("PLGA-PEG-COOH (chloroform 1)") and 83.0% for the second one ("PLGA-PEG-COOH (chloroform 2)"). Considering that synthetized PLGA-PEG-COOH samples were subject to a washing procedure in contrast with the PLGA+PEG mixture, it would be expectable that the obtained samples would present lower efficiency values as compared to the mixture (60.8%) if no conjugation occurred. Thus, such results appear to indicate that conjugation may have been successful, although not in full extent. Moreover, the absence of amide-related protons in spectra, either due to lack of sensitivity of the technique or actual absence of such chemical groups, leaves the question of effective amide formation opened. Such issue, however, has not been unquestionably addressed so far in the literature pertaining to PLGA-PEG synthesis (29, 116-118, 122, 123, 126-129), including by current manufacturers of this type of copolymer (*e.g.*, Sigma Aldrich, PolySciTech).

Table 4.5. Estimated efficiency of H_2N-PEG-COOH bonding to PLGA-COOH during the synthesis of PLGA-PEG-COOH conjugation reaction, determined by ^1H NMR.

Sample	PEG peak	PLGA peaks			PEG "bonding" efficiency
	3.6 ppm	5.2 ppm	4.8 ppm	1.4 ppm	
PLGA+PEG mixture	2.24	1	1.74	2.79	60.8%
PLGA-PEG-COOH (chloroform 1)	2.57	1	1.79	3.04	66.1%
PLGA-PEG-COOH (chloroform 2)	2.97	1	1.69	2.68	83.0%

Overall, the techniques used to characterize PLGA-PEG-COOH copolymer samples provided worthy indications that at least partial conjugation may have been successful. However,

additional efforts are required in order to fully characterize the products obtained by the proposed methodologies.

4.2. Production, functionalization and characterization of PLGA-PEG nanoparticles

Different types of PLGA-PEG-based NPs, including NPs, DAPTA-f-NPs, C6-NPs, C6-NHS-NPs, C6-gly-NPs, C6-DAPTA-a-NPs and C6-DAPTA-f-NPs (see **Table 3.1** in Chapter 3), were produced by nanoprecipitation (or solvent-displacement technique). This simple yet versatile methodology has been commonly used for obtaining nanocarriers for drug delivery applications, particularly when considering hydrophobic compounds (147). Moreover, experience with nanoprecipitation is extensive at the Nanomedicines & Translational Drug Delivery group at i3S/INEB (65, 148), making it a suitable methodology for the purposes of this work. Furthermore, pre-formed NPs were tentatively modified by covalent bonding of DAPTA to the carboxylic acid of PLGA-PEG-COOH present at the interface in order to provide targeting ability to CCR5 as previously explained. The utilization of a longer PEG-COOH linker (7.5 kDa) than the remaining PEG chains at the surface of NPs (5 kDa, from PLGA-PEG, Sigma Aldrich) was intended to minimize steric hindrance during amide coupling between DAPTA and carboxylic acids from PLGA-PEG-COOH. It could also avoid possible steric hindrance in the interaction of DAPTA with the CCR5 (149, 150). This polymer comprised 10% of the NPs matrix, while PLGA-PEG (Sigma Aldrich) comprised 90%. However, due to the abovementioned difficulties in obtaining the PLGA-PEG-COOH copolymer (44 kDa – 7.5 kDa), a commercial PLGA-PEG-COOH copolymer (40 kDa – 5 kDa, from PolySciTech) was also used for NP production. Data on the characterization of produced PLGA-PEG-based NPs are presented and discussed in the following.

4.2.1. Size and surface charge

All prepared NP formulations were analyzed through DLS and ELS, for the determination of their size (mean hydrodynamic diameter), polydispersity index (PdI) and surface charge (zeta potential). DLS measures particle size through determination of the diffusion coefficient. In fact, what is measured is the diameter of the sphere that diffuses at the same speed as the particle being measured, thus being expressed as the hydrodynamic diameter. In ELS mode, the velocity of a charged particle under an applied electric field is used to measure the charge of the diffuse layer around the particle. This feature is expressed as the zeta potential and provides an indirect measure of the surface charge (151). Size and surface charge obtained for each NP formulation are presented in **Table 4.6.**

Table 4.6. Size, polydispersity index and zeta potential values for NP formulations. Data presented as mean ± SD.

PLGA-PEG-COOH origin	Formulation	n [c]	Hydrodynamic diameter (nm)	PdI	Zeta potential (mV)
None	NPs	1	163.0 ± 0.5	0.06 ± 0.02	-3.0 ± 0.4
Commercial [a]	NPs	4	167 ± 8	0.05 ± 0.01	-5 ± 2
	DAPTA-f-NPs	2	164 ± 5	0.064 ± 0.004	-5.0 ± 0.9
	C6-NPs	4	175 ± 2	0.07 ± 0.02	-5 ± 1
	C6-NHS-NPs	2	176 ± 2	0.06 ± 0.01	-5.2 ± 0.6
	C6-gly-NPs	1	170 ± 2	0.06 ± 0.03	-3.8 ± 0.9
	C6-DAPTA-a-NPs	1	166 ± 3	0.07 ± 0.02	-3.3 ± 0.2
	C6-DAPTA-f-NPs	2	172 ± 1	0.062 ± 0.009	-4.6 ± 0.1
Synthesized [b]	NPs	2	172 ± 2	0.05 ± 0.02	-8.5 ± 0.4
	DAPTA-f-NPs	1	172 ± 1	0.05 ± 0.02	-7.6 ± 0.7
	C6-NPs	3	181 ± 3	0.06 ± 0.01	-7.6 ± 0.3
	C6-NHS-NPs	1	180 ± 1	0.04 ± 0.02	-7.3 ± 0.5
	C6-gly-NPs	1	181 ± 3	0.06 ± 0.02	-9 ± 1
	C6-DAPTA-a-NPs	1	184 ± 4	0.06 ± 0.04	-8 ± 2
	C6-DAPTA-f-NPs	1	183 ± 1	0.05 ± 0.02	-8.7 ± 0.4

[a] PLGA-PEG-COOH 40 kDa – 5 kDa (PolySciTech).
[b] PLGA-PEG-COOH 44 kDa – 7.5 kDa (synthesized).
[c] For n=1, the SD corresponds to the three measurements performed by DLS for a single sample.

All obtained particles had average diameter values between 160 and 180 nm, typically within the size range reported for suitable mucus penetration (around 100-500 nm) (152, 153). Such feature may be important for the tentative use of the nanosystems in microbicide development, namely for reaching HIV-susceptible cells present at the epithelial level. Also, no apparent differences were observed between using commercial and synthetized PLGA-PEG-COOH, indicating that these can potentially be used interchangeably. All NP formulations were considered relatively monodisperse, presenting PdI values below 0.1. As expected, and given the small size of the DAPTA peptide (eight amino acids), no significant differences were detected in size for functionalized and non-functionalized NPs, as well as for control formulations.

Zeta potential values ranging from -9 to –3 mV indicated that NPs presented nearly neutral (or slightly negative) surface charge. Values of zeta potential for NPs within five millivolts from zero (*i.e.*, 0 ± 5 mV) are usually considered as denoting dense PEGylation (154). The presence of carboxylic acid groups, which would be ionized at the pH of sodium chloride 10 mM solution (around 6), may still have contributed to slightly more negative values. As DAPTA would be close to neutrality at the pH of the dispersing medium of NPs, no appreciable differences were expected for zeta potential upon functionalization. The presence of either Sulfo-NHS or glycine also did not influence notably the NPs surface charge. This can be due to the low amounts of the tested surface moieties as compared to the extension of the polymer matrix, particularly the PEG content presumably at the surface of particles. The neutral (or slightly negative) character of the NP formulations may further

point towards low cytotoxic potential, since negative and neutral particles are reported to be generally less toxic than positively charged ones, as related to the decreased ability to interact with and destabilize negatively charged cell membranes (155).

4.2.2. Morphology

Transmission electron microscopy (TEM) images of plain NPs were taken to assess their morphology and possibly confirm the size previous determined by DLS (**Figures 4.7-4.10**). The designations "comm." and "synth." have been assigned, respectively, for NPs containing commercially available PLGA-PEG-COOH from PolySciTech and the synthesized copolymer. NPs generally presented a spherical shape and relatively homogeneous dimensions. A few aggregates were however observed, as well as some smaller particles, which is typical of NPs produced by nanoprecipitation (147).

Figure 4.7 displays TEM images of the NPs comm. (non-functionalized), with different magnifications. The size histogram embedded in TEM images (obtained by image processing with ImageJ software, as described in Chapter 3) allowed the determination of an average diameter of 125 ± 42 nm, roughly in accordance with DLS data. Differences between diverse techniques, such as the ones used, have been widely described (156). Possible explanations to larger values in the case of DLS might be related to the overestimation caused by possible particle aggregates (counted as single particles) and/or shrinkage of NPs upon drying during sample processing for TEM or due to the vacuum atmosphere inside the electron microscope. Moreover, the determination of the hydrodynamic radius is based on the evaluation of the diffusion coefficient and assumes perfectly spherical particles (not the case as shown by TEM imaging), typically leading to larger values than the effective particle diameter (157).

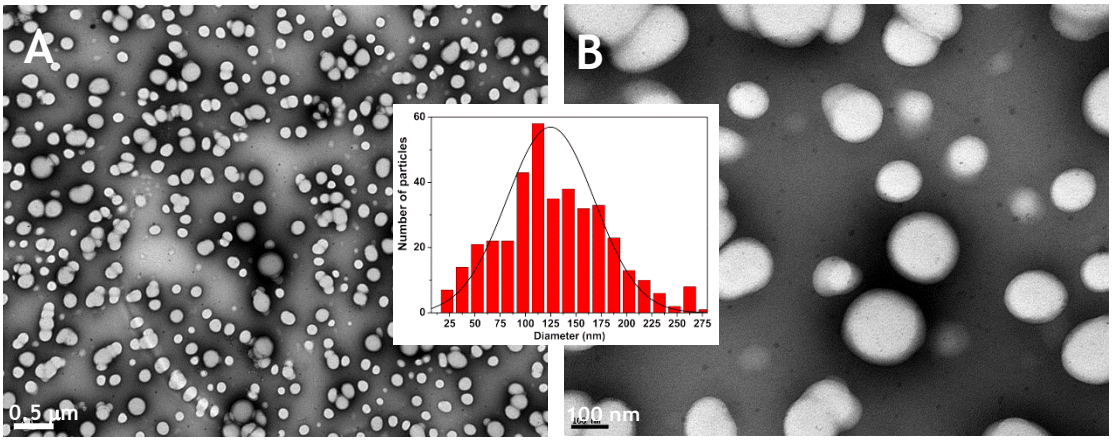

Figure 4.7. Representative TEM images of NPs comm. with different magnifications: **(A)** 25,000× and **(B)** 100,000×. Inset: Size histogram of image **(A)** and fitting to a Gaussian distribution.

In the case of DAPTA-f-NPs comm. (**Figure 4.8**), a similar procedure allowed determining an average diameter of 103 ± 45 nm. Differences from DLS measures may be explained by the same reasons indicated above for non-functionalized NPs. Comparing with the non-functionalized ones, it can be concluded that the functionalization did not cause a significant increase in the NPs size. It can also be concluded that the NPs functionalization does not appear to change the morphology significantly, generally retaining the spherical shape.

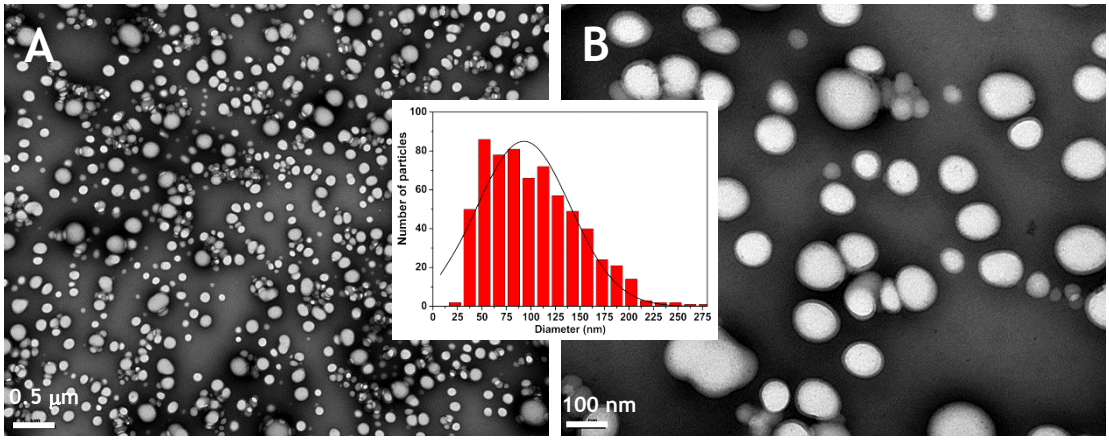

Figure 4.8. Representative TEM images of DAPTA-f-NPs comm. with different magnifications: **(A)** 25,000× and **(B)** 100,000×. Inset: Size histogram of image **(A)** and fitting to a Gaussian distribution.

NPs synth. exhibited a size distribution of 94 ± 51 nm (**Figure 4.9**), being slightly smaller than the previous and presenting a larger size distribution. However, the image obtained with 25,000× magnification (**Figure 4.9B**), does not evidence the presence of any aggregates in the synthetized NPs. Still, differences appear to be negligible and likely associated with variability from the production process of NPs and/or TEM imaging procedures.

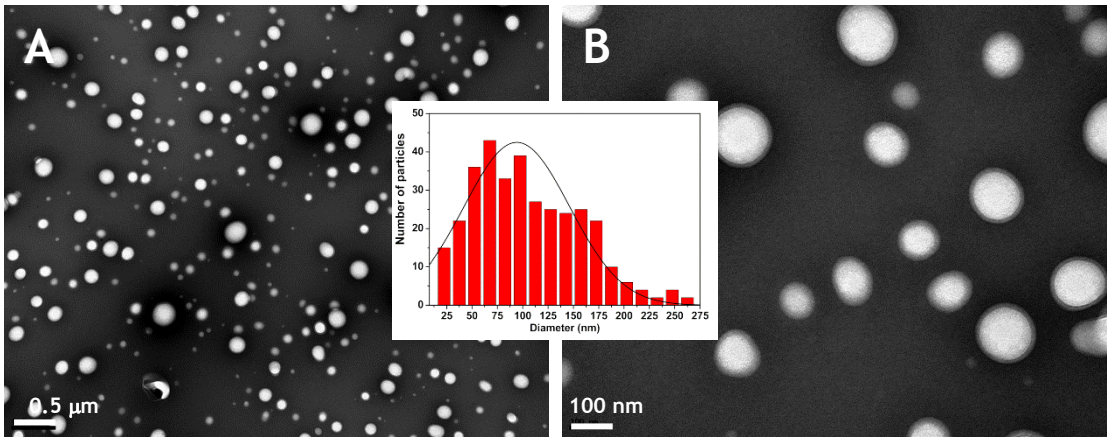

Figure 4.9. Representative TEM images of NPs synth. with different magnifications: **(A)** 25,000× and **(B)** 100,000×. Inset: Size histogram of image **(A)** and fitting to a Gaussian distribution.

Regarding the DAPTA-f-NPs synth. (**Figure 4.10**), a size distribution of 110 ± 45 nm was obtained. In terms of size, these NPs were very similar to the DAPTA-f-NPs comm., as previously shown. The NPs containing synthetic polymer also exhibited a spherical shape.

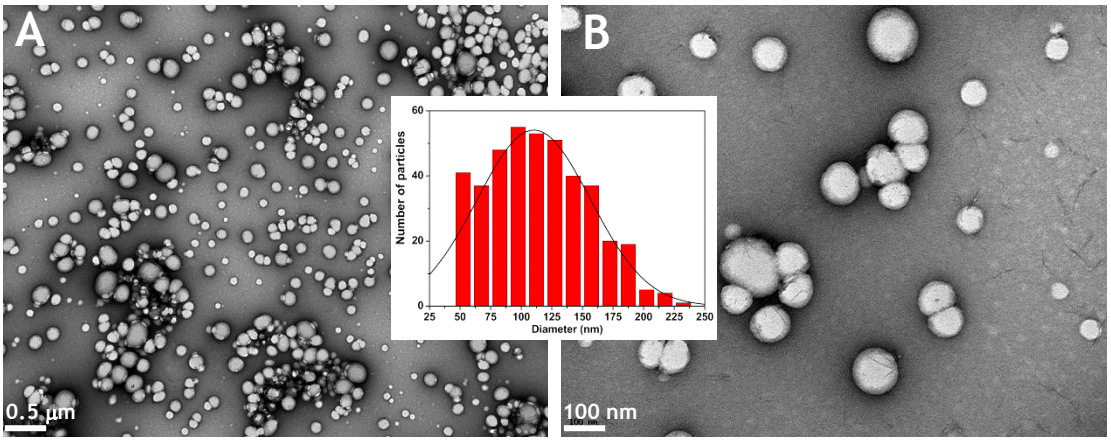

Figure 4.10. Representative TEM images of DAPTA-f-NPs synth. with different magnifications: **(A)** 25,000× and **(B)** 100,000×. Inset: Size histogram of image **(A)** and fitting to a Gaussian distribution.

4.2.3. Assessment of NP functionalization with DAPTA

Functionalized NPs were characterized by MALDI-TOF MS, FTIR and ^{1}H NMR in order to potentially confirm the association of DAPTA. Non-fuctionalized NPs, as well as polymers used in the production of the NPs and DAPTA, were also analyzed for comparison purposes. In this sub-section, "PLGA-PEG" denotes the PLGA-PEG (55 kDa – 5 kDa) from Sigma Aldrich. PLGA-PEG-COOH polymers are attributed with the designations "comm." for commercially available PLGA-PEG-COOH from PolySciTech (40 kDa – 5 kDa) and "synth." for the synthesized one (44 kDa – 7.5 kDa), as stated previously for NPs.

For the purpose of confirming the functionalization of NPs with the DAPTA peptide, MALDI-TOF MS may be useful in the sense that it could allow the detection of a shift in the spectra of functionalized NPs when compared to the ones of non-functionalized NPs, being differences putatively attributable to the contribution of DAPTA (around 857 Da) to the total Mw. A bimodal distribution may be expected for NP samples given that they are composed of both PLGA-PEG (~60 kDa, ~90%) and PLGA-PEG-COOH (~10%), either commercial (~45 kDa) or synthesized (~51.5 kDa). The MALDI-TOF spectra are presented in **Figures 4.11-4.13**.

For tested samples, a MALDI-TOF analysis in the range of 20-100 kDa should have been enough for detecting shifts in Mw. However, as in the previous case, only PEG peaks could be detected, possibly due to PLGA degradation. Still, as DAPTA would bind to the PEG-COOH chains, possible shifts could eventually be detected in PEG Mw.

Regarding PLGA-PEG-COOH comm. (**Figure 4.11A**), analyzed as a control, only a band centered around 5 kDa could be detected, which is in accordance with the expected Mw of the PEG arm. As for PLGA-PEG-COOH synth. (**Figure 4.11B**), the abovementioned band centered at 7.8 kDa is roughly in accordance with PEG Mw.

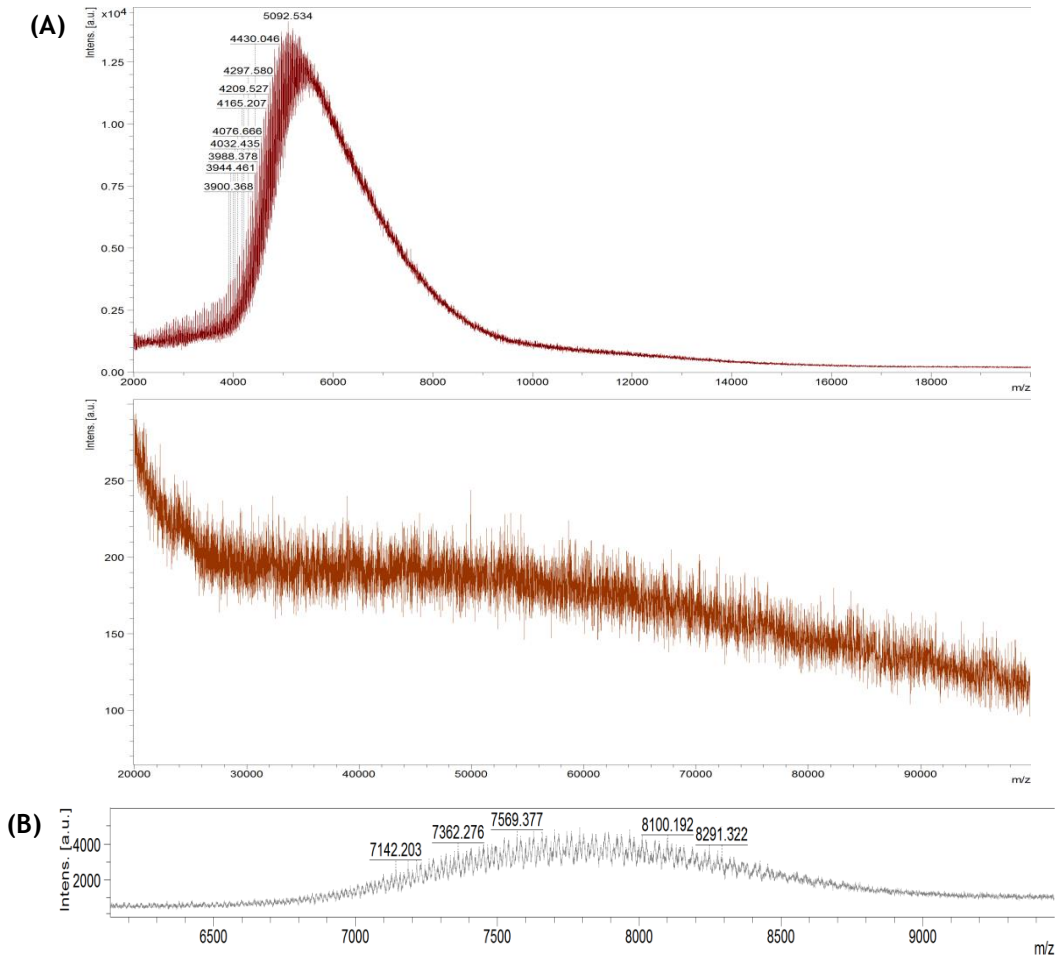

Figure 4.11. MALDI-TOF spectra of **(A)** PLGA-PEG-COOH comm. (2-20 kDa and 20-100 kDa) and **(B)** PLGA PEG-COOH synth. (6-10 kDa).

The spectrum of NPs comm. (**Figure 4.12A**) presents two peaks in the 2-20 kDa range. The left peak (~5.4 kDa) may be assigned to the 5 kDa PEG chains of both PLGA-PEG and PLGA-PEG-COOH comm., while the right peak (~7.7 kDa) may be attributable to PLGA or PLGA-PEG degradation residue. In the spectrum of DAPTA-f-NPs comm. (**Figure 4.12B**), a band centered at ~7.9 kDa was detected, also attributable to PLGA or PLGA-PEG degradation. A shoulder at ~5.8 kDa could be detected, which could presumably be attributed to the PEG-DAPTA arm (5 kDa + 0.86 kDa).

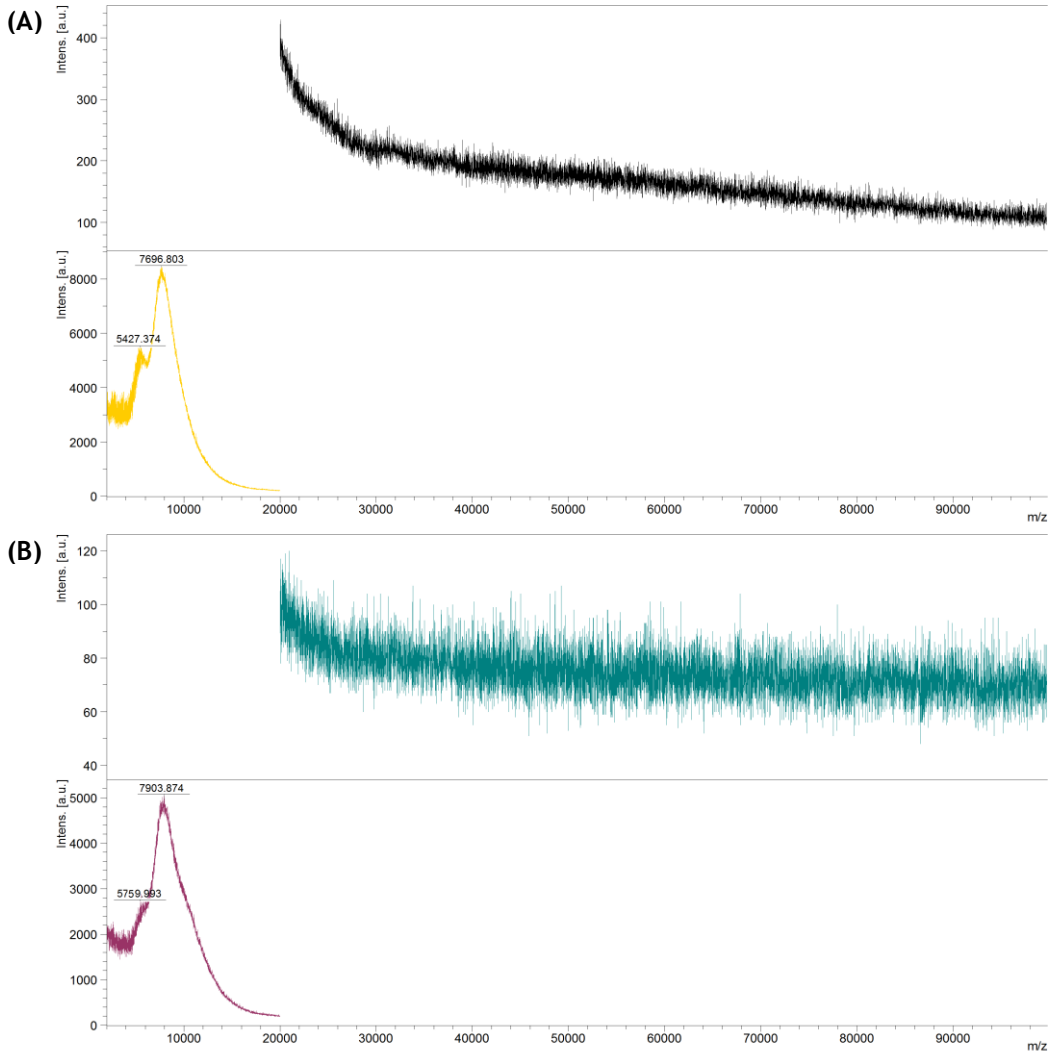

Figure 4.12. MALDI-TOF spectra of **(A)** NPs comm. (2-20 kDa and 20-100 kDa) and **(B)** DAPTA-f-NPs comm. (2-20 kDa and 20-100 kDa).

The spectrum of NPs synth. (**Figure 4.13A**) presented two peaks at ~5.4 kDa and ~7.7 kDa, which are roughly in accordance with the Mw of the PEG chains of PLGA-PEG (5 kDa) and PLGA-PEG-COOH synth. (7.5 kDa). The same features could be detected in the DAPTA-f-NPs synth. spectrum (**Figure 4.13B**), with peaks at ~5.6 kDa and ~7.2 kDa. No shifts were observed that could be attributable to a possible functionalization with DAPTA.

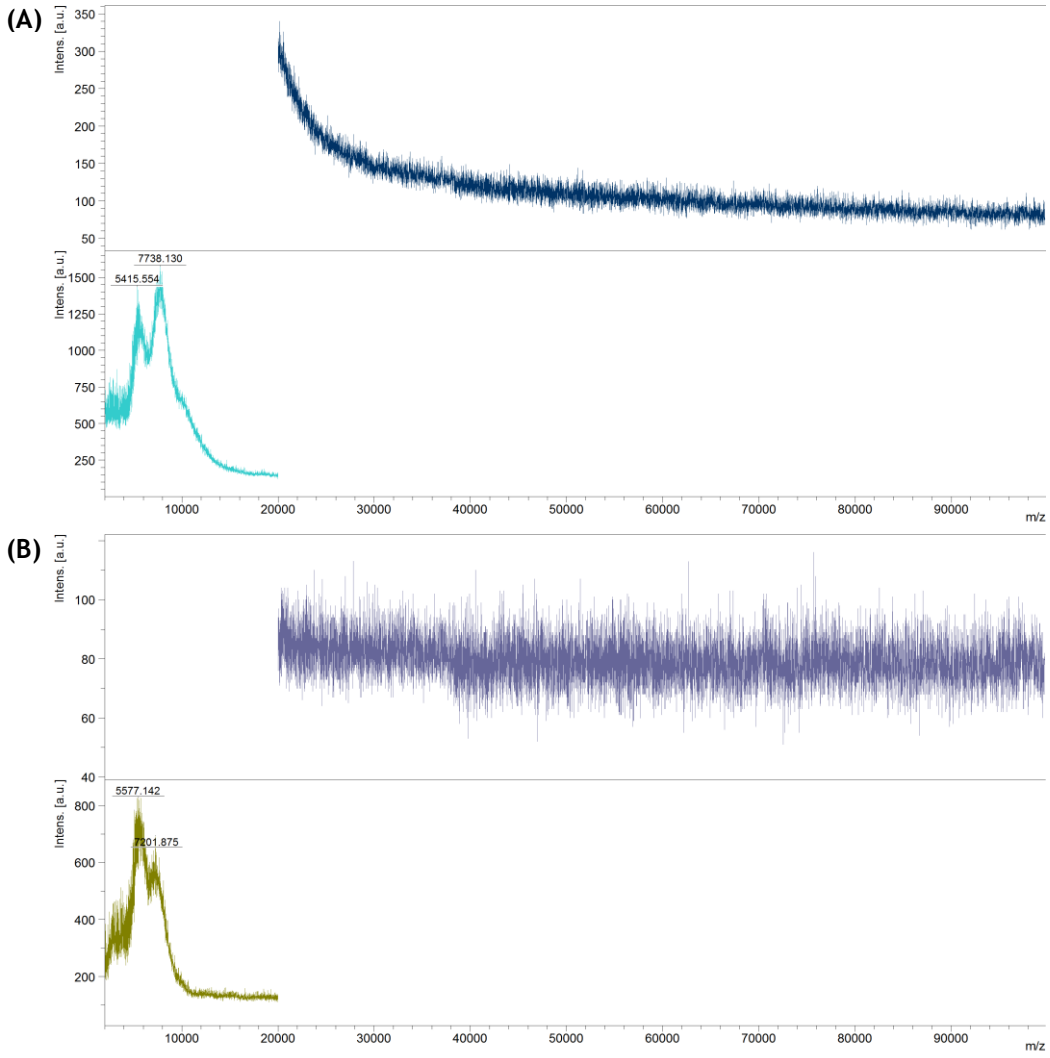

Figure 4.13. MALDI-TOF spectra of **(A)** NPs synth. (2-20 kDa and 20-100 kDa) and **(B)** DAPTA-f-NPs synth. (2-20 kDa and 20-100 kDa).

Overall, MALDI-TOF analyzes provided some indication that the functionalization was presumably successful in the case of NPs contaning commercial PLGA-PEG, but not in the case of NPs containing the synthesized polymer. However, the possible interference of PLGA and PLGA-PEG degradation residue may have influenced these results and further methodological developments of the protocol used for MALDI-TOF analysis may provide more information in the future.

A FTIR analysis was also performed in an attempt to detect DAPTA functional groups in the spectra of functionalized NPs. The spectra of NPs samples, as well as DAPTA and precursor polymers are presented in **Figure 4.14**. In the FTIR spectrum of DAPTA, there was evidence of the presence of amide I and amide II bands (1,500-1,700 cm^{-1}), respectively due to C=O stretching vibrations, υ(C=O), and C-N stretching vibrations, υ(C-N), in combination with N-H bending, δ(N-H). These bands are possibly overlapped with the aromatic bands (occurring in the region 1,650-2,000 cm^{-1}). In the region of 3,100-3,500 cm^{-1}, DAPTA also exhibited typical

bands due to N-H stretching, υ(N-H) (139). All the spectra of NPs were roughly similar to that of the PLGA-PEG copolymer, which constitutes ~90% of their matrix. The magnification of the FTIR spectra in the region of 1,400-1,900 cm^{-1} did not show either the presence of amides (as before) or other characteristic bands of the DAPTA peptide.

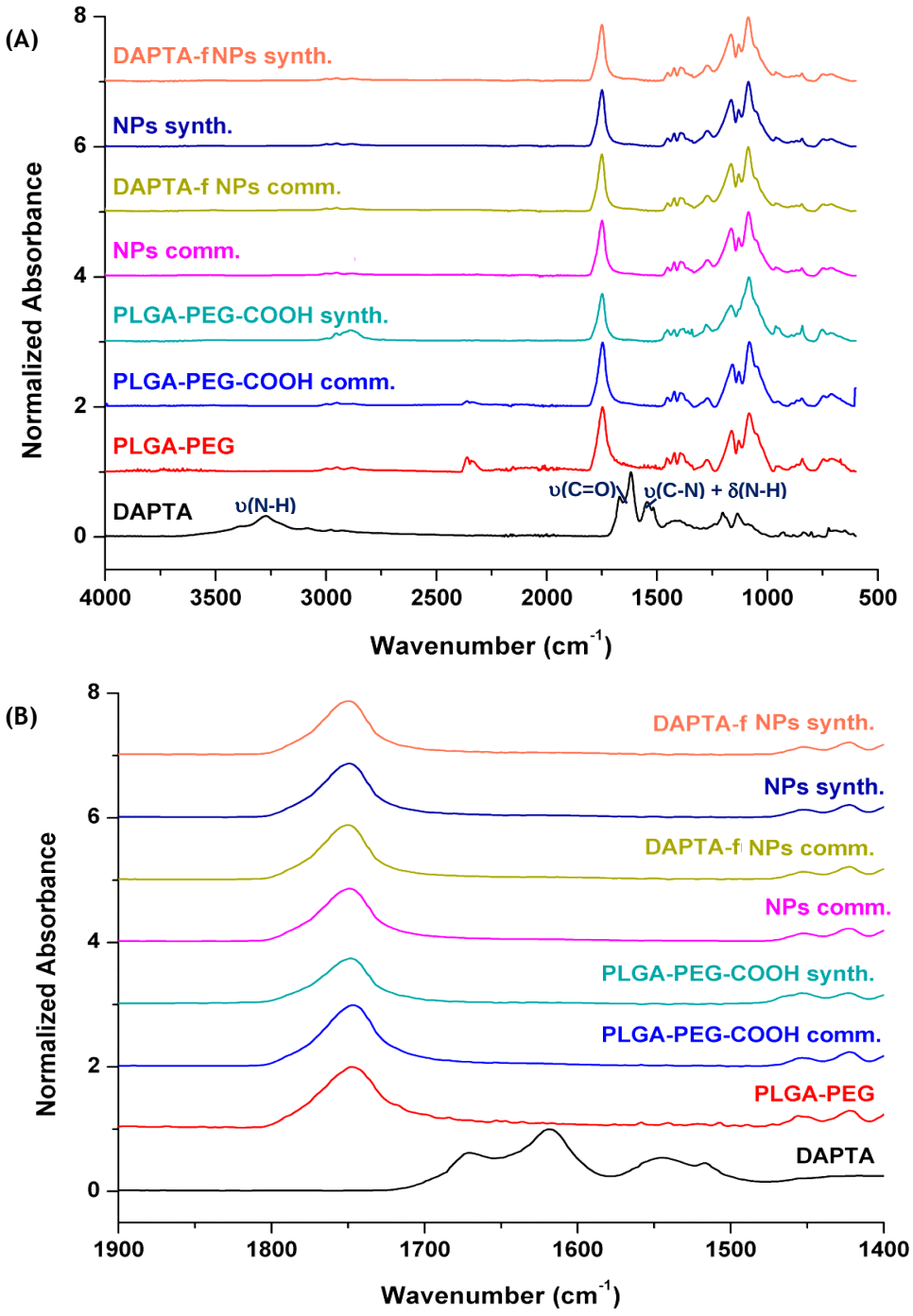

Figure 4.14. FTIR analysis of NPs. **(A)** Full spectra of DAPTA, PLGA-PEG polymers and PLGA-PEG NPs (functionalized and non-functionalized). **(B)** Magnification of the previous spectra in the 1,400-1,900 cm^{-1} region.

In a further attempt to prove the presence of the peptide in the functionalized particles, the FTIR normalized spectra of non-functionalized particles were subtracted from those of the functionalized ones, but the resulting spectra did not allow identifying any peaks or bands (data not shown). Therefore, it was not possible to prove the functionalization of the NPs with DAPTA by FTIR. As in the case of polymer samples, it is possible that the amount of DAPTA relative to the total polymer quantity was too low to allow detection, as it constitutes only, at best, 0.2% (w/w) of the particle composition.

The ^{1}H NMR analysis was also performed in an attempt to demonstrate the presence of DAPTA protons. Due to the predictably low amount of DAPTA present on the surface of NPs, spectra were collected at a higher frequency (600 MHz instead of 400 MHz) and more reading accumulations were considered. The spectra of NPs comm. and DAPTA-f-NPs comm., as well as DAPTA alone are presented in **Figure 4.15.** In the spectra presented in **Figure 4.15A**, apart from DMSO-*d6* and water signals (2.5 ppm and 3.3 ppm), it is possible to observe the presence of the peaks previously described for PLGA (1.4, 4.8 and 5.2 ppm) and PEG (3.6 ppm), in accordance with their major composition in PLGA-PEG. After functionalization, the peaks related with PLGA and PEG did not suffer any chemical shift. Besides, it was not possible to clearly detect any peaks of DAPTA in the spectra of functionalized NPs, presumably due to its low concentration, which hampered its identification. However, after magnification of NMR spectra between 6 and 9 ppm (**Figure 4.15B**), it was possible to observe the appearance of peaks in the aromatic zone (144) (between 6.9 and 7.3 ppm) in both DAPTA only and DAPTA-f-NPs comm. spectra. Since only the peptide presents an aromatic group in its structure (tyrosine residue), the presence of DAPTA in the DAPTA-f-NPs comm. sample may then be inferred. Moreover, the small chemical shifts in the signals related with aromatic groups of DAPTA for the plain peptide and DAPTA-f-NPs comm. may indicate the establishment of new interactions occurring due to bonding. The association of functionalized NPs with the DAPTA peptide seemed therefore to be confirmed by ^{1}H NMR analysis for the case of NPs containing the commercially available PLGA-PEG-COOH. However, additional analytical work may be appropriate in order to fully elucidate (amide) bonding formation and the extension of functionalization. Due to the difficulties in obtaining the synthesized polymer, it was not possible to analyze the corresponding NPs by ^{1}H NMR within the time frame of this work. Such analysis should be performed in a near future, in order to confirm the proper functionalization of these NPs.

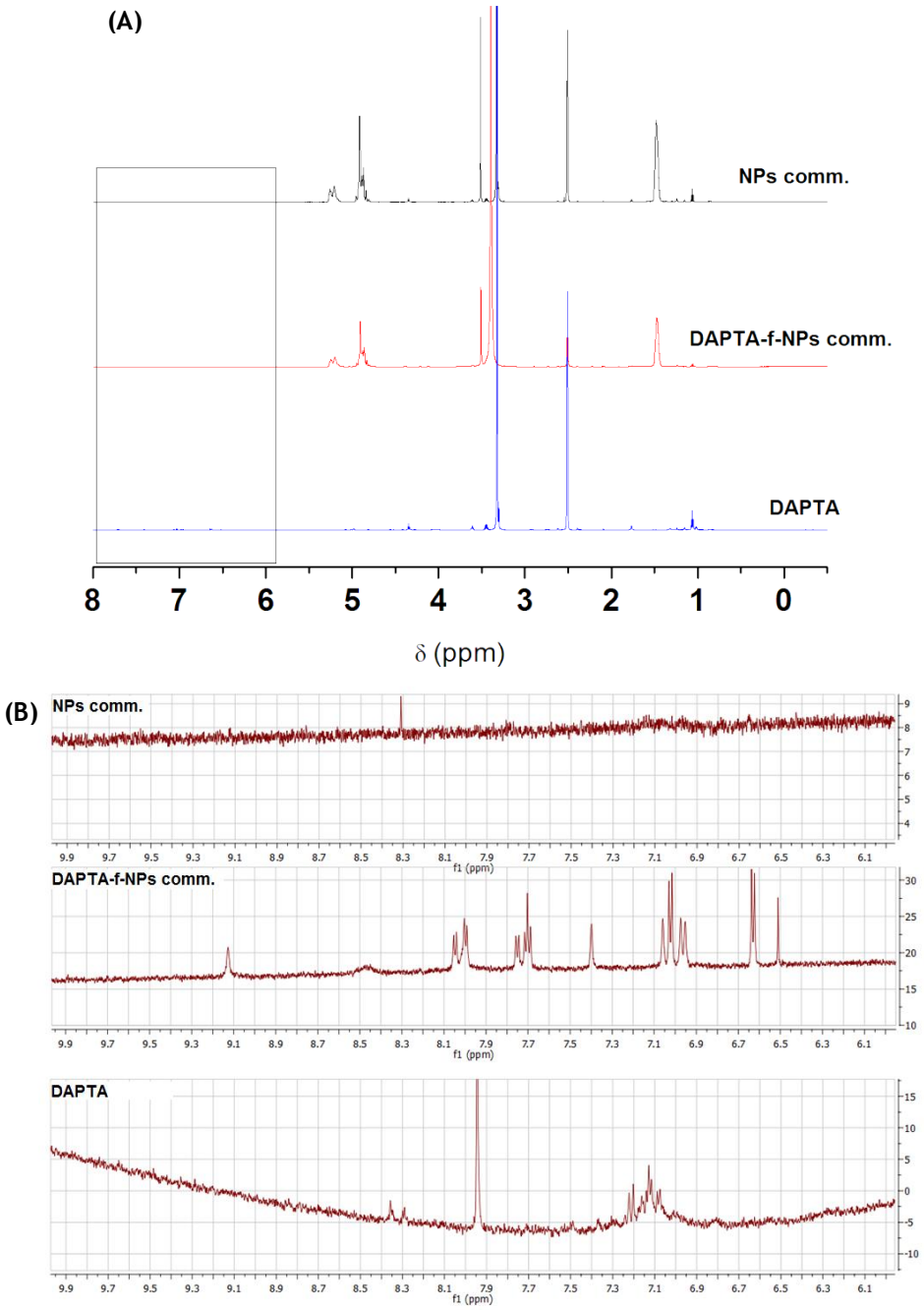

Figure 4.15. NMR analysis of NPs. **(A)** ^{1}H NMR spectra of NPs comm., DAPTA-f-NPs comm. and DAPTA, in DMSO-*d6* at 600 MHz. **(B)** Magnification of the spectra between 6 and 9 ppm using MNova software (Mestrelab Research, Santiago de Compostela, Spain).

4.3. *In vitro* cell studies

4.3.1. Cytotoxicity of DAPTA and nanoparticle formulations

The toxicity of all NP formulations to Ghost Hi-5 cells was investigated by the MTT reduction assay. This is a colorimetric assay commonly used to evaluate the cellular metabolism and possible interferences on cell viability resulting from the interactions with test compounds. It measures the activity of cellular enzymes that reduce the MTT compound to form insoluble formazan crystals of a dark purple color. Upon solubilization of the crystals, the amount of formazan produced can be assessed by measuring the absorbance at 570 nm (158). According to the International Organization for Standardization (ISO) standard pertaining to *in vitro* cytotoxicity testing of medical devices (ISO standard 10993-5), a compound at a given concentration possesses cytotoxic potential if cell viability is reduced to less than 70% of the blank when using the MTT reduction assay (159). Although not directly concerning drug delivery systems, namely nanocarriers, this threshold is commonly used as guidance (160-162).

As a preliminary test, the safety of DAPTA alone was assessed (**Figure 4.16**). DAPTA showed low cytotoxic potential up to 10^5 nM, as inferred from determined viability values that were generally around or above 70%. The value registered at 10 nM, although significant, may be due to possible errors during the experimental procedures or simply the variability associated with this kind of biological assays. These results corroborate the safety profile of DAPTA, which had been previously demonstrated in early clinical trials (28). Also, cytotoxicity data seems to assure that no deleterious effects might be observed when further used for functionalizing NPs formulations.

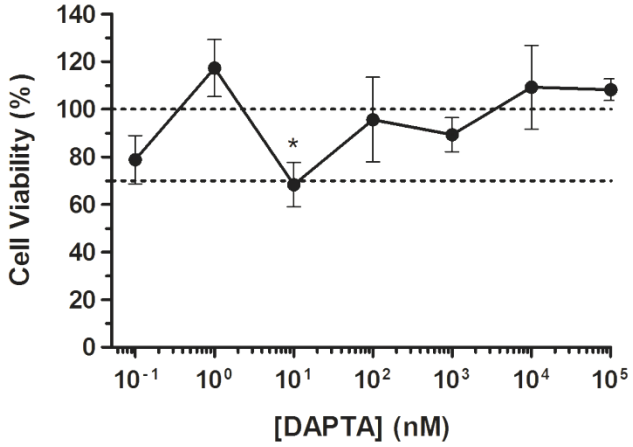

Figure 4.16. Viability of Ghost Hi-5 cells after 24 h incubation with different concentrations of DAPTA, as assessed by the MTT reduction assay. Individual points and vertical bars represent mean and SD values, respectively (n = 3). (*) denotes a significant difference ($p < 0.05$) when compared to cells incubated with medium only.

In order to define a suitable set of concentrations to evaluate the cytotoxicity of NPs, a correlation was made between DAPTA and NP concentrations, based on the maximum theoretical quantity of DAPTA associated to NPs (*i.e.*, assuming that all available carboxylic acid groups of PLGA-PEG-COOH would be functionalized). The concentrations of NPs that contained, at most, each of the concentration values used for DAPTA were thus calculated. The concentrations used for NPs containing either commercial or synthesized PLGA-PEG-COOH are presented in **Table 4.7**. The slight differences between values for the two types of PLGA-PEG-COOH, approximately 12%, are related to the different Mw of their PLGA and PEG chains. The results of the MTT reduction assays for the different NP formulations (NPs, DAPTA-f-NPs, C6-NPs, C6-NHS-NPs, C6-gly-NPs, C6-DAPTA-a-NPs and C6-DAPTA-f-NPs) are depicted in **Figure 4.17**.

Table 4.7. Concentrations of NPs used in the MTT reduction assays.

[DAPTA] (nM)	[NPs] (μg/mL)	
	Commercial PLGA-PEG-COOH	Synthesized PLGA-PEG-COOH
10^{-1}	0.045	0.051
1	0.45	0.51
10	4.5	5.1
10^{2}	45	51
10^{3}	450	510
10^{4}	4,500	5,100

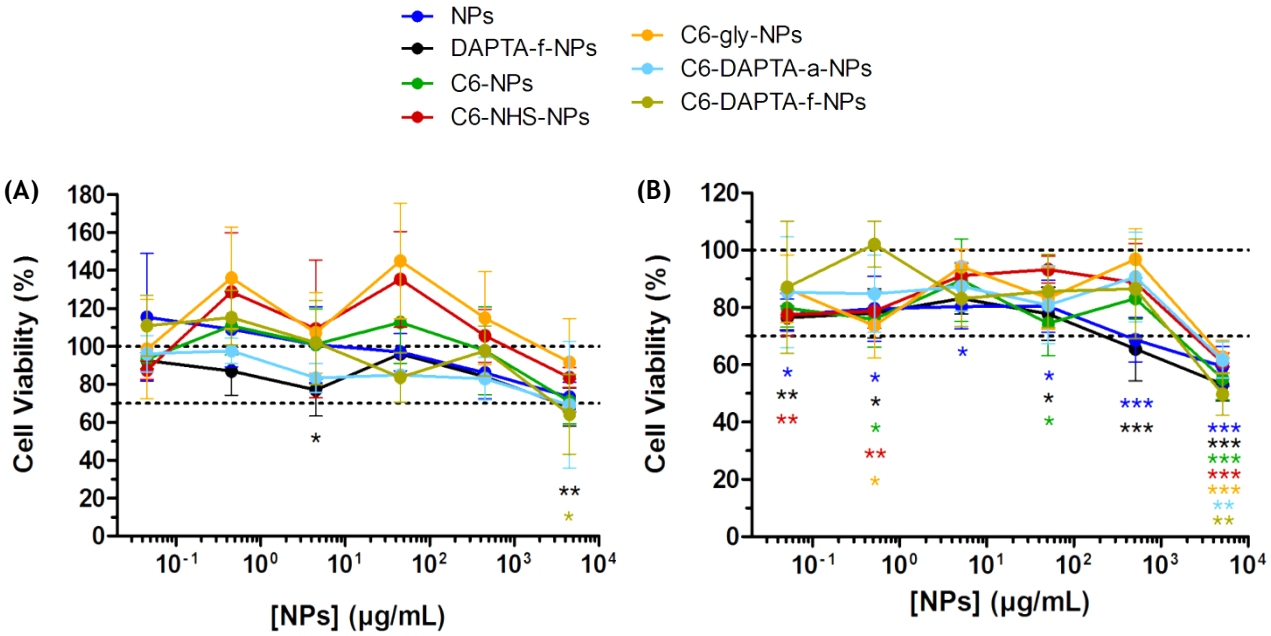

Figure 4.17. Viability of Ghost Hi-5 cells after 24 h incubation with different concentrations of several NP formulations, as assessed by the MTT reduction assay. **(A)** NPs containing commercial PLGA-PEG-COOH; **(B)** NPs containing the synthesized PLGA-PEG-COOH. Individual points and vertical

bars represent mean and SD values, respectively (n = 3). (*), (**) and (***), denote a significant difference at $p < 0.05$, $p < 0.01$ and $p < 0.001$, respectively, when compared to cells incubated with media only. The colors of the asterisks refer to the correspondent NPs. Comparison between NP formulations are not shown for the sake of clarity.

All NP formulations, in general, induced only mild changes to cell viability, with the exception of the highest concentration tested. In this last case, relevant toxicity for all NPs containing synthethized PLGA-PEG-COOH (viability values below 70%) or a few NPs containing the commercial polymer was observed. This is probably due to the considerable amount of solid material that has been added (aroung 5 mg/mL), probably too much to allow proper compound exchange between cells and medium. The formation of a physical barrier does not necessarily mean that cytotoxicity is specific but may rather be a limitation of the assay itself (163). Moreover, the inability to concentrate the NPs enough to avoid a significant diluiton of the medium, which was around 1:5 for this concentration, could be responsible for higher toxicity. The apparently lesser cytotoxicity for NPs comprising PLGA-PEG-COOH from a commercial supplier may have to deal with the presence of residual amounts of solvents or coupling reagents in the synthetized PLGA-PEG-COOH. Also, adding to the intrinsic variability of the assay, no significant differences were found at each concentration when comparing either the polymer type composing the NPs or the different NP formulations. Overall, tested NPs may be considered as having low cytotoxicity, namely to Ghost Hi-5 cells. Also important, no apparent increase in the cytotoxicity of NPs has arised from the incorporation of C6, NHS, DAPTA or glycine. The obtained cytotoxicity results further allowed establishing a safe concentration for performing further NP uptake studies (0.1 mg/mL).

Despite promising, presented results may only be considered preliminary, namely considering the possible application of NPs in microbicide development. Ghost Hi-5 cells do not represent main cell types populating the vaginal or rectal mucosae, namely of epithelial origin. Studies in cervicovaginal and colorectal cell lines would be required to assess the safety profile of the proposed nanosystems.

4.3.2. Nanoparticle uptake studies

FACS studies were performed in order to quantitatively assess the uptake of NPs by Ghost Hi-5 cells. Higher association with cells was expected for fluorescent DAPTA-functionalized NPs, as compared with non-functionalized particles, in order to attest, at least partially, the targeting ability. FACS is a flow cytometry technique that, by using antibodies labeled with fluorescent conjugates, allows to collect data for a high number of different parameters simultaneously. Forward-scatter, side-scatter and fluorescent signal data are collected just like in conventional flow cytometry (164). The signal of fluorescent NPs can also be analyzed

using this technique. Although commonly referred to as uptake studies, data from FACS only ascertain that NP-cell association occurred. For example, NPs may be linked to the cell membrane without actual cellular internalization (formal uptake).

Before proceeding with NP uptake studies, a preliminary study was performed in order to confirm the expression of CCR5 by Ghost Hi-5 cells. Cells from passages 9 and 20 were incubated for 1h with an APC-labelled anti-CCR5 antibody and analyzed by FACS using the BD FACSCanto™ II instrument. Detection was performed through the APC channel, upon excitation with the 633 nm laser. HeLa cervical cells, not expressing CCR5, were used as the negative control.

The population distribution and gating strategy adopted to perform the analysis are shown in **Figure 4.18**. The left panel shows the selection of the viable cell population on a Forward Scatter Area (FSC-A) vs. Side Scatter Area (SSC-A) dot plot. The middle panel shows the exclusion of cell doublets and aggregates, being selected the single cells population, on a FSC-A vs. Forward Scatter Height (FSC-H) dot plot. The right panel represents the fluorescence histogram detected on the APC channel for an unstained sample. Therefore, the fluorescent signal presented by these samples is excluded and events presenting fluorescence values above that threshold are considered APC-positive values (*i.e.*, $CCR5^+$ cells). Obtained results are presented as percentage of positive cells in **Figure 4.19**.

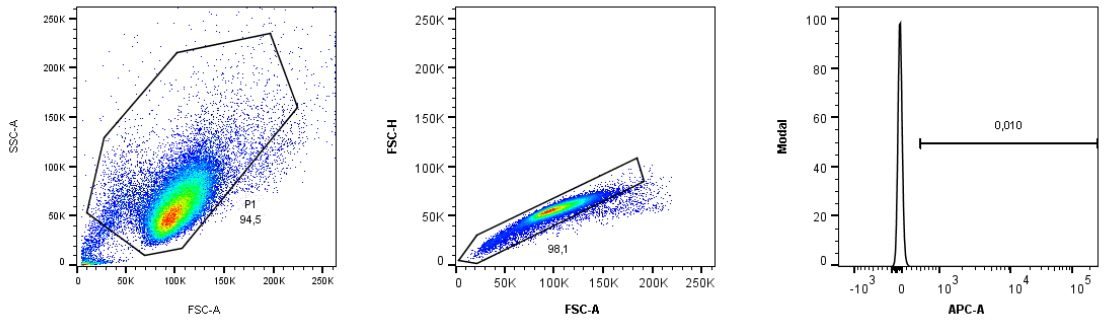

Figure 4.18. Representative population distribution and gates applied in FACS for the CCR5 expression experiment.

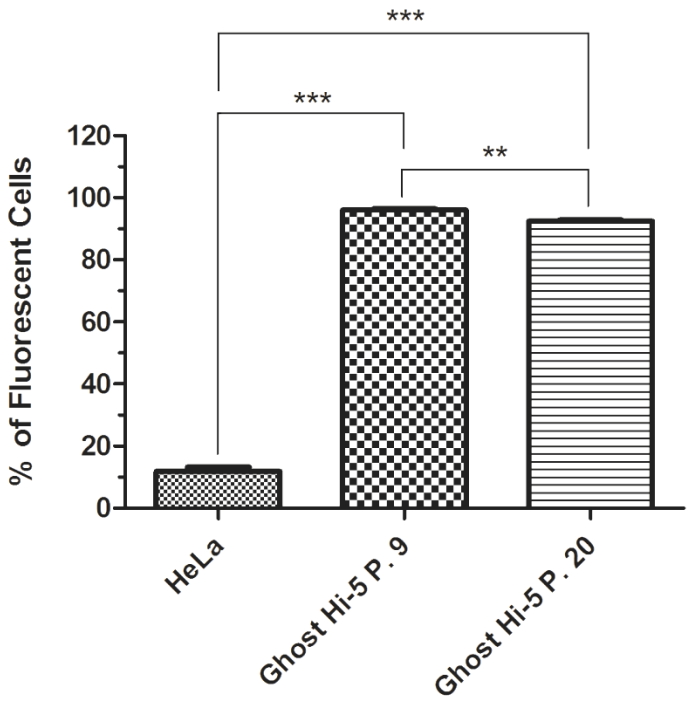

Figure 4.19. CCR5 expression by Ghost Hi-5 cells at different passages. Data presented as mean ± SD (n = 3). (**) and (***) denote a significant difference at $p < 0.01$ and $p < 0.001$, respectively.

Cells at passage 9 were 96.1±0.4% positive for CCR5, while at passage 20 this value slightly decreased to 92.5±0.4%. HeLa cells were only 11.8±1.5% positive, a value that could be further reduced if slightly narrowing the APC-positive gate. Still, such levels are commonly associated with non-specific binding of antibodies (165). The presented results confirmed the high CCR5 expression by Ghost Hi-5 cells, as compared to the negative control. Despite being significantly different, results for passages 9 and 20 are probably not biologically relevant. Results presented as Mean Fluorescence Intensity (MFI) showed a similar behavior (not shown). Although it is recommended that Ghost Hi-5 cells are used for no longer than passages 10-15 due to possible phenotype changes (113), presented results appear to indicate no relevant CCR5 receptor loss until at least passage 20. Only a more thorough study of CCR5 expression at different passages could confirm this assumption. Nevertheless, since uptake studies were performed between passages 10 and 12, the influence of possible CCR5 receptor loss in subsequent NP uptake studies could be ruled out.

NP uptake experiments were performed using four time-points for incubation with NPs, spanning from 15 min to 2h. NPs incorporated the fluorescent molecule coumarin-6 (λ_{ex} = 443 nm; λ_{em} = 505 nm), providing a detectable green signal in the FITC channel of the BD FACSCanto™ II instrument, upon excitation with its 488 nm laser. Functionalized (C6-DAPTA-f-NPs) and non-functionalized (C6-NPs) samples were evaluated, as well as NPs that were only activated with EDC/Sulfo-NHS (C6-NHS-NPs). In this last case, no DAPTA was added in the functionalization step of NPs. Since Sulfo-NHS is a reactive group, an additional

control formulation was also evaluated, in which NPs were capped with the glycine amino acid in order to inactivate the Sulfo-NHS group (C6-gly-NPs). Also, a control in which the DAPTA peptide was added to the NPs without EDC/Sulfo-NHS was performed, to attest the possibility of a non-covalent peptide adsorption to NPs leading to changes in uptake (C6-DAPTA-a-NPs). All NPs were subject to the same buffer incubations and number of washing steps. Both formulations containing the commercial or synthesized PLGA-PEG-COOH were evaluated.

In order to assure that cells would be at a sufficient growth rate and metabolic activity at the time of the experiments, the ideal seeding density for Ghost Hi-5 in 24-well plates was previously determined to be 5×10^4 cells/well, reaching 60-70% of confluence after 24h incubation. To avoid possible trypsin-mediated cleavages of the amide bond between the NPs and DAPTA, as well as bonds within the peptide, Versene™ (0.48 mM EDTA) was used as dissociation reagent. In the first assays using PFA as fixative, it was impossible to recover enough cells for FACS analysis, probably due to the reduced number of initially seeded cells and losses related with the multiple cell washing and centrifugation steps required for fixation with PFA. The replacement of PFA for sodium azide as a fixative led to the reduction of the required washing and centrifugation steps, allowing the successful recovery of a sufficient number of cells for analysis.

The population distribution and gating strategy adopted for optimized settings of uptake experiments are presented in **Figure 4.20.** After selection of viable cells (FSC-A vs. SSC-A) and exclusion of doublets and aggregates (FSC-A vs. FSC-H), the fluorescent cell gate was defined from the fluorescence histogram of an unstained sample in the FITC channel. Uptake results for NPs containing either commercial or synthesized PLGA-PEG-COOH are depicted in **Figure 4.21**. Data are presented as percentage of fluorescent cells. Results presented in MFI further showed similar behavior (not shown).

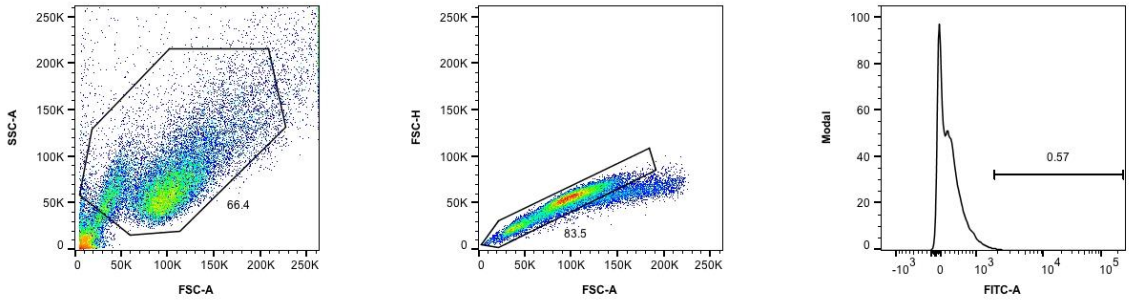

Figure 4.20. Representative population distribution and gates applied in FACS for NP uptake experiments.

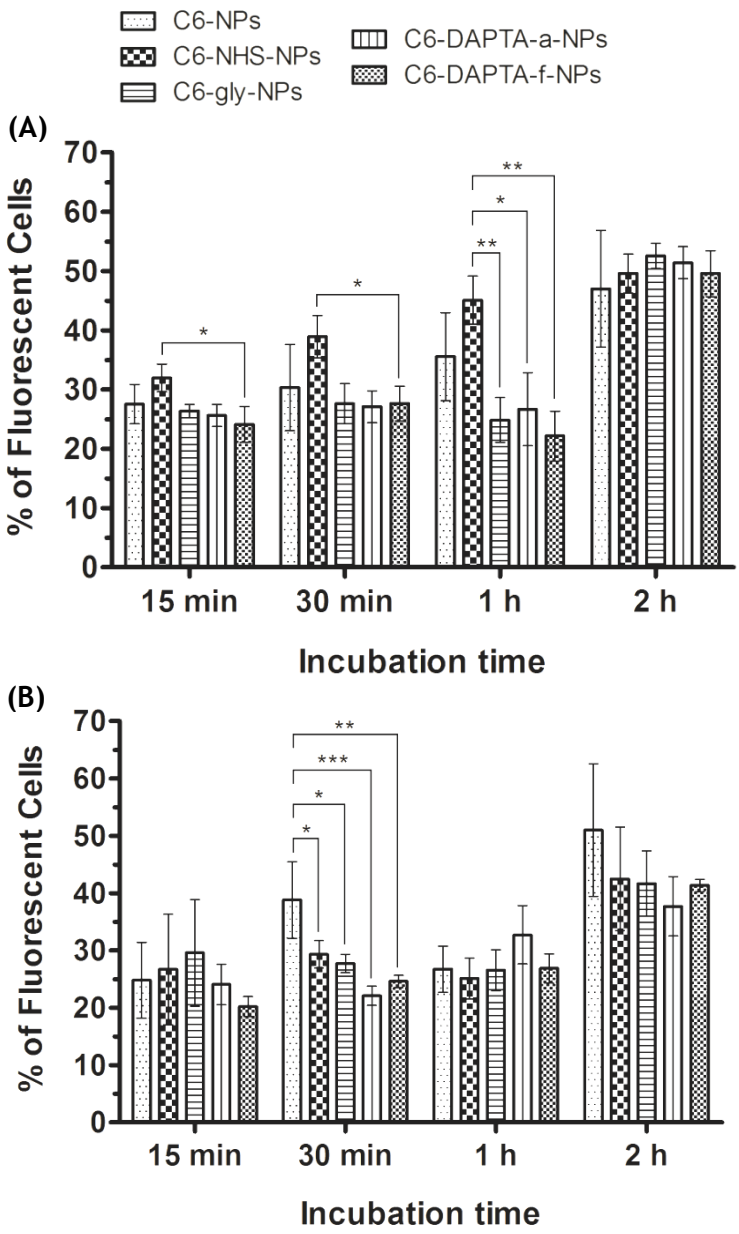

Figure 4.21. Quantitative results for NP uptake by Ghost Hi-5 cells. **(A)** NPs containing commercial PLGA-PEG-COOH; **(B)** NPs containing synthesized PLGA-PEG-COOH. Data presented as mean ± SD (n = 3). (*), (**) and (***) denote a significant difference at $p < 0.05$, $p \leq 0.01$ and $p \leq 0.001$, respectively.

In general, no significant differences were detected between C6-DAPTA-f-NPs and C6-NPs. Also, no significant differences were observed when comparing C6-DAPTA-f-NPs with the controls C6-gly-NPs and C6-DAPTA-a-NPs. One exception occurred at 30 min of incubation with NPs containing synthesized PLGA-PEG-COOH, in which NP-cell association seemed to be favored for non-functionalized NPs (C6-NPs) as compared to all other formulations. However, other incubation times showed no differences between NP formulations, which may indicate the presence of outliers. In the case of NPs containing commercial PLGA-PEG-COOH, C6-NHS-NPs exhibited higher association with cells at earlier time-points of incubation but

the differences were attenuated at 2h (**Figure 4.21A**). The reactivity of the activated Sulfo-NHS groups could be implicated in such observations as linkage of the polymer with cell membrane residues of primary amines could occur (115). Preliminary experiments using trypsin seemed to have corroborated this effect (**Figure 4.22**). In this case and excluding the 15 min time-point (which may be too early to draw clear conclusions), no differences were found between C6-NHS-NPs and C6-DAPTA-NPs, which may be due to the action of trypsin in cleaving possible amide bonds formed by Sulfo-NHS. However, such possibility was not confirmed when NPs containing synthetized PLGA-PEG-COOH featuring Sulfo-NHS activated groups were used (**Figure 4.21B**). As mentioned before, the presence of a longer PEG-COOH chain in the synthetized copolymer was intended to avoid possible steric hindrance of DAPTA when binding to CCR5 (149, 150). This longer PEG arm would allow for DAPTA to be more exposed and thus potentially more available for interacting with CCR5. This feature should also be applicable when considering Sulfo-NHS, as the reactive group would also be more exposed. Nonetheless, data were unable to corroborate such possibility. Still considering the rational for the longer PEG chain attached to DAPTA, no improvement in the interaction of C6-DAPTA-f-NPs with cells was observed. A possible explanation for these unexpected results may be low yield of the synthetized PLGA-PEG-COOH copolymer. Also, the effective functionalization of these NPs with DAPTA was not fully assessed and, therefore, inefficient functionalization with DAPTA may have occurred.

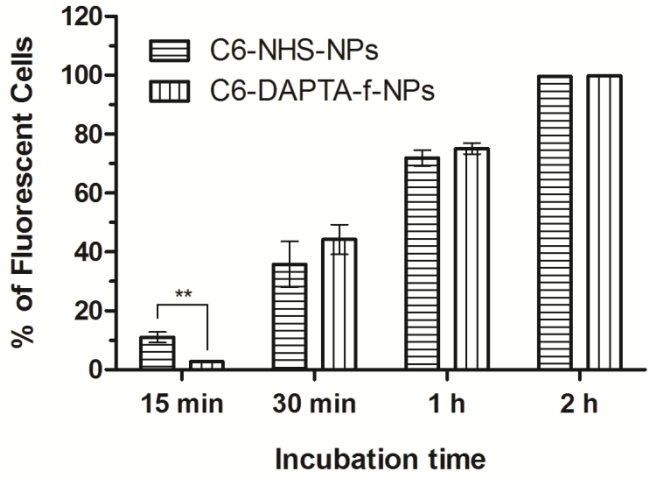

Figure 4.22. Results of preliminary NP uptake studies in Ghost Hi-5 cells using trypsin as dissociation agent for NPs containing commercial PLGA-PEG-COOH. In this case, an unpaired Student t-test was used for statistical analysis. Data presented as mean ± SD (n = 3). (**) denotes a significant difference at $p < 0.01$.

Results for C6-DAPTA-a-NPs did not show any differences when comparing to C6-DAPTA-f-NPs (**Figure 4.21**). Since C6-DAPTA-f-NPs were unable to improve NP-cell

association, it was not possible to assess the actual importance of covalent bonding between DAPTA and NPs for cell association (assuming it occurred in C6-DAPTA-f-NPs). Besides the type of linkage, one important issue to be considered when evaluating targeted systems is the orientation of the ligand. For the case of DAPTA, only the five terminal amino acids (Thr-Thr-Asn-Tyr-Thr) seem to be crucial for activity (166). Since DAPTA has one single primary amine at the alanine residue, which is located on the opposite side of the previous sequence, carbodiimide-mediated amide bond formation could only occur at this site. Thus avoidance of interference with the binding ability of DAPTA due to tethering at the surface of NPs seems conceivable. Still, being such a small peptide, it is possible that the presence of large entities such as PEG or even the whole nanosystem may counteract the ability of DAPTA to bind CCR5. To circumvent this issue, changing DAPTA by other possible CCR5 ligands may be an option, namely antibodies (167, 168); or aptamers, these last having already shown potential in targeted siRNA carriers for CCR5-postive cells (97).

Overall, generated data appears to support that functionalization of NPs with DAPTA, namely by following the adopted methodologies, was unable to improve the association with cells and, thus, the targeting ability of the proposed nanosystems could not be demonstrated.

CHAPTER 5

Conclusions and Future Work

In the present work, polymeric NPs were successfully developed by using PLGA-PEG copolymers and further functionalized with the DAPTA peptide, in order to target the CCR5 cell membrane receptor. Such nanosystems were designed as a potentially innovative targeted carrier for improving the efficacy and safety of anti-HIV microbicide drugs.

A PLGA-PEG-COOH copolymer was initially synthesized through carbodiimide-mediated coupling of PLGA-COOH and H_2N-PEG-COOH. The newly formed copolymer has the potential to provide a valuable tool for engineering NPs featuring carboxylic acid groups at their surface, which may further allow covalent tethering of DAPTA. PLGA-PEG-COOH was likely obtained as collectively verified by using MALDI-TOF MS, FTIR and ^{1}H NMR. Still, no unequivocal proof of the formation of a covalent bonding between the two block polymers could be attained, requiring additional efforts to fully characterize the products obtained. The copolymer mass recovery was also modest and the procedure leading to the production of PLGA-PEG-COOH requires additional optimization. In particular, the precipitation steps necessary for copolymer recovery and, possibly, the extent of conjugation need to be improved.

PLGA-PEG-based NPs containing 10% (w/w) of either the above mentioned synthesized PLGA-PEG-COOH or a commercially available surrogate were successfully produced by nanoprecipitation. NPs were then functionalized with DAPTA through carbodiimide-mediated coupling. Both functionalized and non-functionalized NPs featured similar colloidal properties, namely spherical shape and average hydrodynamic diameter values between 160 and 180 nm and nearly neutral surface charge. Moreover, produced particles were relatively monodisperse as confirmed by DLS and TEM analysis. Overall, such properties may be considered suitable for the desired application, namely for effectively penetrating mucosal fluids and reaching HIV-susceptible cells at the epithelial level. Furthermore, the presence of

DAPTA associated to functionalized NPs was confirmed by ^{1}H NMR analysis, thus potentially conferring the ability for targeting cells expressing CCR5.

Finally, all NP formulations were shown to present low cytotoxic potential, namely when tested with CCR5-positive cells. Still, further expanded studies, namely using other cell types relevant to mucosal application are required in order to confirm the safety of the nanosystems. The interaction of fluorescent NPs with CCR5-positive cells was further tested using FACS. However, quantitative data suggested that NPs modified with DAPTA were unable to significantly improve the association with cells as compared to non-functionalized NPs. Still, additional protocol optimization and complementary studies (e.g., using other cell types, alternative techniques or competitive assays) are deemed necessary in order to definitely clarify this apparent lack of targeting of the proposed NPs.

Overall, DAPTA-modified PLGA-PEG-based NPs were successfully produced and widely characterized for relevant physicochemical and biological properties, presenting suitable features for potential use in anti-HIV microbicide development. Still, enhanced association of functionalized NPs to CCR5-expressing cells could not be demonstrated and further complementary studies are required.

Keeping in mind the abovementioned conclusions of this work, as well as its innovative and possibly seminal character, several questions remain to be addressed and justify additional research. For instance, the proposed synthesis of the PLGA-PEG-COOH copolymer, or possibly an appropriate surrogate, is far from optimal. Changes in the concentration of coupling reagents and polymers, use of alternative coupling agents (*e.g.*, DCC or DIC (115)), modification of solvent media in which the reactions occur and/or, in particular, optimization of the polymer precipitation and washing steps (*e.g.*, modify the ratio between ethyl ether and methanol, use of alternative washing solvent systems or techniques) could improve the outcomes of PLGA-PEG-COOH synthesis, both in terms of conjugation success and copolymer recovery.

Another important aspect concerns the improvement of polymer characterization, either by testing different settings for techniques used throughout this work or by exploring alternative ones. In the case of the former, adjusting the wavelength of the incident laser in MALDI-TOF MS assays could help preventing the presumable degradation of PLGA. Using chemical shifts of different elements for NMR (*e.g.*, ^{13}C NMR) may also enrich the information regarding chemical composition of the synthesized materials. When considering different techniques, Gel Permeation Chromatography (GPC, also known as Size Exclusion Chromatography, SEC) could be particularly useful in order to attest the Mw of newly formed polymers. GPC is a chromatographic assay that separates polymer chains by size: in general, the largest the size, the lowest the retention volume of the chromatographic gel column (169). With appropriate standards of known Mw, the Mw value of the newly formed copolymer could be determined, as well as any unbound PLGA or remaining PEG. Moreover,

this technique can be used in a preparative mode, using columns with high loading capacity, thus allowing to directly purify the synthesized copolymer, separating it from unbound PEG and PLGA, and eventually avoid washing and precipitation steps (170). Static Light Scattering (SLS) could also be exploited for complementary characterization of polymers. This technique allows the determination of the absolute Mw using the relationship between the intensity of scattered light and the molecular weight and size of the particle, as described by the Rayleigh theory. This last states that larger molecules scatter more light than smaller ones and, thus, the intensity of the scattered light is proportional to the Mw (171). Moreover, by combining SLS with a separation technique such as GPC, calculation of absolute molecular weight at any point in the eluting chromatogram becomes possible (and, therefore, determining the Mw of any population in a mixed sample) (171).

Concerning the production of NPs, major issues requesting further insights seem to be those related with functionalization with DAPTA. From the point of view of the plain characterization of the success and extension of surface tethering of the polymer, additional research is critical. Confirmation of the presence of the peptide at the surface of NPs could be pursued by, for instance, using similar strategies and techniques as the one described above for polymer characterization. As for quantification, this could be performed by direct or indirect assay of bound or unbound peptide from purified NP samples or their washing supernatants, respectively. Techniques used for protein quantification, namely at minimal levels (e.g., bicinchoninic acid (BCA), Coomassie Brilliant Blue G-250, *ortho*-phthalaldehyde (OPA) and fluorescamine assays (172-176)) could be tested for that purpose. One predictable problem with direct testing could be scattering effects caused by the NPs in spectrophotometric detection; yet, such issue could be abbreviated by using indirect quantification.

Expanding on the studies of the interactions between NPs and cells will be determinant in assessing the potential of DAPTA functionalization. As mentioned before, despite no significant interference with cell metabolic activity being identified, as shown by the MTT reduction assay, other types of cytotoxicity may be possible to occur, namely at the membrane level or due to mutagenesis. Several well accepted *in vitro* assays are available and could be included in testing proposed NPs (*e.g.*, lactate dehydrogenase leakage assay, comet assay, micronucleus test). Pro-inflammatory effects should also be ruled out, namely by assessing levels of secreted cytokine/chemokine levels by cells upon challenge with NPs (66). This array of tests should also be expanded to other cell types, particularly those relevant to vaginal or rectal drug delivery.

Finally, one important question left open in this work concerns the ability of DAPTA to allow targeting of CCR5-expressing cells. FACS studies could be repeated using optimized protocols. New studies should include the use of CCR5-negative cells lines, as well as competitive uptake experiments using CCR5 inhibitors, namely maraviroc or DAPTA itself. The

inclusion of inhibitors of specific endocytic pathways could also provide insights to the mechanisms involved in NP uptake. Moreover, other types of techniques including fluorescent, confocal or electron microscopy could be helpful in complementing FACS data. These essentially qualitative techniques could help determining if NPs are effectively internalized or just associated with the cell membrane. The use of *in vitro* models relevant to nanotechnology-based mucosal drug delivery (*e.g.*, cell monolayer models, multilayered cell constructs (177)) could also be of value in order to better mimic actual *in vivo* scenarios.

The proposed future work will be determinant in attesting the general strategy followed in this work for engineering CCR5-targeted NPs. In case the proposed DAPTA-modified PLGA-PEG-based NPs are proven promising for advancing in the development pipeline, additional studies leading to the adequate association of promising microbicide drugs and subsequent *in vivo* studies for assessing mucosal distribution, pharmacokinetics, safety and efficacy may be appropriate to pursue (178). Conversely, alternative approaches to CCR5 targeting may be considered appropriate, namely by (i) modifying the process of copolymer and/or NP production (*e.g.*, conjugating DAPTA to PLGA-PEG-COOH before obtaining NPs); (ii) using another type of carrier that allows more structural control (for example, dendrimers, metal NPs); or (iii) changing DAPTA by another more suitable targeting moiety (*e.g.*, anti-CCR5 antibodies or aptamers).

References

1. GBD 2015 HIV Collaborators. Estimates of global, regional, and national incidence, prevalence, and mortality of HIV, 1980-2015: the Global Burden of Disease Study 2015. Lancet HIV. 2016;3(8):e361-87.

2. Maiese EM, Johnson PT, Bancroft T, Goolsby Hunter A, Wu AW. Quality of life of HIV-infected patients who switch antiretroviral medication due to side effects or other reasons. Curr Med Res Opin. 2016;32(12):2039-46.

3. UNAIDS. AIDS data. UNAIDS: Geneva, Switzerland, 2016.

4. De Cock KM, Jaffe HW, Curran JW. The evolving epidemiology of HIV/AIDS. AIDS. 2012;26(10):1205-13.

5. Teeraananchai S, Kerr SJ, Amin J, Ruxrungtham K, Law MG. Life expectancy of HIV-positive people after starting combination antiretroviral therapy: a meta-analysis. HIV Med. 2017;18(4):256-66.

6. Krishnaratne S, Hensen B, Cordes J, Enstone J, Hargreaves JR. Interventions to strengthen the HIV prevention cascade: a systematic review of reviews. Lancet HIV. 2016;3(7):e307-17.

7. Arien KK, Jespers V, Vanham G. HIV sexual transmission and microbicides. Rev Med Virol. 2011;21(2):110-33.

8. Karim QA, Baxter C. Microbicides for the prevention of sexually transmitted HIV infection. Expert Rev Anti Infect Ther. 2013;11(1):13-23.

9. Baeten J, Celum C. Systemic and topical drugs for the prevention of HIV infection: antiretroviral pre-exposure prophylaxis. Annu Rev Med. 2013;64:219-32.

10. Baeten JM, Palanee-Phillips T, Brown ER, Schwartz K, Soto-Torres LE, Govender V, et al. Use of a vaginal ring containing dapivirine for HIV-1 prevention in women. N Engl J Med. 2016;375(22):2121-32.

11. Nel A, van Niekerk N, Kapiga S, Bekker LG, Gama C, Gill K, et al. Safety and efficacy of a dapivirine vaginal ring for HIV prevention in women. N Engl J Med. 2016;375(22):2133-43.

12. das Neves J, Martins JP, Sarmento B. Will dapivirine redeem the promises of anti-HIV microbicides? Overview of product design and clinical testing. Adv Drug Deliv Rev. 2016;103:20-32.

13. van de Wijgert JH, Shattock RJ. Vaginal microbicides: moving ahead after an unexpected setback. AIDS. 2007;21(18):2369-76.

14. Romano J, Kashuba A, Becker S, Cummins J, Turpin J. Pharmacokinetics and pharmacodynamics in HIV prevention; Current status and future directions: A summary of the DAIDS and BMGF sponsored think tank on pharmacokinetics (PK)/pharmacodynamics (PD) in HIV prevention. AIDS Res Hum Retroviruses. 2013;29(11):1418-27.

15. Adams JL, Kashuba AD. Formulation, pharmacokinetics and pharmacodynamics of topical microbicides. Best Pract Res Clin Obstet Gynaecol. 2012;26(4):451-62.

16. Bertrand N, Wu J, Xu X, Kamaly N, Farokhzad OC. Cancer nanotechnology: the impact of passive and active targeting in the era of modern cancer biology. Adv Drug Deliv Rev. 2014;66:2-25.

17. Toy R, Bauer L, Hoimes C, Ghaghada KB, Karathanasis E. Targeted nanotechnology for cancer imaging. Adv Drug Deliv Rev. 2014;76:79-97.

18. Zhu X, Radovic-Moreno AF, Wu J, Langer R, Shi J. Nanomedicine in the management of microbial infection - Overview and perspectives. Nano Today. 2014;9(4):478-98.

19. Wilen CB, Tilton JC, Doms RW. HIV: cell binding and entry. Cold Spring Harb Perspect Med. 2012;2(8).

20. Sharma S, Parmar A, Kori S, Sandhir R. PLGA-based nanoparticles: A new paradigm in biomedical applications. Trends Anal Chem. 2016;80:30-40.

21. Danhier F, Ansorena E, Silva JM, Coco R, Le Breton A, Preat V. PLGA-based nanoparticles: an overview of biomedical applications. J Control Release. 2012;161(2):505-22.

22. das Neves J, Nunes R, Rodrigues F, Sarmento B. Nanomedicine in the development of anti-HIV microbicides. Adv Drug Deliv Rev. 2016;103:57-75.

23. Harris JM. Poly(Ethylene Glycol) Chemistry: Biotechnical and Biomedical Applications. New York: Plenum Press; 1992.

24. das Neves J, Amiji M, Sarmento B. Mucoadhesive nanosystems for vaginal microbicide development: friend or foe? Wiley Interdiscip Rev Nanomed Nanobiotechnol. 2011;3(4):389-99.

25. Lederman MM, Offord RE, Hartley O. Microbicides and other topical strategies to prevent vaginal transmission of HIV. Nat Rev Immunol. 2006;6(5):371-82.

26. Klasse PJ, Shattock R, Moore JP. Antiretroviral drug-based microbicides to prevent HIV-1 sexual transmission. Annu Rev Med. 2008;59:455-71.

27. Polianova MT, Ruscetti FW, Pert CB, Ruff MR. Chemokine receptor-5 (CCR5) is a receptor for the HIV entry inhibitor peptide T (DAPTA). Antiviral Res. 2005;67(2):83-92.

28. Ruff MR, Polianova M, Yang Q-e, Leoung GS, Ruscetti FW, Pert CB. Update on D-ala-peptide T-amide (DAPTA): a viral entry inhibitor that blocks CCR5 chemokine receptors. Curr HIV Res. 2003;1(1):51-67.

29. Sanna V, Siddiqui IA, Sechi M, Mukhtar H. Resveratrol-loaded nanoparticles based on poly(epsilon-caprolactone) and poly(D,L-lactic-co-glycolic acid)-poly(ethylene glycol) blend for prostate cancer treatment. Mol Pharm. 2013;10(10):3871-81.

30. Maartens G, Celum C, Lewin SR. HIV infection: epidemiology, pathogenesis, treatment, and prevention. Lancet. 2014;384(9939):258-71.

31. Shen R, Richter HE, Smith PD. Early HIV-1 target cells in human vaginal and ectocervical mucosa. Am J Reprod Immunol. 2011;65(3):261-7.

32. Klasse PJ. The molecular basis of HIV entry. Cell Microbiol. 2012;14(8):1183-92.

33. Haqqani AA, Tilton JC. Entry inhibitors and their use in the treatment of HIV-1 infection. Antiviral Res. 2013;98(2):158-70.

34. Clayton R, Ohagen A, Nicol F, Del Vecchio AM, Jonckers THM, Goethals O, et al. Sustained and specific in vitro inhibition of HIV-1 replication by a protease inhibitor encapsulated in gp120-targeted liposomes. Antiviral Res. 2009;84(2):142-9.

35. Song E, Zhu P, Lee S-K, Chowdhury D, Kussman S, Dykxhoorn DM, et al. Antibody mediated in vivo delivery of small interfering RNAs via cell-surface receptors. Nat Biotechnol. 2005;23(6):709-17.

36. Zhou J, Li H, Li S, Zaia J, Rossi JJ. Novel dual inhibitory function aptamer-siRNA delivery system for HIV-1 therapy. Mol Ther. 2008;16(8):1481-9.

37. Neff CP, Zhou J, Remling L, Kuruvilla J, Zhang J, Li H, et al. An aptamer-siRNA chimera suppresses HIV-1 viral loads and protects from helper CD4(+) T cell decline in humanized mice. Sci Transl Med. 2011;3(66):66ra6-ra6.

38. Endsley AN, Ho RJY. Enhanced anti-HIV efficacy of indinavir after inclusion in CD4-targeted lipid nanoparticles. J Acquir Immune Defic Syndr. 2012;61(4):417-24.

39. Levy JA. HIV and the pathogenesis of AIDS. 3rd ed. Washington, DC, USA: American Society of Microbiology Press; 2007.

40. Anderson DJ, Politch JA, Nadolski AM, Blaskewicz CD, Pudney J, Mayer KH. Targeting Trojan Horse leukocytes for HIV prevention. AIDS. 2010;24(2):163-87.

41. Sosnik A, das Neves J, Sarmento B. Mucoadhesive polymers in the design of nano-drug delivery systems for administration by non-parenteral routes: a review. Prog Polym Sci. 2014;39(12):2030-75.

42. Wang YY, Lai SK, So C, Schneider C, Cone R, Hanes J. Mucoadhesive nanoparticles may disrupt the protective human mucus barrier by altering its microstructure. PLoS One. 2011;6(6):e21547.

43. Dünnhaupt S, Kammona O, Waldner C, Kiparissides C, Bernkop-Schnürch A. Nano-carrier systems: Strategies to overcome the mucus gel barrier. Eur J Pharm Biopharm. 2015;96:447-53.

44. Carias AM, McCoombe S, McRaven M, Anderson M, Galloway N, Vandergrift N, et al. Defining the interaction of HIV-1 with the mucosal barriers of the female reproductive tract. J Virol. 2013;87(21):11388-400.

45. Haase AT. Targeting early infection to prevent HIV-1 mucosal transmission. Nature. 2010;464(7286):217-23.

46. Hladik F, Sakchalathorn P, Ballweber L, Lentz G, Fialkow M, Eschenbach D, et al. Initial events in establishing vaginal entry and infection by human immunodeficiency virus type-1. Immunity. 2007;26(2):257-70.

47. Botting RA, Rana H, Bertram KM, Rhodes JW, Baharlou H, Nasr N, et al. Langerhans cells and sexual transmission of HIV and HSV. Rev Med Virol. 2017;27(2):e1923.

48. Keele BF, Giorgi EE, Salazar-Gonzalez JF, Decker JM, Pham KT, Salazar MG, et al. Identification and characterization of transmitted and early founder virus envelopes in primary HIV-1 infection. Proc Natl Acad Sci U S A. 2008;105(21):7552-7.

49. Wu L, KewalRamani VN. Dendritic-cell interactions with HIV: infection and viral dissemination. Nat Rev Immunol. 2006;6(11):859-68.

50. van Kooyk Y, Geijtenbeek TB. DC-SIGN: escape mechanism for pathogens. Nat Rev Immunol. 2003;3(9):697-709.

51. Geijtenbeek TBH, Kwon DS, Torensma R, Van Vliet SJ, Van Duijnhoven GCF, Middel J, et al. DC-SIGN, a dendritic cell-specific HIV-1-binding protein that enhances trans-infection of T cells. Cell. 2000;100(5):587-97.

52. Ramanathan R, Park J, Hughes SM, Lykins WR, Bennett HR, Hladik F, et al. Effect of mucosal cytokine administration on selective expansion of vaginal dendritic cells to support nanoparticle transport. Am J Reprod Immunol. 2015;74(4):333-44.

53. Park J, Ramanathan R, Pham L, Woodrow KA. Chitosan enhances nanoparticle delivery from the reproductive tract to target draining lymphoid organs. Nanomedicine. 2017.

54. Torchilin VP. Passive and active drug targeting: drug delivery to tumors as an example. In: Schäfer-Korting M, editor. Drug Deliv. Heidelberg, Germany: Springer; 2010. p. 3-53.

55. Nowacek AS, Balkundi S, McMillan J, Roy U, Martinez-Skinner A, Mosley RL, et al. Analyses of nanoformulated antiretroviral drug charge, size, shape and content for uptake, drug release and antiviral activities in human monocyte-derived macrophages. J Control Release. 2011;150(2):204-11.

56. Ece Gamsiz D, Shah LK, Devalapally H, Amiji MM, Carrier RL. A model predicting delivery of saquinavir in nanoparticles to human monocyte/macrophage (Mo/Mac) cells. Biotechnol Bioeng. 2008;101(5):1072-82.

57. Mainardes RM, Gremiao MP, Brunetti IL, da Fonseca LM, Khalil NM. Zidovudine-loaded PLA and PLA-PEG blend nanoparticles: influence of polymer type on phagocytic uptake by polymorphonuclear cells. J Pharm Sci. 2009;98(1):257-67.

58. das Neves J, Bahia MF, Amiji MM, Sarmento B. Mucoadhesive nanomedicines: characterization and modulation of mucoadhesion at the nanoscale. Expert Opin Drug Deliv. 2011;8(8):1085-104.

59. Meng J, Zhang T, Agrahari V, Ezoulin MJ, Youan BB. Comparative biophysical properties of tenofovir-loaded, thiolated and nonthiolated chitosan nanoparticles intended for HIV prevention. Nanomedicine (Lond). 2014;9(11):1595-612.

60. Meng J, Sturgis TF, Youan BB. Engineering tenofovir loaded chitosan nanoparticles to maximize microbicide mucoadhesion. Eur J Pharm Sci. 2011;44(1-2):57-67.

61. Xu Q, Ensign LM, Boylan NJ, Schon A, Gong X, Yang JC, et al. Impact of Surface Polyethylene Glycol (PEG) Density on Biodegradable Nanoparticle Transport in Mucus ex Vivo and Distribution in Vivo. ACS Nano. 2015;9(9):9217-27.

62. Sadio A, Amaral AL, Nunes R, Ricardo S, Sarmento B, Almeida R, et al. A mouse intra-intestinal infusion model and its application to the study of nanoparticle distribution. Front Physiol. 2016;7:579.

63. Maisel K, Ensign L, Reddy M, Cone R, Hanes J. Effect of surface chemistry on nanoparticle interaction with gastrointestinal mucus and distribution in the gastrointestinal tract following oral and rectal administration in the mouse. J Control Release. 2015;197:48-57.

64. Nunes R, Sousa C, Sarmento B, das Neves J. Nanotechnology-based systems for microbicide development. In: das Neves J, Sarmento B, editors. Drug Delivery and Development of Anti-HIV Microbicides. Singapore: Pan Stanford; 2014. p. 415-58.

65. das Neves J, Michiels J, Arien KK, Vanham G, Amiji M, Bahia MF, et al. Polymeric nanoparticles affect the intracellular delivery, antiretroviral activity and cytotoxicity of the microbicide drug candidate dapivirine. Pharm Res. 2012;29(6):1468-84.

66. das Neves J, Araujo F, Andrade F, Michiels J, Arien KK, Vanham G, et al. In vitro and ex vivo evaluation of polymeric nanoparticles for vaginal and rectal delivery of the anti-HIV drug dapivirine. Mol Pharm. 2013;10(7):2793-807.

67. das Neves J, Sarmento B. Precise engineering of dapivirine-loaded nanoparticles for the development of anti-HIV vaginal microbicides. Acta Biomater. 2015;18:77-87.

68. Ham AS, Cost MR, Sassi AB, Dezzutti CS, Rohan LC. Targeted delivery of PSC-RANTES for HIV-1 prevention using biodegradable nanoparticles. Pharm Res. 2009;26(3):502-11.

69. Zolla-Pazner S, Cardozo T. Structure-function relationships of HIV-1 envelope sequence-variable regions refocus vaccine design. Nat Rev Immunol. 2010;10(7):527-35.

70. Hayakawa T, Kawamura M, Okamoto M, Baba M, Niikawa T, Takehara S, et al. Concanavalin A-immobilized polystyrene nanospheres capture HIV-1 virions and gp120: potential approach towards prevention of viral transmission. J Med Virol. 1998;56(4):327-31.

71. Di Gianvincenzo P, Marradi M, Martínez-Ávila OM, Bedoya LM, Alcamí J, Penadés S. Gold nanoparticles capped with sulfate-ended ligands as anti-HIV agents. Bioorg Med Chem Lett. 2010;20(9):2718-21.

72. Lara HH, Ixtepan-Turrent L, Garza-Trevino EN, Rodriguez-Padilla C. PVP-coated silver nanoparticles block the transmission of cell-free and cell-associated HIV-1 in human cervical culture. J Nanobiotechnology. 2010;8:15.

73. Lara HH, Ayala-Nunez NV, Ixtepan-Turrent L, Rodriguez-Padilla C. Mode of antiviral action of silver nanoparticles against HIV-1. J Nanobiotechnology. 2010;8:1.

74. Jiménez JL, Pion M, de la Mata FJ, Gomez R, Muñoz E, Leal M, et al. Dendrimers as topical microbicides with activity against HIV. New J Chem. 2012;36(2):299-309.

75. Nandy B, Saurabh S, Sahoo AK, Dixit NM, Maiti PK. The SPL7013 dendrimer destabilizes the HIV-1 gp120-CD4 complex. Nanoscale. 2015;7(44):18628-41.

76. Telwatte S, Moore K, Johnson A, Tyssen D, Sterjovski J, Aldunate M, et al. Virucidal activity of the dendrimer microbicide SPL7013 against HIV-1. Antiviral Res. 2011;90(3):195-9.

77. Tyssen D, Henderson SA, Johnson A, Sterjovski J, Moore K, La J, et al. Structure activity relationship of dendrimer microbicides with dual action antiviral activity. PLoS One. 2010;5(8):e12309.

78. Jiang YH, Emau P, Cairns JS, Flanary L, Morton WR, McCarthy TD, et al. SPL7013 gel as a topical microbicide for prevention of vaginal transmission of SHIV89.6P in macaques. AIDS Res Hum Retroviruses. 2005;21(3):207-13.

79. Patton DL, Cosgrove Sweeney YT, McCarthy TD, Hillier SL. Preclinical safety and efficacy assessments of dendrimer-based (SPL7013) microbicide gel formulations in a nonhuman primate model. Antimicrob Agents Chemother. 2006;50(5):1696-700.

80. Cohen CR, Brown J, Moscicki AB, Bukusi EA, Paull JR, Price CF, et al. A phase I randomized placebo controlled trial of the safety of 3% SPL7013 Gel (VivaGel(R)) in healthy young women administered twice daily for 14 days. PLoS One. 2011;6(1):e16258.

81. Moscicki AB, Kaul R, Ma Y, Scott ME, Daud, II, Bukusi EA, et al. Measurement of mucosal biomarkers in a phase 1 trial of intravaginal 3% StarPharma LTD 7013 gel (VivaGel) to assess expanded safety. J Acquir Immune Defic Syndr. 2012;59(2):134-40.

82. Chonco L, Pion M, Vacas E, Rasines B, Maly M, Serramia MJ, et al. Carbosilane dendrimer nanotechnology outlines of the broad HIV blocker profile. J Control Release. 2012;161(3):949-58.

83. Sepúlveda-Crespo D, Serramía MJ, Tager AM, Vrbanac V, Gómez R, De La Mata FJ, et al. Prevention vaginally of HIV-1 transmission in humanized BLT mice and mode of antiviral action of polyanionic carbosilane dendrimer G2-S16. Nanomedicine. 2015;11(6):1299-308.

84. Huang J, Ofek G, Laub L, Louder MK, Doria-Rose NA, Longo NS, et al. Broad and potent neutralization of HIV-1 by a gp41-specific human antibody. Nature. 2012;491(7424):406-12.

85. Tan J, Su M, Zeng Y, Wang C. Design, synthesis and activity evaluation of novel peptide fusion inhibitors targeting HIV-1 gp41. Bioorg Med Chem. 2016;24(2):201-6.

86. Liu S, Wu S, Jiang S. HIV entry inhibitors targeting gp41: from polypeptides to small-molecule compounds. Curr Pharm Des. 2007;13(2):143-62.

87. Wickline SA, Lanza G, Hood J, inventorsNanoparticulate compositions which employ membrane-integrating peptides to effect contraception and/or protection against infection by sexually transmitted virus are described patent 20120100186. 2012.

88. Hood JL, Jallouk AP, Campbell N, Ratner L, Wickline SA. Cytolytic nanoparticles attenuate HIV-1 infectivity. Antivir Ther. 2013;18(1):95-103.

89. Zhu J, Paul WE. CD4 T cells: fates, functions, and faults. Blood. 2008;112(5):1557-69.

90. Wheeler LA, Trifonova R, Vrbanac V, Basar E, McKernan S, Xu Z, et al. Inhibition of HIV transmission in human cervicovaginal explants and humanized mice using CD4 aptamer-siRNA chimeras. J Clin Invest. 2011;121(6):2401-12.

91. Davis KA, Lin Y, Abrams B, Jayasena SD. Staining of cell surface human CD4 with 2'-F-pyrimidine-containing RNA aptamers for flow cytometry. Nucleic Acids Res. 1998;26(17):3915-24.

92. Wheeler LA, Vrbanac V, Trifonova R, Brehm MA, Gilboa-Geffen A, Tanno S, et al. Durable knockdown and protection from HIV transmission in humanized mice treated with gel-formulated CD4 aptamer-siRNA chimeras. Mol Ther. 2013;21(7):1378-89.

93. Yang S, Chen Y, Gu K, Dash A, Sayre CL, Davies NM, et al. Novel intravaginal nanomedicine for the targeted delivery of saquinavir to CD4+ immune cells. Int J Nanomedicine. 2013;8:2847-58.

94. Salazar-Gonzalez JF, Salazar MG, Keele BF, Learn GH, Giorgi EE, Li H, et al. Genetic identity, biological phenotype, and evolutionary pathways of transmitted/founder viruses in acute and early HIV-1 infection. J Exp Med. 2009;206(6):1273-89.

95. Kakinuma T, Hwang ST. Chemokines, chemokine receptors, and cancer metastasis. J Leukoc Biol. 2006;79(4):639-51.

96. Lopalco L. CCR5: From natural resistance to a new anti-HIV strategy. Viruses. 2010;2(2):574-600.

97. Zhou J, Satheesan S, Li H, Weinberg MS, Morris KV, Burnett JC, et al. Cell-specific RNA aptamer against human CCR5 specifically targets HIV-1 susceptible cells and inhibits HIV-1 infectivity. Chem Biol. 2015;22(3):379-90.

98. Chittasupho C, Lirdprapamongkol K, Kewsuwan P, Sarisuta N. Targeted delivery of doxorubicin to A549 lung cancer cells by CXCR4 antagonist conjugated PLGA nanoparticles. Eur J Pharm Biopharm. 2014;88(2):529-38.

99. Wang RT, Zhi XY, Yao SY, Zhang Y. LFC131 peptide-conjugated polymeric nanoparticles for the effective delivery of docetaxel in CXCR4 overexpressed lung cancer cells. Colloids Surf B Biointerfaces. 2015;133:43-50.

100. Martínez-Ávila O, Hijazi K, Marradi M, Clavel C, Campion C, Kelly C, et al. Gold manno-glyconanoparticles: multivalent systems to block HIV-1 gp120 binding to the lectin DC-SIGN. Chemistry. 2009;15(38):9874-88.

101. Martínez-Ávila O, Bedoya LM, Marradi M, Clavel C, Alcami J, Penadés S. Multivalent manno-glyconanoparticles inhibit DC-SIGN-mediated HIV-1 trans-infection of human T cells. Chembiochem. 2009;10(11):1806-9.

102. Garcia-Vallejo JJ, Koning N, Ambrosini M, Kalay H, Vuist I, Sarrami-Forooshani R, et al. Glycodendrimers prevent HIV transmission via DC-SIGN on dendritic cells. Int Immunol. 2013;25(4):221-33.

103. Berzi A, Varga N, Sattin S, Antonazzo P, Biasin M, Cetin I, et al. Pseudo-mannosylated DC-SIGN ligands as potential adjuvants for HIV vaccines. Viruses. 2014;6(2):391-403.

104. Varga N, Sutkeviciute I, Ribeiro-Viana R, Berzi A, Ramdasi R, Daghetti A, et al. A multivalent inhibitor of the DC-SIGN dependent uptake of HIV-1 and Dengue virus. Biomaterials. 2014;35(13):4175-84.

105. Jolly C, Mitar I, Sattentau QJ. Adhesion molecule interactions facilitate human immunodeficiency virus type 1-induced virological synapse formation between T cells. J Virol. 2007;81(24):13916-21.

106. Kim S-S, Peer D, Kumar P, Subramanya S, Wu H, Asthana D, et al. RNAi-mediated CCR5 silencing by LFA-1-targeted nanoparticles prevents HIV infection in BLT mice. Mol Ther. 2010;18(2):370-6.

107. Kamp W, Breij EC, Nottet HS, Berk MB. Interactions between major histocompatibility complex class II surface expression and HIV: implications for pathogenesis. Eur J Clin Invest. 2001;31(11):984-91.

108. Bestman-Smith J, Désormeaux A, Tremblay MJ, Bergeron MG. Targeting cell-free HIV and virally-infected cells with anti-HLA-DR immunoliposomes containing amphotericin B. AIDS. 2000;14(16):2457-65.

109. Gagné JF, Désormeaux A, Perron S, Tremblay MJ, Bergeron MG. Targeted delivery of indinavir to HIV-1 primary reservoirs with immunoliposomes. Biochim Biophys Acta. 2002;1558(2):198-210.

110. Gu J, Yang S, Ho EA. Biodegradable film for the targeted delivery of siRNA-loaded nanoparticles to vaginal immune cells. Mol Pharm. 2015;12(8):2889-903.

111. Cunha-Reis C, Machado A, Barreiros L, Araújo F, Nunes R, Seabra V, et al. Nanoparticles-in-film for the combined vaginal delivery of anti-HIV microbicide drugs. J Control Release. 2016;243:43-53.

112. Nunes R, Sarmento B, das Neves J. Formulation and delivery of anti-HIV rectal microbicides: advances and challenges. J Control Release. 2014;194:278-94.

113. GHOST (3) CCR5+ Cells (Hi-5): NIH Aids Reagent Program; 2017 [updated 22 June 2017. Available from: https://www.aidsreagent.org/reagentdetail.cfm?t=cell_lines&id=343.

114. HeLa (ATCC® CCL-2™) American Type Culture Collection (ATCC); 2016 [Available from: https://www.lgcstandards-atcc.org/Products/All/CCL-2.aspx.

115. Hermanson GT. Bioconjugate Techniques. 2nd ed. Oxford, UK: Academic Press; 2008.

116. Cheng J, Teply BA, Sherifi I, Sung J, Luther G, Gu FX, et al. Formulation of functionalized PLGA-PEG nanoparticles for in vivo targeted drug delivery. Biomaterials. 2007;28(5):869-76.

117. Chan JM, Valencia PM, Zhang L, Langer R, Farokhzad OC. Polymeric nanoparticles for drug delivery. Methods Mol Biol. 2010;624:163-75.

118. Liu CW, Lin WJ. Polymeric nanoparticles conjugate a novel heptapeptide as an epidermal growth factor receptor-active targeting ligand for doxorubicin. Int J Nanomedicine. 2012;7:4749-67.

119. Ghahremankhani AA, Dorkoosh F, Dinarvand R. PLGA-PEG-PLGA Tri-Block Copolymers as In Situ Gel-Forming Peptide Delivery System: Effect of Formulation Properties on Peptide Release. Pharm Dev Technol. 2008;13(1):49-55.

120. Nicolas J, Mura S, Brambilla D, Mackiewicz N, Couvreur P. Design, functionalization strategies and biomedical applications of targeted biodegradable/biocompatible polymer-based nanocarriers for drug delivery. Chem Soc Rev. 2013;42(3):1147-235.

121. Guo J, Gao X, Su L, Xia H, Gu G, Pang Z, et al. Aptamer-functionalized PEG-PLGA nanoparticles for enhanced anti-glioma drug delivery. Biomaterials. 2011;32(31):8010-20.

122. Zhou W, Zhou Y, Wu J, Liu Z, Zhao H, Liu J, et al. Aptamer-nanoparticle bioconjugates enhance intracellular delivery of vinorelbine to breast cancer cells. J Drug Target. 2014;22(1):57-66.

123. Kang T, Gao X, Hu Q, Jiang D, Feng X, Zhang X, et al. iNGR-modified PEG-PLGA nanoparticles that recognize tumor vasculature and penetrate gliomas. Biomaterials. 2014;35(14):4319-32.

124. Gomes MJ, Fernandes C, Martins S, Borges F, Sarmento B. Tailoring Lipid and Polymeric Nanoparticles as siRNA Carriers towards the Blood-Brain Barrier - from Targeting to Safe Administration. J, Neuroimmune Pharmacol. 2017;12(1):107-19.

125. Schindelin J, Arganda-Carreras I, Frise E, Kaynig V, Longair M, Pietzsch T, et al. Fiji: an open-source platform for biological-image analysis. Nat Methods. 2012;9(7):676-82.

126. Koopaei MN, Dinarvand R, Amini M, Rabbani H, Emami S, Ostad SN, et al. Docetaxel immunonanocarriers as targeted delivery systems for HER 2-positive tumor cells: preparation, characterization, and cytotoxicity studies. Int J Nanomedicine. 2011;6:1903-12.

127. Thuy Le DT. Anti-Tumor Activity of Docetaxel PLGA-PEG Nanoparticles with a Novel Anti-HER2 scFv. J Nanomed Nanotechnol. 2015;06(02).

128. Kamaly N, Fredman G, Subramanian M, Gadde S, Pesic A, Cheung L, et al. Development and in vivo efficacy of targeted polymeric inflammation-resolving nanoparticles. Proc Natl Acad Sci U S A. 2013;110(16):6506-11.

129. Vasconcelos A, Vega E, Perez Y, Gomara MJ, Garcia ML, Haro I. Conjugation of cell-penetrating peptides with poly(lactic-co-glycolic acid)-polyethylene glycol nanoparticles improves ocular drug delivery. Int J Nanomedicine. 2015;10:609-31.

130. Staros JV, Wright RW, Swingle DM. Enhancement by N-hydroxysulfosuccinimide of water-soluble carbodiimide-mediated coupling reactions. Anal Biochem. 1986;156(1):220-2.

131. Özdemir C, Güner A. Solubility profiles of poly(ethylene glycol)/solvent systems, I: Qualitative comparison of solubility parameter approaches. Eur Polym J. 2007;43(7):3068-93.

132. Yu L, Zhang H, Ding J. Effects of precipitate agents on temperature-responsive sol–gel transitions of PLGA–PEG–PLGA copolymers in water. Colloid Polym Sci. 2010;288(10-11):1151-9.

133. Lebouille JGJL, Stepanyan R, Slot JJM, Cohen Stuart MA, Tuinier R. Nanoprecipitation of polymers in a bad solvent. Colloids Surf A Physicochem Eng Asp. 2014;460(Supplement C):225-35.

134. Pottorf RS, Szeto P, Srinivasarao M. 1-Ethyl-3-(3′-dimethylaminopropyl) carbodiimide Hydrochloride. e-EROS Encyclopedia of Reagents for Organic Synthesis.1-5.

135. Singhal N, Kumar M, Kanaujia PK, Virdi JS. MALDI-TOF mass spectrometry: an emerging technology for microbial identification and diagnosis. Front Microbiol. 2015;6:791.

136. Cobo F. Application of MALDI-TOF Mass Spectrometry in Clinical Virology: A Review. Open Virol J. 2013;7:84-90.

137. Shibata A, Yada S, Terakawa M. Biodegradability of poly(lactic-co-glycolic acid) after femtosecond laser irradiation. Sci Rep. 2016;6:27884.

138. Smith BC. Fundamentals of Fourier transform infrared spectroscopy. USA: CRC press; 2011.

139. Silverstein RM, Webster FX, Kiemle DJ, Bryce DL. Spectrometric identification of organic compounds. 8th ed. USA: John Wiley & Sons; 2014.

140. Xiao H, Wang L. Effects of X-shaped reduction-sensitive amphiphilic block copolymer on drug delivery. Int J Nanomedicine. 2015;Volume 10(1):5309-25.

141. Muthiah M, Vu-Quang H, Kim YK, Rhee JH, Kang SH, Jun SY, et al. Mannose-poly(ethylene glycol)-linked SPION targeted to antigen presenting cells for magnetic resonance imaging on lymph node. Carbohydr Polym. 2013;92(2):1586-95.

142. Loganathan S, Sankaran S. Surface Chemical Studies on Silicon Carbide Suspensions in the Presence of Poly (Ethylene Glycol) and Chitosan. Colloid Surf Sci. 2017;2(1):6-20.

143. Jelinski LW. Modern NMR Spectroscopy. Chem Eng News. 1984;62(45).

144. Starkey LS. ^{1}H NMR Chemical Shifts Pomona, CA, USA: California State Polytechnic University; [Available from: https://www.cpp.edu/~lsstarkey/courses/NMR/NMRshifts1H-general.pdf.

145. Fulmer GR, Miller AJM, Sherden NH, Gottlieb HE, Nudelman A, Stoltz BM, et al. NMR Chemical Shifts of Trace Impurities: Common Laboratory Solvents, Organics, and Gases in Deuterated Solvents Relevant to the Organometallic Chemist. Organometallics. 2010;29(9):2176-9.

146. Heald CR, Stolnik S, Kujawinski KS, De Matteis C, Garnett MC, Illum L, et al. Poly(lactic acid)−Poly(ethylene oxide) (PLA−PEG) Nanoparticles: NMR Studies of the Central Solidlike PLA Core and the Liquid PEG Corona. Langmuir. 2002;18(9):3669-75.

147. Martinez Rivas CJ, Tarhini M, Badri W, Miladi K, Greige-Gerges H, Nazari QA, et al. Nanoprecipitation process: From encapsulation to drug delivery. Int J Pharm. 2017;532(1):66-81.

148. das Neves J, Amiji M, Bahia MF, Sarmento B. Assessing the physical-chemical properties and stability of dapivirine-loaded polymeric nanoparticles. Int J Pharm. 2013;456(2):307-14.

149. Bulte JW, Modo M. Nanoparticles in biomedical imaging: emerging technologies and applications: Springer Science & Business Media; 2007.

150. Maruyama K. PEG-immunoliposome. Biosci Rep. 2002;22(2):251-66.

151. Zetasizer Nano Series User Manual. Worcestershire, UK: Malvern Instruments Ltd.; 2013.

152. Lai SK, O'Hanlon DE, Harrold S, Man ST, Wang YY, Cone R, et al. Rapid transport of large polymeric nanoparticles in fresh undiluted human mucus. Proc Natl Acad Sci U S A. 2007;104(5):1482-7.

153. Lai SK, Wang YY, Cone R, Wirtz D, Hanes J. Altering mucus rheology to "solidify" human mucus at the nanoscale. PLoS One. 2009;4(1):e4294.

154. Yang M, Lai SK, Wang YY, Zhong W, Happe C, Zhang M, et al. Biodegradable nanoparticles composed entirely of safe materials that rapidly penetrate human mucus. Angew Chem Int Ed Engl. 2011;50(11):2597-600.

155. Frohlich E. The role of surface charge in cellular uptake and cytotoxicity of medical nanoparticles. Int J Nanomedicine. 2012;7:5577-91.

156. Domingos RF, Baalousha MA, Ju-Nam Y, Reid MM, Tufenkji N, Lead JR, et al. Characterizing manufactured nanoparticles in the environment: multimethod determination of particle sizes. Environ Sci Technol. 2009;43(19):7277-84.

157. Bootz A, Vogel V, Schubert D, Kreuter J. Comparison of scanning electron microscopy, dynamic light scattering and analytical ultracentrifugation for the sizing of poly(butyl cyanoacrylate) nanoparticles. Eur J Pharm Biopharm. 2004;57(2):369-75.

158. Mosmann T. Rapid colorimetric assay for cellular growth and survival: application to proliferation and cytotoxicity assays. J Immunol Methods. 1983;65(1-2):55-63.

159. Biological evaluation of medical devices. Tests for in vitro cytotoxicity. Switzerland: International Organization for Standardization; 2009.

160. Petersen S, Steiniger F, Fischer D, Fahr A, Bunjes H. The physical state of lipid nanoparticles influences their effect on in vitro cell viability. Eur J Pharm Biopharm. 2011;79(1):150-61.

161. Dionisio M, Cordeiro C, Remunan-Lopez C, Seijo B, Rosa da Costa AM, Grenha A. Pullulan-based nanoparticles as carriers for transmucosal protein delivery. Eur J Pharm Biopharm. 2013;50(1):102-13.

162. Wu M, Guo K, Dong H, Zeng R, Tu M, Zhao J. In vitro drug release and biological evaluation of biomimetic polymeric micelles self-assembled from amphiphilic deoxycholic acid-phosphorylcholine-chitosan conjugate. Mater Sci Eng C Mater Biol Appl. 2014;45:162-9.

163. Hillegass JM, Shukla A, Lathrop SA, MacPherson MB, Fukagawa NK, Mossman BT. Assessing nanotoxicity in cells in vitro. Wiley Interdiscip Rev Nanomed Nanobiotechnol. 2010;2(3):219-31.

164. Lugli E, Zanon V, Mavilio D, Roberto A. FACS Analysis of Memory T Lymphocytes. Methods Mol Biol. 2017;1514:31-47.

165. Hulspas R, O'Gorman MR, Wood BL, Gratama JW, Sutherland DR. Considerations for the control of background fluorescence in clinical flow cytometry. Cytometry B Clin Cytom. 2009;76(6):355-64.

166. Ruff MR, Martin BM, Ginns EI, Farrar WL, Pert CB. CD4 receptor binding peptides that block HIV infectivity cause human monocyte chemotaxis: Relationship to vasoactive intestinal polypeptide. FEBS Lett. 1987;211(1):17-22.

167. Olson WC, Rabut GE, Nagashima KA, Tran DN, Anselma DJ, Monard SP, et al. Differential inhibition of human immunodeficiency virus type 1 fusion, gp120 binding, and CC-chemokine activity by monoclonal antibodies to CCR5. J Virol. 1999;73(5):4145-55.

168. Trkola A, Ketas TJ, Nagashima KA, Zhao L, Cilliers T, Morris L, et al. Potent, broad-spectrum inhibition of human immunodeficiency virus type 1 by the CCR5 monoclonal antibody PRO 140. J Virol. 2001;75(2):579-88.

169. Brandrup J, Immergut EH, Grulke EA. Polymer Handbook. 4th ed. USA2003.

170. Preparative Gel Permeation Chromatography – Loading (Technical Overview). USA: Agilent Technologies, Inc.; 2015.

171. Static Light Scattering technologies for GPC-SEC explained. Worcestershire, UK: Malvern Instruments Ltd.; 2015.

172. Bradford MM. A rapid and sensitive method for the quantitation of microgram quantities of protein utilizing the principle of protein-dye binding. Anal Biochem. 1976;72(1):248-54.

173. Congdon RW, Muth GW, Splittgerber AG. The binding interaction of Coomassie blue with proteins. Anal Biochem. 1993;213(2):407-13.

174. Smith PK, Krohn RI, Hermanson GT, Mallia AK, Gartner FH, Provenzano MD, et al. Measurement of protein using bicinchoninic acid. Anal Biochem. 1985;150(1):76-85.

175. Zuman P. Reactions of orthophthalaldehyde with nucleophiles. Chem Rev. 2004;104(7):3217-38.

176. Bohlen P, Stein S, Dairman W, Udenfriend S. Fluorometric assay of proteins in the nanogram range. Arch Biochem Biophys. 1973;155(1):213-20.

177. Sarmento B, editor. Concepts and Models for Drug Permeability Studies: Cell and Tissue Based In Vitro Culture Models. Cambridge, UK: Woodhead Publishing; 2016.

178. das Neves J, Sarmento B, editors. Drug Delivery and Development of Anti-HIV Microbicides. Singapore: Pan Stanford; 2014.